NOAA Technical Memorandum OAR PMEL-136

# SCIENTIFIC AND TECHNICAL ISSUES IN TSUNAMI HAZARD ASSESSMENT OF NUCLEAR POWER PLANT SITES

Science Review Working Group

Pacific Marine Environmental Laboratory
Seattle, WA

Pacific Marine Environmental Laboratory
Seattle, WA
May 2007


**UNITED STATES DEPARTMENT OF COMMERCE**

**Carlos M. Gutierrez**
**Secretary**

NATIONAL OCEANIC AND ATMOSPHERIC ADMINISTRATION

VADM Conrad C. Lautenbacher, Jr.
Under Secretary for Oceans and Atmosphere/Administrator

Office of Oceanic and Atmospheric Research

Richard W. Spinrad
Assistant Administrator

NOTICE from NOAA

Mention of a commercial company or product does not constitute an endorsement by NOAA/OAR. Use of information from this publication concerning proprietary products or the tests of such products for publicity or advertising purposes is not authorized. Any opinions, findings, and conclusions or recommendations expressed in this material are those of the authors and do not necessarily reflect the views of the National Oceanic and Atmospheric Administration.

**Science Review Working Group:**

Frank González (Chair), NOAA Center For Tsunami Research, PMEL, Seattle, WA
Eddie Bernard, NOAA Center for Tsunami Research, PMEL, Seattle, WA
Paula Dunbar, NOAA National Geophysical Data Center, Boulder, CO
Eric Geist, USGS Coastal and Marine Geology Division, Menlo Park, CA
Bruce Jaffe, USGS Pacific Science Center, Santa Cruz, CA
Utku Kânoğlu, Middle East Technical University, Ankara, Turkey
Jacques Locat, Université Laval, Quebec, Canada
Harold Mofjeld, NOAA Center For Tsunami Research, PMEL, Seattle, WA
Andrew Moore, Kent State University, Kent, OH
Costas Synolakis, USC Tsunami Research Center, Los Angeles, CA
Vasily Titov, NOAA Center For Tsunami Research, PMEL, Seattle, WA
Robert Weiss, NOAA Center For Tsunami Research, PMEL, Seattle, WA

This report should be cited as:

González, F.I., E. Bernard, P. Dunbar, E. Geist, B. Jaffe, U. Kânoğlu, J. Locat, H. Mofjeld, A. Moore, C. Synolakis, V. Titov, and R. Weiss (Science Review Working Group) (2007): Scientific and technical issues in tsunami hazard assessment of nuclear power plant sites. NOAA Tech. Memo. OAR PMEL-136, Pacific Marine Environmental Laboratory, Seattle, WA, 125 pp. + appendices on CD.

Contribution No. 3031 from NOAA/Pacific Marine Environmental Laboratory

Also available from the National Technical Information Service (NTIS)
(`http://www.ntis.gov`)

# Contents

# List of Figures

# Scientific and technical issues in tsunami hazard assessment of nuclear power plant sites

Science Review Working Group

**Abstract.** This report provides a review and discussion of existing scientific and technical reports related to tsunami hazard assessment, and organizes the information in the form of a "Template Tsunami Hazard Assessment (THA)." This provides a general scientific and technical framework that can serve as a starting point for the development of improved and more detailed procedures to guide Nuclear Regulatory Commission (NRC) reviews of applications to build and operate nuclear power plants.

## Executive Summary

*by Eddie Bernard*

This study was undertaken at the request and under the sponsorship of the Nuclear Regulatory Commission (NRC), in support of a program to upgrade procedures that guide NRC reviews of applications to build and operate nuclear power plants. The purpose of the study was to provide a framework for upgrading the tsunami portion of these procedures, in a way that embodies the current state of the art in the science and technology of Tsunami Hazard Assessment (THA). To this end, an interdisciplinary team was assembled, composed of experts in the geoscientific and hydrodynamic aspects of such assessments. Relevant reports are reviewed, summarized, and discussed in Sections 1–7 of the report, and key reports are provided in Appendices A–D, for convenient reference. In Section 8, this information is organized into a "Template THA," a scientific and technical framework for development of improved, more detailed tsunami hazard assessment review procedures.

The primary components of the Template THA methodology recommended as the basis for NRC reviews are

- ***Conduct an Initial Screening Study***, with the goal of establishing the presence or absence of a tsunami hazard at the site, on the basis of existing information and best available scientific interpretation of this information. If a tsunami hazard is established, or the study is inconclusive, additional THA must be conducted, as follows.

- ***Develop a Site-specific THA Database***, including specification of potential sources, the results of a parametric tsunami inundation modeling study, and the development of hazard metrics specific to the nuclear power plant (NPP) location, physical setting, and engineering design.

- ***Establish the Tsunami Hazard Level*** through analysis of tsunami hazard metric values in the context of the proposed NPP design.

- ***Evaluate the Feasibility of Real-time THA*** at the site, to provide

effective, continual tsunami hazard assessment in real time, during an actual event.

Recommendations on scientific and technical issues related to THA are provided in each of Sections 2–8, which deal with specific aspects of THA. In addition, more general recommendations are provided in Section 9, which would facilitate improvements in nuclear power plant THA, and associated NRC reviews, through collaboration and coordination with other Federal agencies and programs. These recommendations are reproduced here, for convenience.

A. Establish a formal, interagency partnership of NRC, NOAA, USGS, and FEMA to leverage existing expertise and resources, avoid duplication, and address national needs for tsunami hazard assessment of NPP sites in a federally consistent and cost-effective manner.

B. Require that tsunami hazard assessments be conducted with source specification and tsunami numerical modeling that meet USGS and NOAA standards, respectively, to ensure Federal consistency of all tsunami hazard assessment methods and the resulting products.

C. Request that NOAA investigate and determine the means and needed resources by which (a) Tsunami Warning Centers can provide site-specific warnings for threatened NPPs, and (b) real-time tsunami measurement systems can be established near each NPP to enhance site-specific tsunami forecasts, warnings, and real-time tsunami hazard assessment during an actual event.

# 1. Introduction

*by Frank González*

## 1.1 Background

Applications to build and operate up to 26 new nuclear power reactors are expected over the next few years, increasing the current level of 104 nuclear power reactors licensed to operate in the U.S. at 65 sites in 31 states (Fig. 1-1); this renewed interest is due to various factors, including the rising price of fuel, the aging of the U.S. electric power supply system, reduced licensing delays resulting from amendments to the Atomic Energy Act, and a tax credit for nuclear generation provided by the Energy Policy Act of 2005 (Smolik and Newell, 2006; Parker and Holt, 2006). Some candidate nuclear power plant (NPP) sites may be located on coasts subject to tsunamis, and the devastation to coastal infrastructure caused by the Indian Ocean tsunami of 26 December 2004 has increased awareness of this hazard to NPPs.

The Nuclear Regulatory Commission (NRC) is responsible for the licensing and regulation of nuclear power plants. In particular, NRC staff in the Office of New Reactors are responsible for performing safety reviews of the plant design and the plant site proposed in the application. Guidance for NRC staff reviewers is provided by the Standard Review Plan for the Review of Safety Analysis Reports for Nuclear Power Plants (U.S. NRC, 1996), also

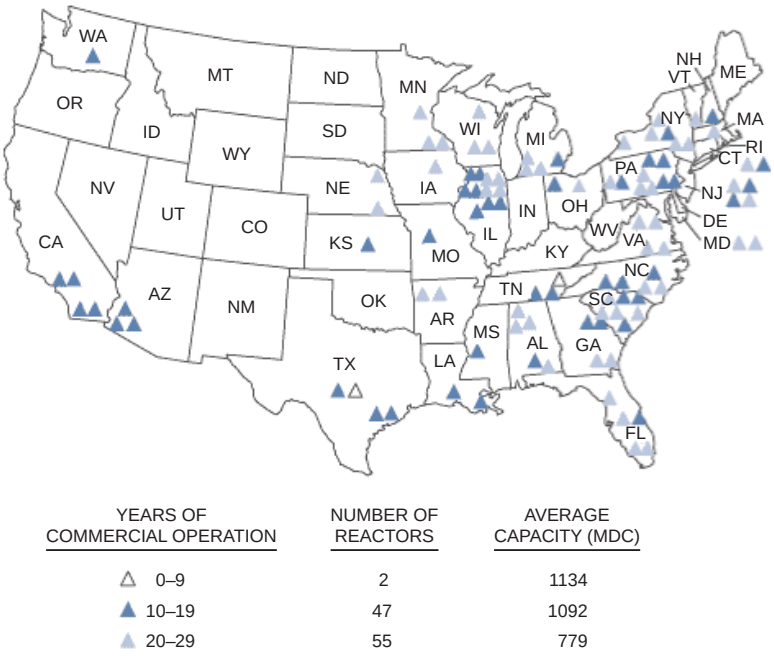


**Figure 1-1:** Location of U.S. nuclear reactor sites. (Map available at `http://www.nrc.gov/reactors/operating/map-power-reactors.html`)

known as NUREG-0800. A program to update the Standard Review Plan (SRP) was initiated by NRC in 2006 and will be completed in 2007. The tsunami hazard is addressed by Section 2.4.6 of the SRP, entitled "Probable Maximum Tsunami Flooding"; consequently, as part of the SRP Update Program, the NRC requested that the National Oceanic and Atmospheric Administration (NOAA) and the U.S. Geological Survey (USGS) form a team of tsunami experts to develop this report, to serve as scientific guidance for carrying out tsunami hazard analysis at nuclear power plant sites as recommended by this section of the SRP.

## 1.2 Relevant Federal Agencies and Programs

Several Federal Agencies are charged with missions that are highly relevant to the responsibility of the NRC to review tsunami hazard assessment (THA) at potential NPP sites and administer programs focused on developing, applying, and improving the needed technology.

NOAA bears national responsibility for tsunami warnings and has established and maintains the Pacific Tsunami Warning Center (PTWC), located at Ewa Beach, Hawaii, and the West Coast and Alaska Tsunami Warning Center (WCATWC), located in Palmer, Alaska. NOAA also leads the National Tsunami Hazard Mitigation Program (NTHMP), a partnership with the U.S. Geological Survey, the Federal Emergency Management Agency (FEMA), the National Science Foundation, and all U.S. coastal states. The NOAA Center for Tsunami Research (NCTR) was established to conduct research and development in support of the NOAA mission to reduce the loss of U.S. life and property by providing tsunami warning and hazard mitigation products. The NCTR research and development focuses on the improvement and application of tsunami measurement and modeling technology.

USGS also bears national responsibility for minimizing the loss of life and property to natural hazards by providing reliable geoscientific information. Tsunami research conducted by the USGS Coastal and Marine Geology Program focuses on the identification, description, and modeling of potential tsunami sources. As such, the USGS and NOAA work in close scientific collaboration on tsunami research issues.

FEMA administers the National Flood Insurance Program, and is responsible for the development of Flood Insurance Rate Maps (FIRMs) that govern insurance rates for individual homeowners and businesses. FEMA is in the process of updating flooding hazard assessment technology for many flood phenomena through its Map Modernization Program, and supported a pilot study at Seaside, Oregon, to improve tsunami hazard assessment methods (Tsunami Pilot Study Working Group, 2006).

## 1.3 Tsunami Characteristics

A tsunami is a series of propagating water waves generated impulsively by an undersea earthquake or, much less frequently, by sources such as a volcanic eruption or meteor impact; submarine slumps or coastal landslides can accompany these events and act as important sources of additional energy.

**Figure 1-2:** A tsunami generated on 12 July 1993 by a magnitude 7.8 earthquake off Aonae, Okushiri Island, Japan, completely denuded the exposed Aonae peninsula of built structures and caused severe damage to the port facilities. Maximum wave height and current speed were estimated to be approximately 10 m and 18 m/s, respectively.

Although primarily an oceanic phenomena, tsunamis can also be generated in lakes and other inland bodies of water by similar mechanisms, i.e., earthquakes and slope failures—associated or not associated with earthquakes.

The impact of the extremely high waves and currents of a large tsunami event can cause massive destruction of the built environment (Fig. 1-2). Clearly, such destruction can affect the critical infrastructure of a power reactor by interfering with the cooling water supply, or by damaging a safety-related structure. These events can also inflict a huge number of fatalities; historical tsunamis believed to have caused more than 1,000 deaths are presented in Table 1-1. This table was compiled by querying the online NOAA Historical Tsunami Database, and includes estimated damage, when available. Appendix A discusses sources of historical and pre-historic data, and Section 2 provides a summary and discussion of tsunamis that have impacted the U.S.

An understanding of tsunami dynamics, including inundation, runup, and drawdown are needed for specific sites exposed to a variety of potential tsunamigenic sources. Accordingly, tsunami characteristics are discussed in detail in Sections 4–7 and Appendix B of this report. However, a few simple physical ideas and some simple relationships derived from linear long wave theory can provide first order approximations that are informative and help build physical intuition.

Basically, ranges of values for various tsunami parameters are governed by both the source characteristics and by the details of the bathymetry and topography of the propagation path. Thus, we start with the expression for linear, long wave phase speed,

$$c = (gd)^{1/2} = \lambda/\tau \ , \tag{1.1}$$

**Table 1-1:** Large historical tsunamis, based on information from NOAA Historical Tsunami Database. Source abbreviations are Eq: Earthquake; Vol: Volcano; LS: Landslide; Unk: Unknown.

| Yr | Mo | Dy | Country | Location | Eq Mag | Other Source | Max Runup (m) | Deaths | Damage ($) |
|---|---|---|---|---|---|---|---|---|---|
| 2004 | 12 | 26 | Indonesia | W. Coast Sumatra | 9 | | 34.9 | 297,248 | >25M |
| 1998 | 7 | 17 | PNG | | 7 | | 15 | 2,182 | |
| 1992 | 12 | 12 | Indonesia | Flores Sea | 7.8 | | 26.2 | 1,000 | |
| 1976 | 8 | 16 | Philippines | Moro Gulf | 8.1 | | 4.48 | 2,349 | 130M |
| 1960 | 5 | 22 | Chile | Central Chile | 9.5 | | 25 | 1,260 | |
| 1946 | 8 | 4 | Dom. Rep. | N.E. Coast | 8.1 | | 5 | 1,790 | 5–24M |
| 1941 | 6 | 26 | India | Andaman Sea | 7.6 | | | 5,000 | |
| 1933 | 3 | 2 | Japan | Sanriku | 8.4 | | 29.3 | 3,064 | 5–25M |
| 1923 | 9 | 1 | Japan | Tokaido | 7.9 | | 12.1 | 2,144 | |
| 1906 | 1 | 31 | Ecuador | Off Coast | 8.8 | | 5 | 1,000 | 5–24M |
| 1902 | 5 | 7 | St. Vincent, Grenadines | Soufriere Volcano | | Vol | | 1,565 | |
| 1899 | 9 | 30 | Indonesia | Banda Sea | 7.8 | | 12 | 3,620 | |
| 1896 | 6 | 15 | Japan | Sanriku | 7.6 | | 38.2 | 27,122 | 5–24M |
| 1883 | 8 | 27 | Indonesia | Krakatau | | Vol | 35 | 36,500 | |
| 1861 | 3 | 9 | Indonesia | S.W. Sumatra | 7 | | | 1,700 | |
| 1854 | 12 | 24 | Japan | Nankaido | 8.4 | | 28 | 3,000 | 5–24M |
| 1819 | 6 | 16 | India | Kutch | 8.3* | | | 1,543 | |
| 1815 | 11 | 22 | Indonesia | Bali Sea | 7 | | | 1,200 | |
| 1792 | 5 | 21 | Japan | S.W. Kyushu Is. | 6.4 | Vol | 11 | 4,300 | 5–24M |
| 1771 | 4 | 24 | Japan | Ryukyu Is. | 7.4 | | 85.4 | 13,486 | |
| 1766 | 3 | 8 | Japan | Sanriku | 6.9 | Unk | 0.9 | 1,700 | |
| 1746 | 10 | 29 | Peru | | 8 | | 24 | 3,800 | |
| 1741 | 8 | 29 | Japan | W. Hokkaido Is. | 6.9 | Vol | 9 | 1,607 | |
| 1707 | 10 | 28 | Japan | Tokaido-Nankaido | 8.4 | | 25.7 | 30,000 | >25M |
| 1703 | 12 | 31 | Japan | Tokaido-Kashima | 8.2 | | 10.5 | 5,233 | |
| 1700 | 4 | 1 | Japan | S.W. Kyushu Is. | | LS | | 1,000 | |
| 1692 | 6 | 7 | Jamaica | Port Royal | 7.7 | | 1.8 | 2,000 | 5–24M |
| 1674 | 2 | 17 | Indonesia | Banda Sea | 6.8 | | 100 | 2,243 | 5–24M |
| 1611 | 12 | 2 | Japan | Sanriku | 8 | | 25 | 5,000 | |
| 1605 | 2 | 3 | Japan | Nankaido | 8.1 | | 10 | 5,000 | 5–24M |
| 1605 | 2 | 3 | Japan | Enshunada | 8 | | | 1,000 | 5–24M |
| 1586 | 1 | 18 | Japan | Tokaido | 8.2 | | | 8,000 | 5–24M |
| 1570 | 2 | 8 | Chile | Old Concepcion | 8 | | | 2,000 | 5–24M |
| 1498 | 9 | 20 | Japan | Nankaido | Unk | | 10 | 31,201 | 5–24M |
| 1341 | 10 | 31 | Japan | Jusanko | 7 | | | 2,600 | |
| 1026 | 6 | 16 | Japan | Masuda | 7.5 | | 10 | 1,000 | 5–24M |
| 869 | 7 | 13 | Japan | Sanriku | 8.6 | | 10 | 1,000 | 5–24M |
| 744 | 6 | 30 | Japan | S.W. Kyushu Is. | | Unk | 2 | 1,520 | |

*Computational method could not be determined.

where

$c$ = wave phase speed
$g$ = acceleration due to gravity
$d$ = water depth
$\lambda$ = wavelength
$\tau$ = wave period

Initially, the tsunami wavelength, $\lambda$, is determined by the length scale, $L$, of the source. Thus, e.g., if an earthquake produces an ocean bottom deformation of characteristic length scale $L$, then, to a first approximation, an identical sea surface deformation is produced, and a tsunami is generated with an initial wavelength that is approximately

$$\lambda_0 \cong 2L \ . \tag{1.2}$$

Similarly, the dominant tsunami period (in reality, there will likely be a narrow band of individual wave periods associated with multiple source length scales) is set by the generation length scale, as

$$\tau \cong \lambda_0/(gd_0)^{1/2} \cong 2L/(gd_0)^{1/2} \ , \tag{1.3}$$

where $d_0$ is the initial water depth. Since the period $\tau$ is invariant, the wavelength varies with water depth, as

$$\lambda \cong \tau(gd)^{1/2} \ . \tag{1.4}$$

Finally, the associated maximum tsunami currents are given approximately by

$$u \cong \eta/(gd)^{1/2} \ , \tag{1.5}$$

where $\eta$ is the tsunami amplitude, and the currents are vertically uniform.

Field observations and modeling indicate that the majority of tsunamis of interest, i.e., those potentially destructive, are characterized by periods in the range of 5–60 min, deep ocean amplitudes that range from 0.01 to 1 m, and amplitudes in shallow coastal waters that can be 10 m or more. Accordingly, Table 1-2 provides the corresponding range of tsunami parameter values in the deep ocean and shallow coastal waters, based on the relationships presented above.

## 1.4 Purpose, Scope, and Content of Report

The purpose of this report is to summarize what is currently believed to be the "best available science" that bears directly on the issue of tsunami hazard assessment, especially as it relates to nuclear power plants, to serve as guidance for the development of improved, detailed procedures and protocols for NRC reviews of such assessments. To that end, the focus of this study is to summarize and cast relevant information into a logical framework that will provide scientific and technical guidance for developing these improved and more detailed NRC review procedures. As such, the actual development

**Table 1-2:** Approximate range of tsunami parameters in the deep ocean and shallow coastal waters.

| | | | |
|---|---|---|---|
| ***Deep Ocean*** | | | |
| Depth | $1000 \leq$ | $h$ | $\leq 5000$ m |
| Period | $5 \leq$ | $\tau$ | $\leq 60$ min |
| Amplitude | $0.01 \leq$ | $\eta$ | $\leq 1$ m |
| Wavelength | $30 \leq$ | $\lambda$ | $\leq 800$ km |
| Speed | $0.10 \leq$ | $c$ | $\leq 0.22$ km/sec |
| Max current | $0.05 \leq$ | $u$ | $\leq 9.9$ cm/sec |
| ***Shallow Water*** | | | |
| Depth | $10 \leq$ | $h$ | $\leq 1000$ m |
| Period | $5 \leq$ | $\tau$ | $\leq 60$ min |
| Amplitude | $1 \leq$ | $\eta$ | $\leq 10$ m |
| Wavelength | $3 \leq$ | $\lambda$ | $\leq 356$ km |
| Speed | $0.01 \leq$ | $c$ | $\leq 0.10$ km/sec |
| Max current | $9.9 \leq$ | $u$ | $\leq 990$ cm/sec |

of comprehensive, step-by-step guidance for NRC review of tsunami hazard assessments is beyond the scope of this study.

The content of this report is drawn from existing studies, previously published reports, and expert opinions, including those of the authors and colleagues expert in the disciplines that must be brought to bear on THA. Section 2 summarizes U.S. tsunami occurrences, including several measures of their severity, and Appendix A describes national and international sources of tsunami data; for a more detailed and comprehensive assessment of the U.S. Tsunami Hazard, see Dunbar *et al.* (2006). Section 3 discusses the acquisition of paleotsunami field data and the interpretation of such prehistoric evidence. Sections 4–7 and Appendices B and D provide detailed discussions of tsunami sources and the theory and numerical modeling of tsunami dynamics; Appendix C presents standards and procedures for tsunami modeling that are in the process of being adopted by NOAA and the international community. Section 8 draws on all of the preceding sections to develop a Template THA that provides a framework for NPP tsunami hazard assessment and subsequent NRC reviews; the Template THA methodology includes an initial screening study, application of the concept of "Probable Maximum Tsunami" adopted by the NRC, and an evaluation of real-time THA (RTHA) feasibility and effectiveness as an integral part of the assessment; an example of a site-specific tsunami hazard assessment study is also provided in Appendix D. Sections 2–8 also provide specific scientific/technical recommendations related to THA, while Section 9 provides more general recommendations to improve both tsunami hazard assessments and the procedures that guide the subsequent NRC review.

# 2. U.S. Tsunami Occurrences

*by Paula Dunbar*

## 2.1 NOAA/NGDC Data Overview

The NOAA/National Geophysical Data Center (NGDC) is one of three environmental data centers within the National Environmental Satellite, Data and Information Service (NESDIS). Appendix A of this report provides an overview of the NGDC tsunami data acquisition, processing, distribution, and archival effort. This section utilizes the NGDC tsunami databases to create Table 2-1 and provide a brief history and summary of tsunamis that have impacted the U.S. coast. Tsunami events with validities $\geq$3, i.e., definite or confirmed (see Appendix A), were used to calculate the statistics described in this section.

The earliest description of a tsunami in the U.S. states or territories was a Hawaiian chant composed in the 16th century that described a huge wave that came on the west coast of Molokai and killed the inhabitants. The next listing of a U.S. tsunami occurs after the migration of the Puritans to New England. Since that time, there have been over 200 tsunami events that have caused more than 2700 recordings or descriptions (runup observations) of tsunami effects in the coastal states and territories of the U.S. The majority of these runup observations were in Hawaii (58%), California (15%), and Alaska (13%).

## 2.2 Source Mechanism Statistics

Most of the tsunamis affecting the U.S. were generated by earthquakes (84%) or earthquakes that caused landslides (14%). The remaining events were caused by landslides (1%), volcanic eruptions (<1%), and unknown sources (<1%). The distribution of sources affecting the U.S. is 61% distant (>1000 km), 21% regional (200–1000 km), and 18% local (<200 km). Most of the distant sources were from large earthquakes in the Pacific Basin including Kamchatka and Kuril Island (17%), South Pacific (17%), west coast of South America (16%), west coast of North and Central America (13%), Alaska (11%), and Japan (12%). These distant tsunami sources caused the majority (80%) of the tsunami effects in the U.S. states. This percentage is dominated by the large number of recordings in Hawaii (>1500) due to its location in the middle of the Pacific Basin and extensive fieldwork that was done in Hawaii after several major tsunamis.

## 2.3 Damage and Deaths

Since 1837, tsunamis have caused over 700 deaths and over $200 million damage in the U.S. states and territories. Of these 700 deaths, 328 occurred in Hawaii from eight events (1837–1975). In Puerto Rico, a magnitude 7.3 earthquake in 1918 generated a tsunami that killed more than 142 people and caused $4 million in damage. The most significant economic loss due to a tsunami in the U.S. resulted from the 28 March 1964 magnitude $M_w = 9.2$

**Table 2-1:** U.S. tsunami events and runup measurements by State, territory and region, deaths, and dollar damage from the NOAA/NGDC tsunami database from 1690 to the present.

| State/Territory | No. events with any observed runup | No. events with measured max runup 0.01 − 0.5 m | No. events with measured max runup 0.5 − 1.0 m | No. events with measured max runup 1.0 − 3.0 m | No. events with measured max runup 3.0 − 5.0 m | No. events with measured max runup >5.0 m | Total no. observations | No. deaths | Millions dollars damage |
|---|---|---|---|---|---|---|---|---|---|
| **U.S. Atlantic East Coast** | | | | | | | | | |
| Maine | 1 | | | | | | 3 | | |
| New Hampshire | 1 | | | | | | 1 | | |
| Massachusetts | 1 | | | | | | 2 | | |
| Rhode Island | 2 | 1 | | | | | 3 | | |
| Connecticut | 1 | | | | | | 1 | | |
| New York | 2 | 1 | | | | | 7 | | |
| New Jersey | 6 | 2 | 1 | | | | 8 | | |
| Pennsylvania | | | | | | | | | |
| Delaware | | | | | | | | | |
| Maryland | 1 | 1 | | | | | 1 | | |
| Virginia | | | | | | | | | |
| North Carolina | | | | | | | | | |
| South Carolina | 2 | 1 | | | | | 2 | | |
| Georgia | | | | | | | | | |
| Florida | 4 | 1 | | | | | 5 | | |
| **Totals** | 21 | 7 | 1 | 0 | 0 | 0 | 33 | 0 | 0 |
| **U.S. Gulf Coast** | | | | | | | | | |
| Florida | | | | | | | | | |
| Alabama | | | | | | | | | |
| Mississippi | | | | | | | | | |
| Louisiana | | | | | | | | | |
| Texas | 1 | | | | | | 1 | | |
| **Totals** | 1 | 0 | 0 | 0 | 0 | 0 | 1 | 0 | 0 |
| **Puerto Rico and Virgin Islands** | | | | | | | | | |
| Puerto Rico | 9 | 3 | 2 | 2 | | 1 | 33 | 142 | 4 |
| Virgin Islands | 7 | 1 | 1 | 1 | 1 | 1 | 15 | 30 | |
| **Totals** | 16 | 4 | 3 | 3 | 1 | 2 | 48 | 172 | 4 |

**Table 2-1:** (continued).

| State/Territory | No. events with any observed runup | No. events with measured max runup 0.01 – 0.5 m | No. events with measured max runup 0.5 – 1.0 m | No. events with measured max runup 1.0 – 3.0 m | No. events with measured max runup 3.0 – 5.0 m | No. events with measured max runup >5.0 m | Total no. observations | No. deaths | Millions dollars damage |
|---|---|---|---|---|---|---|---|---|---|
| Alaska | 79 | 46 | 3 | 6 | 1 | 15 | 357 | 222 | 122 |
| **U.S. West Coast** | | | | | | | | | |
| Washington* | 18 | 12 | 1 | 2 | 1 | | 68 | | 2 |
| Oregon* | 21 | 15 | 1 | 2 | 2 | | 76 | 5 | 1 |
| California* | 74 | 46 | 8 | 9 | 3 | 2 | 423 | 19 | 19 |
| **W Coast Totals** | 113 | 73 | 10 | 13 | 6 | 2 | 567 | 24 | 22 |
| Hawaii | 112 | 74 | 7 | 11 | 9 | 10 | 1580 | 328 | 59 |
| **U.S. Western Pacific island territories** | | | | | | | | | |
| Guam | 16 | 10 | 1 | 1 | | 1 | 24 | 1 | |
| Northern Marianas | 1 | | | | | | 1 | | |
| American Samoa | 53 | 37 | 4 | 3 | | | 58 | | |
| **W Pacific Totals** | 70 | 47 | 5 | 4 | 0 | 1 | 83 | 1 | 0 |
| **American Totals** | 412 | 251 | 29 | 37 | 17 | 30 | 2669 | 747 | 207 |

*Include Cascadia tsunami deposit sites

Alaskan earthquake and ensuing tsunami, which caused a total of 124 deaths and $119 million in property loss in the U.S. ($97 million and 106 deaths in Alaska). The 1964 tsunami caused damage and fatalities on the west coast of the U.S., including 10 fatalities in Crescent City, California.

Local tsunami events are usually the most devastating: it is interesting to note that local tsunamis in the U.S. resulted in 455 deaths, regional tsunamis caused 28 deaths, and distant tsunamis caused 264 deaths. A comparison of damage produces similar results; local tsunamis caused $73M damage, regional tsunamis $54M damage, and distant tsunamis $80M damage.

## 2.4 Regional and State Analysis

The NGDC tsunami database was queried to determine the earliest historical accounts of tsunamis impacting the U.S. states and territories. The first report was the 16th Century Hawaiian chant described previously. In 1811, an earthquake in Chile generated a tsunami that was observed on the Island of Hawaii. A Kamchatka earthquake in 1737 generated the first tsunami observed in Alaska. There was a confirmed report of a tsunami in 1732 in Acapulco, Mexico; the first tsunami reported on the west coast of the U.S. was in 1806 in Santa Barbara, California. There were a few unconfirmed accounts of tsunamis as early as 1767 in the Pacific islands of Guam, American Samoa, and the Northern Marianas Islands; the first confirmed account was in 1837 in American Samoa. Caribbean tsunamis were reported as early as 1498 in Venezuela; the first observation in the U.S. territories was in 1690 in the Virgin Islands. On the east coast of North America there were unconfirmed reports of tsunamis as early as 1688; the first confirmed report was from the 1755 Lisbon event that was observed on the east coast of Canada. The first confirmed tsunami reports on the U.S. east coast were from the 1886 Charleston, South Carolina, tsunami that was observed in South Carolina and Florida. An earthquake in Puerto Rico in 1918 generated a small tsunami that was recorded on a tide gauge in Galveston, Texas, in 1918.

Table 2-1 provides a count of tsunami events and runup heights recorded in the U.S. states and territories. The second column was a result of searching the tsunami runup database by state with no other conditions and dividing the runup measurements into individual events using the date and time. Multiple tsunami runup measurements over several hours from great subduction zone earthquakes, such as 1960 Chile or 1964 Alaska, were considered as one event. This table does not include tsunamis reported on inland waters, such as Lake Erie or Roosevelt Lake in Washington, but it does include tsunamis in Puget Sound and all reported tsunamis in the bays of southeastern Alaska, including those with local landslide sources. Although observed seiches are not included in Table 2-1, they are discussed in Section 2.5.

The above procedure generated a count of tsunami events recorded in each state. Reported runup heights were then used to develop additional details of the tsunami runup distribution. For each individual tsunami event, the events were binned based on the maximum recorded runup height in each state. Tsunami runup heights were subdivided into five groups:

- 0.01 m $\leq$ runup $\leq$ 0.5 m

- 0.5 m $<$ runup $\leq$ 1.0 m
- 1.0 m $<$ runup $\leq$ 3.0 m
- 3.0 m $<$ runup $\leq$ 5.0 m
- 5.0 m $<$ runup

For example, if a tsunami was recorded in Oregon with two measured runup values of 0.5 m and 1.4 m, the tsunami was binned into the 1.0 m $<$ runup $\leq$ 3.0 m group. The same tsunami, if recorded in Washington with runup values of 0.05 m, 0.15 m, and 0.6 m would be binned into the second group, 0.5 m $<$ runup $\leq$ 1.0 m.

Table 2-1 shows the results of these database selections. Finally, deaths, millions of dollars in damage reported as due to tsunamis, and the total number of tsunami events were summed for each state.

The results in Table 2-1 are organized into seven broad regions: Atlantic Coast, Gulf Coast, Puerto Rico and Virgin Islands, West Coast, Alaska, Hawaii, and Western Pacific. Florida's coast is divided between the Atlantic and Gulf coast regions because of the differences in tsunami source zones affecting the state. The Western Pacific includes Guam, Northern Mariana, and American Samoa. It should be noted that the numbers in Table 2-1 do not represent the number of total individual tsunamis, but the number of tsunamis per state with reported runup events. For instance, the 1964 Alaska earthquake counts as a recorded tsunami runup in many states, e.g., Washington, Oregon, Alaska, California, Hawaii, Texas, and so on. Thus, the runup numbers in Table 2-1 are essentially state runup events.

The number of state runup events range from none in Pennsylvania, Delaware, Virginia, North Carolina, Georgia, Alabama, Mississippi, and Louisiana to 112 events in Hawaii, 74 in California, and 79 in Alaska. The state runup events include both local sources of all types as well as distant events resulting in runup. In terms of the state runup events, about 10% of the events are in the Atlantic basin (Atlantic, Gulf, Puerto Rico, and Virgin Islands) and 90% in the Pacific (West Coast, Alaska, Hawaii, and Western Pacific). Again, one tsunami is often counted in several states.

Of the total 412 state runup events, there are 364 state runup events with measured runup values. The remaining state runup events were observed, but there were no measurements reported. The results of binning are in columns 3 through 7 in Table 2-1. The totals for each maximum runup category show the particular issue with tsunamis. The large total number of runup observations (251) between 0.01 m and 0.5 m is driven primarily by distant tsunamis. For example, American Samoa has 53 recorded tsunami runup events and 44 have measured runup amplitudes (37+4+3+0+0 in columns 3–7). Of the 44 measured runup events in American Samoa, 37 are less than 0.5 m. As the measured runup height increases, the total number of tsunami runup events decreases quickly from 251 for $<$0.5 m, to 29 for 0.5 m to 1.0 m heights, but increases to 37 between 1.0 m and 3.0 m, and increases again to 47 events over 3.0 m. These numbers reflect the fact that in the subduction zones, local earthquakes generate severe tsunamis with amplitudes in excess of 10 m.

The Pacific basin has 44 of the 47 state runup events with wave heights

greater than 3.0 m. There are no measured runup values along the Atlantic Coast greater than 3.0 m. The number of runup events greater than 3.0 m for Alaska (16 events) and Hawaii (19 events) points out the very severe nature of the tsunami threat in those states. The large number of local sources in Alaska along both the mainland and Aleutian arc contributes to the tsunami hazard facing Alaska. Both significant local tsunami sources and frequent devastating distant tsunamis strike Hawaii.

For the Atlantic coastline, there is only one event with a measured tsunami runup exceeding 0.5 m. The 0.68-m runup is from the 1929 Grand Banks earthquake and was observed in New Jersey. This magnitude 7.3 earthquake caused an underwater landslide that generated the tsunami.

## 2.5 Seiches

The NGDC tsunami database was also queried to determine where seiches have been observed in the U.S. There are four main areas that have experienced seiches:

- Arkansas-Missouri area from more than 200 earthquakes that occurred on the New Madrid fault between 16 December 1811 and 15 March 1812. The New Madrid earthquakes generated several waves in the rivers, raised water levels, agitated waters, and affected navigation.
- From 1944 to 1953, eight seiches were generated in R.D. Roosevelt Lake, Washington, from landsliding. The runup heights ranged from 3 to 19 m and one caused $3,000 damage to a lumber company. An earthquake in 1891 generated a landslide that caused a 2 m seiche in Lake Washington.
- A magnitude $M_s = 7.5$ earthquake in 1959 generated a landslide that caused a 30 m wave in Hebgen Lake, Montana.

Seiches were set up in the Gulf of Mexico (Freeport, Texas) and in many lakes in the United States by the magnitude 9.2 Prince William Sound, Alaska, earthquake in 1964.

## 2.6 Recommendation

Conduct a region-wide search of the NOAA/NGDC database and all other sources of tsunami data for potential sources and tsunami occurrences. This conservative, regional approach is recommended because of the sparse nature of historic and pre-historic tsunami data.

# 3. Geologic Evidence of Tsunamis

*by Andrew Moore and Bruce Jaffe*

## 3.1 Purpose and Scope

The 26 December 2004 tsunami dramatically illustrated the vulnerability of the world's coastlines to the threat of tsunamis. Although the Sunda Subduction Zone had experienced M < 9 earthquakes historically, some of which produced small tsunamis, there was no historical precedent for the December 26th tsunami. Even in India and Sri Lanka, with a 500-yr written history, no clear mention is made of similarly destructive tsunamis.

This lack of historical data points out a problem—large tsunamis are infrequent, high-hazard events. It is unlikely that most areas in the U.S. that have been struck by such tsunamis have experienced them during the short period of written history. As a result, in order to adequately assess the risk of tsunami in a given area, planners must turn to the geologic record of tsunamis.

This document describes the type of evidence left by ancient tsunamis in the geologic record, methods for detecting these traces, and recommendations for what actions should be taken to look for these traces before siting a NPP. It is of limited scope, and should not be considered exhaustive—individuals seeking further information are encouraged to contact the authors.

## 3.2 Definitions

Subaerial tsunami deposits are sediments (including grain sizes from boulders to mud) deposited on land above mean sea level during the passage of a tsunami. The material may come from offshore, or may be reworked material from the beach and onshore. Modern tsunami deposits have been used to help establish the landward limit of inundation (Fig. 3-1) and the direction water flowed over an area, but tsunami deposits are most often used to infer the passage of prehistoric tsunamis.

Lacustrine tsunami deposits are sediment deposited in a lake above mean sea level during the passage of a tsunami. As is the case with subaerial tsunami deposits, sediments may come from offshore, or may be reworked material from the beach and onshore. Lacustrine tsunami deposits have been used to help establish the magnitude and recurrence interval for ancient tsunamis in the Pacific Northwest (Kelsey *et al.*, 2005).

## 3.3 Deposits as Indicators of Past Tsunamis

Prehistoric tsunamis have been identified solely on the basis of their deposits in the Pacific Northwest (Atwater and Moore, 1992; Benson *et al.*, 1997; Peters *et al.*, 2003; Peters *et al.*, in press), Kamchatka (Pinegina and Bourgeois, 2001; Pinegina *et al.*, 2003), Japan (Nanayama *et al.*, 2003), the North Sea (Dawson *et al.*, 1988), and Hawaii (Moore, 2000; Moore *et al.*, 1994), among others. These studies have helped scientists and disaster

**Figure 3-1:** Satellite photos taken of northern Sumatra before (left) and after (right) the 2004 South Asia tsunami. Sand and mud (tan and brown colors) have eroded and transported elsewhere in most areas inundated by the tsunami, forming a marker horizon of this event. However, modification of this layer has already begun, as shown by sediment plumes washing into the ocean.

managers understand the tsunami risk associated with not only these areas (Walsh *et al.*, 2000), but also other areas in the same ocean basin. Tsunami deposits have also been used in a probabilistic tsunami hazard assessment to validate model results (Tsunami Pilot Study Working Group, 2006). In regions where tsunamis are infrequent, paleotsunami deposits may represent the only available means of determining the magnitude and frequency of tsunamis.

The recurrence interval for tsunamis may be developed through dating a series of paleotsunami deposits (Jaffe and Gelfenbuam, 2002). This has been done in several places around the world. For example, in the Pacific Northwest of the U.S. Darienzo and Peterson (1995) dated a series of tsunami deposits and determined that the recurrence interval for subduction zone earthquakes and associated tsunamis is from 200 to 600 yr. For this technique to give accurate recurrence intervals, the dating methods must be robust, there must be positive identification of the deposit as a tsunami deposit, and the record must be long enough to encompass many tsunamis.

The ability to recognize and interpret paleotsunami deposits has improved greatly in the past decade with the rise in the number of studies of modern tsunami deposits, including many studies of the 26 December 2004 tsunami (e.g., Moore *et al.*, 2006; Goff *et al.*, 2006; Jaffe *et al.*, 2006; Kench *et al.*, 2006). Although attempts to "codify" the criteria for paleotsunami deposit recognition have been made (e.g., Chagué-Goff and Goff, 1999; Nanayama *et al.*, 2000; Tuttle *et al.*, 2004; Peters *et al.*, in press), there remains no single criteria for distinguishing tsunami deposits from the deposits of other coastal phenomena such as storms (Morton *et al.*, 2007). This

difficulty has led to vigorous debate on the origin of several paleotsunami deposits described in the scientific literature (e.g., Bryant *et al.*, 1992; Hearty, 1997; Moore and Moore, 1984).

It is of paramount importance to search for tsunami deposits in environments conducive to their formation and preservation. These environments include marshes and low elevation coastal lakes. Any environment near the coast where tsunami deposits are formed and either covered by sediment or isolated from erosion is a potential site of tsunami deposit preservation. When assessing tsunami hazard at a site, the coastline should be searched for many kilometers (order of 100 km) in either direction to identify good environments for recording past tsunamis. The need to search large stretches of coastline adjacent to a site is underscored by lack of tsunami deposits along >150-km-long stretches of coastline with unfavorable environments for recording tsunamis from deposits in the Pacific Northwest (Peters *et al.*, 2003; Peters *et al.*, in press), a region where more than 15 great tsunamis have been recorded in tsunami deposits formed during the past 7000 yr (Kelsey *et al.*, 2005).

Tsunami deposits also have the potential to record the flow parameters of the waves that created them—although several attempts to estimate wave parameters from tsunami deposits have been made (e.g., Jaffe and Gelfenbaum, 2007; Moore *et al.*, in press; Moore and Mohrig, 1994; Nott, 1997; Reinhart, 1991), this subject is still in its infancy. This emerging field has, however, the potential to help assess the risk posed not only by tsunamis, but also by the earthquakes that generate them. In many cases, tsunami deposits are the only record not only of ancient tsunamis, but also of prehistoric earthquakes. In these cases, information on tsunami size over a section of coast can be used to place constraints on the location and nature of earthquake rupture (e.g., Tanioka and Satake, 2001), although such constraints may be more difficult for landslide generated tsunamis.

### 3.4 Identification of Tsunami Deposits

The ability to distinguish the deposits of ancient tsunamis from other coastal deposits remains of vital concern to the tsunami community. Historical records of tsunami do not, typically, extend farther back than 500 yr (with the exception of Japan), and often do not exceed 150 yr in the U.S. Because these records are short relative to recurrence intervals, it is quite difficult to assess tsunami frequency and intensity without some means of extending the historical record. Typically, this has meant extending the record using paleotsunami deposits; this has necessarily meant understanding tsunami deposit characteristics.

Because tsunami sedimentology stems, historically, from an analysis of potential paleotsunami deposits, much research has gone into attempting to distinguish tsunami deposits from the deposits of other coastal phenomena, most notably large storms. Early studies (e.g., Reinhart and Bourgeois, 1989; Hearty, 1997) focused on understanding the hydraulic differences between tsunamis and storms, but most later studies (e.g., Chagué-Goff and Goff, 1999; Nanayama *et al.*, 2000; Tuttle *et al.*, 2004) have adopted a fa-

cies approach—modern storm and tsunami deposits are compared, and their differences tabulated. There is also a growing body of information on the sedimentology of modern tsunami deposits (e.g., Bourgeois and Reinhart, 1993; Dawson *et al.*, 1996; Gelfenbaum and Jaffe, 2003; Moore *et al.*, 2006).

The combination of both the facies and sedimentology approach has resulted in an often-used, if not universally approved, set of criteria for understanding how *sandy* tsunami deposits might be distinguished in the stratigraphic record. These include:

- Sand layers in continuous sheets usually <25 cm thick and laterally continuous over 100s of meters (Gelfenbaum and Jaffe, 2003; Jaffe *et al.*, 2003; Morton *et al.*, 2007; Fig. 3-2)
- The sand sheet generally thins landward (Gelfenbaum and Jaffe, 2003; Jaffe *et al.*, 2003)
- The sand layer typically cuts across stratigraphy and represents an isochronous surface (Moore, 1994)
- These sands contain marine microfossils, often from a range of depths and environments (Nanayama and Shigeno, 2005)
- Sands are often massive or plane laminated, and may have flame structures at the base. Ripples and other bedload structures are rare, although they have been reported in modern deposits (Nanayama *et al.*, 2000)
- The underlying sediments may show evidence of erosion, including rip-up clasts of the underlying sediment incorporated into the tsunami deposit. This does not happen in every case, however, and many tsunami deposits show no evidence for strong erosion. Rather, plants rooted in the pre-tsunami surface can be well preserved in the deposit, often appearing to have grown through it (Fig. 3-3)
- Grain size of the deposit tends to decrease landward and upward, although recent research suggests that inverse grading (that is, layers that increase in size upward) is more prominent in the deposits of large tsunamis (Higman and Jaffe, 2005)
- Relative abundance of marine geochemical tracers such as bromine (Goff and Chagué-Goff, 1999)

In some cases, the presence of marine microfossils and geochemical tracers alone has been used to infer the passage of tsunami—sand need not necessarily be present (Hemphill-Haley, 1995; Kelsey *et al.*, 2005).

Although relatively less studied, muddy tsunami deposits should have similar criteria as sandy deposits. However, because few boulders are moved during a tsunami (compared with the amount of sand or mud) the criteria used to evaluate whether a boulder or boulder field represents the deposit of a tsunami are somewhat different.

**Figure 3-2:** Laterally continuous 1000-yr-old tsunami deposit exposed in a trench, Puget Sound, Washington.

**Figure 3-3:** Marsh grasses (dark mounds) growing through a tsunami sand sheet in a coastal marsh in Puget Sound, Washington.

**Figure 3-4:** Boulder moved by the 1771 Meiwa tsunami in Okinawa, Japan, surrounded by coral rubble also moved by the tsunami.

It is important to note that few modern tsunamis have created extensive boulder fields, so that it is far more common to find individual boulders surrounded by sheets of sand. Only one modern tsunami (the 1771 Meiwa tsunami in southern Okinawa, Japan) is known to have moved an extensive field of boulders from the sea to the land. This boulder field covers most of the inundated area of one island (up to about 30 m above sea level), and consists of large coral blocks from 1 to 3 m in diameter, commonly surrounded by coral rubble (Nakata and Kawana, 1993; Fig. 3-4). Although sandy deposits have been reported from this area (Moore *et al.*, 2001), the boulders now appear as isolated blocks.

Although many paleotsunamis have been inferred from boulder evidence (Bryant *et al.*, 1992; Moore and Moore, 1984; Nott, 1997; Scheffers, 2002), the use of boulders for determining the passage of ancient tsunamis remains controversial, and should be bolstered with sandy deposit evidence whenever possible (Morton *et al.*, 2006).

Last, although evidence for bedrock scouring has been used to identify paleotsunamis (Bryant and Young, 1996), it has been tentatively reported from only one modern event (Aalto *et al.*, 1999). Indeed, even in the areas hit hardest by the 2004 Indian Ocean tsunami, exposed bedrock was not scoured. Use of this feature to identify ancient tsunamis should be made with the greatest caution.

## 3.5 Search Methods

Sandy paleotsunami deposits are most commonly identified in outcroppings of coastal sediment, or in core holes augered into coastal lowlands. Outcrops are commonly cleaned with a flat blade, such as a shovel or machete, and measurements of the thickness, grain size, and sedimentary structures made from the cleared surface (Fig. 3-2). Although possible to clean tens of meters of outcrop, it is usually prohibitive to clean more than a 2-m swath at any one time. Stratigraphy between outcrops is usually inferred. Core holes are most often collected using push corers such as a gouge auger. These augers produce a core 1 m long and about 2 cm wide, and can be extended for deeper recovery. Networks of holes, often in a grid, have often been used to map out the extent and thickness of paleotsunami deposits (e.g., Moore, 1994). A common approach is to use an adaptive grid, starting with a relatively wide spacing such as 40 m, and decreasing the grid spacing in areas of interest. In general, any search for sandy paleotsunami deposits should focus on:

- Finding a layer of sand in an environment (e.g., a coastal marsh) where sand deposition is unusual.
- Establishing that the layer is continuous (i.e., can it be found in only one location, or is it found consistently throughout an area?)

Collecting data on grain size (vertical and lateral), thickness, and stratigraphic position, along with microfossil and geochemical samples.

## 3.6 Recommendation

For the specific task of seeking geologic tsunami evidence, we make the following recommendations:

A. Conduct a search for geologic evidence of tsunami occurrence and potential tsunami sources in all cases for which an initial screening study (Section 8.2) fails to eliminate the possibility of a tsunami hazard.

B. Search coastal sites within 100 km of the proposed NPP location for tsunami sand and boulder deposits, especially in locations likely to preserve tsunami deposits, such as shallow lakes and coastal marshes.

C. Include analyses and documentation of those sites with evidence of events with tsunami generation potential for which no tsunami evidence, per se, is found.

# 4. Tsunami Sources

*By Eric Geist and Jacques Locat*

There are three general types of geologic source that can initiate tsunamis: (1) earthquakes, (2) submarine and subaerial landslides, and (3) a variety of mechanisms associated with volcanism. For each of these tsunami sources, we first describe different sub-types that have been known to cause tsunamis and their geologic/tectonic environment of occurrence. In each case, we provide historic examples of cases that have produced significant or destructive tsunamis and cite information regarding the global distribution of sources. We then describe the methodology with which to compute the generation of tsunamis as input to tsunami propagation computations (see Section 5.1 for standard methodology). Finally, we describe how different source parameters for each source type are measured or estimated from various geological, geotechnical, and geophysical datasets. Other less common tsunami sources, such as asteroids and atmospheric disturbances, are not described in this report.

## 4.1 Earthquakes

### *4.1.1 Source types and environment of occurrence*

Earthquakes are the most common source of tsunamis. The types of earthquakes that generate tsunamis are typically dip-slip events of magnitude (M) 6.5 or greater. Because earthquakes generate tsunamis primarily through vertical coseismic displacement of the seafloor and overlying water column, dip-slip earthquakes are more efficient at generating tsunamis than strike-slip earthquakes (e.g., Ward, 1980; Okal, 1988). In addition, because a substantial amount of slip and large rupture area are needed for earthquakes to generate tsunamis, only large magnitude earthquakes ($M > 6.5$) will typically generate observable tsunamis. In terms of considering tsunamis as an extension of earthquake normal modes, because earthquake excitation occurs near a node, the seismic moment has to be quite large to induce destructive tsunamis (Ward, 1980). The tectonic environment where the conditions for tsunamigenesis apply are primarily subduction zones and, less commonly, oceanic convergence boundaries.

The recent plate tectonic compilation by Bird (2003) includes seven different types of tectonic boundaries. Of these, the commonly known subduction zones (SUB) are convergent boundaries with a well established Benioff zone (i.e., systematic distribution of hypocenters of deep earthquakes) and a parallel volcanic arc of Quaternary age. The majority of all destructive tsunamis originate from the inter-plate thrust or "megathrust" of subduction zones. Examples of these tsunamigenic earthquakes include the $M = 9.5$ (Engdahl and Villaseñor, 2002)[1] 1960 Chile, $M = 9.2$ 1964 Alaska, and $M = 9.2$ (Chlieh *et al.*, 2007) 2004 Sumatra-Andaman earthquakes. Because this is

[1]Unless otherwise indicated, all magnitudes of historic earthquakes are from the catalog of Engdahl and Villaseñor (2002).

the most common mechanism of seismogenic tsunamis, the discussion of how earthquake source parameters affect tsunami generation (Section 3.1.3) is keyed to this type of earthquake. A special class of earthquakes termed "tsunami earthquakes" occurs on the shallow inter-plate thrust or décollement near the trench, seaward of apparent seismic fronts defined by background seismicity (Yoshii, 1979; Byrne *et al.*, 1988). These earthquakes are much more efficient at generating tsunamis than typical inter-plate thrust earthquakes that occur down-dip along the plate interface (Satake and Tanioka, 1999).

In addition to the inter-plate thrust, destructive tsunamis have originated from other dip-slip faults associated with subduction zones (Geist, 1999; Satake and Tanioka, 1999). These include outer-rise normal faults, back-arc thrust faults and, less commonly, deep intra-slab events. Outer-rise earthquakes of sufficient magnitude can potentially yield very destructive tsunamis, because of the deep water overlying the source region and amplification during tsunami shoaling according to Green's Law. Notable examples of outer-rise tsunamigenic earthquakes include the M = 8.4 1933 Sanriku, M = 7.7 1965 Rat Island (Aleutians), M = 8.3 1977 Sumba, and M = 7.4 1990 Mariana earthquakes. The occurrence of outer-rise earthquakes may be related to seismic coupling along the inter-plate thrust (Christensen and Ruff, 1988) and/or stress transfer from inter-plate thrust earthquakes (Dmowska *et al.*, 1988). The global distribution of normal-faulting events associated with subduction zones is given in Choy and Kirby (2004). Back-arc thrust earthquakes beneath marginal seas have also been known to generate destructive tsunamis, as exemplified by the M = 7.7 1983 Japan Sea (Akita-Oki) and M = 7.8 1992 Flores Island earthquakes. Finally, although deep, intra-slab earthquakes can be large, the great focal depth usually limits the amount of coseismic displacement at the seafloor. Seafloor deformation, however, can extend over a large area and in some cases can generate a significant tsunami, as for the M = 8.1 1977 Tonga earthquake (Okal, 1988) (focal depth = 50 km).

Oceanic convergent boundaries (OCB) encompass the other submarine tectonic convergent boundaries that are not classified as subduction zones (Bird, 2003). There is a high degree of diversity in faulting mechanisms for this type of tectonic boundary, including a wide range of obliquity of the relative plate convergence vector and regions of broadly distributed deformation. Examples include the Indo-Australian plate boundary (Abercrombie *et al.*, 2003) and the Macquarie Ridge south of New Zealand (Frohlich *et al.*, 1997; Meckel *et al.*, 2005). Examples of tsunamigenic earthquakes on oceanic convergent boundaries include the highly destructive M = 8.5 (Utsu, 2002) 1755 Lisbon earthquake, as well as the more recent M = 8.0 1945 Makran, and M = 7.6 1991 Costa Rica-Panamá events.

### *4.1.2 Generation mechanism and methodology*

The controlling source parameter that determines tsunami severity is earthquake magnitude, or more specifically, seismic moment defined as $M_0 = \mu \overline{D} A$ where $\mu$ is the shear modulus or rigidity and $\overline{D}$ is the average slip over a

rupture area A. Moment magnitude ($M_w$) is derived from seismic moment according to $M_w = \frac{2}{3}[\log(M_0) - 9.05]$ (Hanks and Kanamori, 1979). Tsunami generation is typically computed through three steps: (1) representation of fault rupture process, ranging from idealized dislocation or crack descriptions to fully dynamic rupture models; (2) computation of vertical and horizontal components of coseismic displacement at the sea floor; and (3) application of tsunami Green's functions to compute initial (or quasi-initial in the case of kinematic or dynamic rupture) wave height conditions from coseismic seafloor displacement. Each of these three steps is described below.

***4.1.2.1 Fault rupture representation.*** Idealized representations of fault rupture used for tsunami generation modeling include, most commonly, elastic dislocations and, less commonly, crack theory. Elastic dislocations involving uniform slip (Rybicki, 1986), termed a Volterra dislocation, are often used in conjunction with the definition of seismic moment ($M_0$) above. For a given magnitude, rupture area, and shear modulus, one can compute an equivalent uniform slip—but it should be clear that the definition of seismic moment is based on average slip (i.e., the mean of a slip distribution that may be non-uniform), rather than uniform slip. For uniform slip dislocations, it should also be noted that there exists a short wavelength artifact in the coseismic vertical displacement field above the updip edge of shallow thrusts (Geist and Dmowska, 1999). The other idealized representation used by Geist and Dmowska (1999) is crack theory, in which a uniform static stress-drop ($\Delta\sigma$) is specified. The expression for seismic moment for a Poisson elastic solid and dip-slip fault in this case is $M_0 = \frac{3}{8}\pi\Delta\sigma W^2 L$, where $W$ and $L$ are the rupture width and length, respectively (Lay and Wallace, 1995). Other ad hoc slip functions have been used in the past for tsunami generation that do not conform to any particular theory of earthquake rupture. In certain respects, these ad hoc slip functions are constrained by interseismic geodetic observations, but it is generally regarded that coseismic slip is much more heterogeneous than interseismic strain accumulation (Mazzotti *et al.*, 2000).

Examination of actual fault ruptures either from seismic waveform inversions or theoretical/numerical studies of rupture dynamics indicates that static slip distribution is strongly heterogeneous, such that slip could rarely, if ever, be considered uniform and only in certain cases conform to crack theory (e.g., Yomogida, 1988). In the far-field, fortunately, the effects of slip heterogeneity on the tsunami wavefield are attenuated, such that tsunami amplitudes are essentially controlled by the scalar seismic moment ($M_0$) (Pelayo and Wiens, 1992; Abe, 1995), regardless of the slip distribution. A sensitivity analysis of different earthquake source parameters on tsunamis in the far-field is given by Titov *et al.* (1999; 2001). In the near-field and at regional distance (depending on the earthquake size), slip heterogeneity does have a significant effect on estimating tsunami amplitudes.

***4.1.2.2 Calculation of coseismic seafloor displacements.*** For those cases in which fault rupture is represented by a Volterra elastic dislocation, coseismic displacement at the sea floor can be computed using analytic expressions for a homogeneous earth structure and a planar, rectangular fault (e.g., Okada, 1985). Similarly for crack models, analytic expressions for

coseismic displacement have been developed using Chebyshev polynomials (Dmowska and Kostrov, 1973; Rudnicki and Wu, 1995). The slip function derived from crack theory or any heterogeneous slip field in general can also be discretized into cells of uniform slip, and the point-source expressions of Okada (1985) can be utilized to compute coseismic displacement. Again, these expressions are developed for planar faults in a homogeneous elastic medium. For non-planar faults, analytic expressions involving triangular dislocations and curved slip zones can be used (Jeyakumaran *et al.*, 1992; Jeyakumaran and Keer, 1994). For both non-planar faults and heterogeneity in elastic media, numerical techniques involving finite-elements and boundary elements are available (e.g., Yoshioka *et al.*, 1989; Zhao *et al.*, 2004).

***4.1.2.3 Computation of initial wave elevation field.*** The vertical component of seafloor displacement dominates tsunami generation. The horizontal component provides a small effect on tsunami generation in regions of steep bathymetry according to the following expression (Tanioka and Satake, 1996): $u_h = u_x(\partial H/\partial x) + u_y(\partial H/\partial y)$, where $H$ is water depth. To account for the attenuation of short wavelengths of coseismic displacement at the sea floor through the water column, the tsunami Green's function of Kajiura (1963) effectively results in a $1/\cosh(kh)$ low-pass filter of the coseismic displacement field (where $k$ is the wavenumber of the coseismic displacement field and $h$ is water depth). If a kinematic or dynamic rupture description is used to model tsunami generation, then the tsunami generation model needs to be coupled with the tsunami propagation model, such that the wave elevation field is updated according to time-dependent slip on the fault and deformation of the seafloor. This would typically necessitate a much smaller time step than what would normally be used in numerical tsunami propagation calculations, and is similar in concept to landslide tsunami generation models.

***4.1.2.4 Initial wave characteristics.*** The initial wave characteristics of seismogenic tsunamis are primarily dependent on the mechanism of the earthquake. For dip-slip earthquakes, the initial wavefield is characterized as a dipole, whereas strike-slip earthquakes result in a quadrupole displacement field. For the most common mechanism, interplate thrusts along subduction zones, the displacement field is characterized by uplift at the seaward (updip) edge of rupture and subsidence at the landward (downdip) edge rupture. This explains the common observation of the sea receding prior to the onset of a local subduction zone tsunami. As the dip increases, the polarity changes such that for steep dip, there is subsidence on the footwall side of the fault and uplift on the hanging wall side (Fig. 4.1-1). Absent effects of changes in water depth and rise time, the tsunami wave profiles for the outgoing (far-field) and incoming (local) waves are nearly identical. This contrasts dramatically with landslide sources as described in Section 5.1.2.

### *4.1.3 Source parameters*

For dislocation modeling, most parameters such as average slip and rupture area scale with seismic moment, whereas other parameters such as fault dip

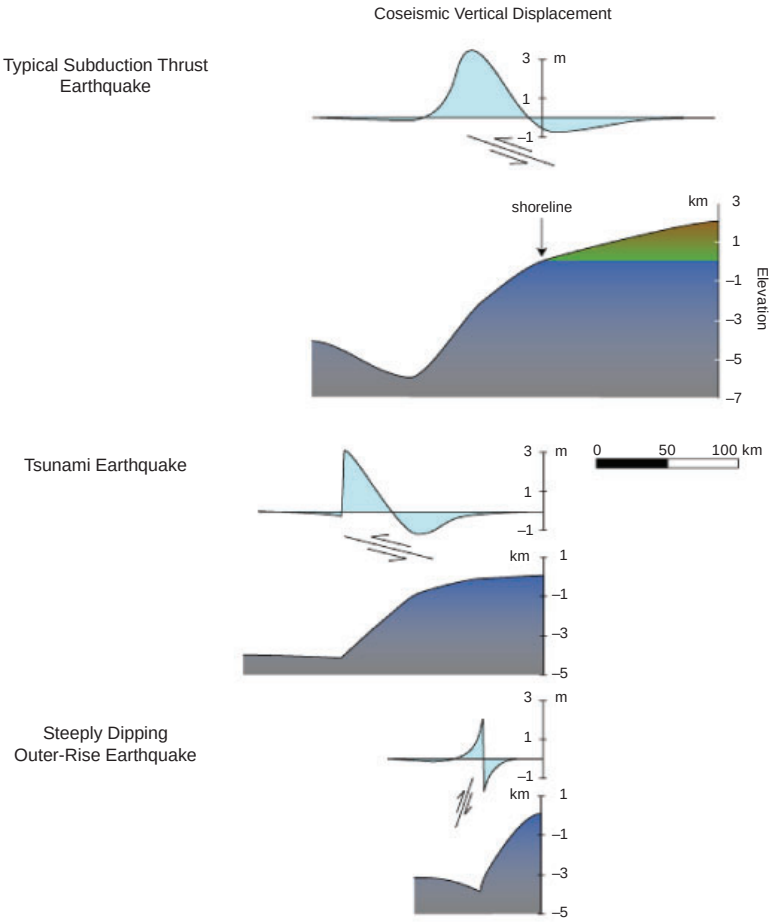


**Figure 4.1-1:** Characteristic coseismic vertical displacement profiles (initial tsunami wave profiles) for three types of subduction zone earthquakes.

and elastic rock properties are determined from analyses of past earthquakes, controlled-source geophysical surveys, and laboratory tests.

***4.1.3.1 Magnitude distribution.*** The frequency-size distribution of seismogenic tsunamis can be directly linked to the frequency-magnitude distribution of the earthquake source—i.e., the well known Gutenberg-Richter (G-R) power-law relationship $\log[N(M_w)] = a - b$ , where $N(M_w)$ is the number of earthquakes with magnitude greater than $M_w$ (Kagan, 2002). Whereas the slope or $b$-value of the G-R relationship is fairly well established, there is much uncertainty in the tail of the distribution for large earthquake magnitudes, due to an incomplete historic earthquake catalog. Fig. 4.1-2 shows four common forms of the size distribution for large magnitudes described by Kagan (2002). There are essentially three widely debated options for defining the G-R distribution tail (which results in what is termed the modified G-R relationship): (1) the characteristic model in which it is assumed that the largest earthquake occurs at approximately the same location between segment boundaries and at approximately the same magnitude, with a G-R distribution specified up to the magnitude of the

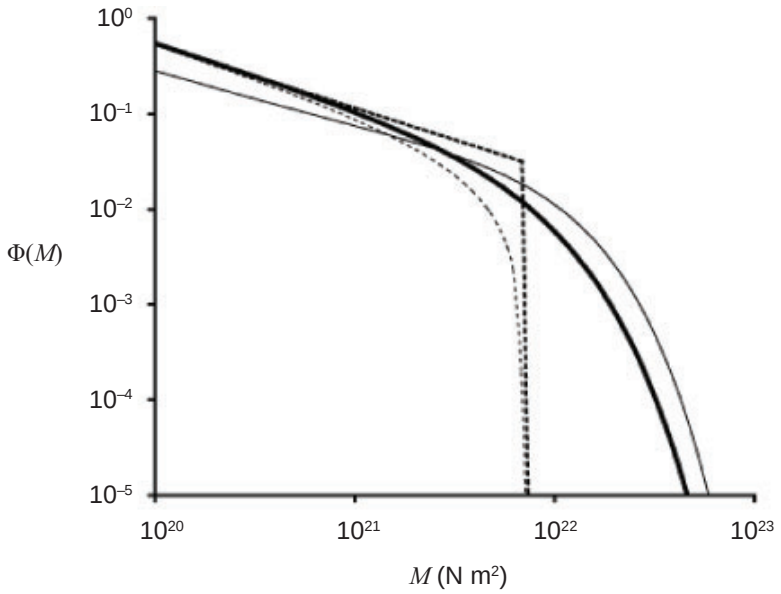


**Figure 4.1-2:** Four different forms of the earthquake size distribution tail (cumulative distribution $\Phi$ as a function of seismic moment): option 1 with hard corners (characteristic—heavy dashed line; truncated G-R—light dashed line), and option 2 with soft corners (tapered G-R—heavy solid line; gamma—light solid line). Adapted from Kagan (2002).

largest aftershock of the characteristic earthquake (Wesnousky, 1994); (2) a regional modified G-R relationship (truncated, tapered, and gamma forms shown in Fig. 4.1-2) that is continuous in magnitude and where the tail is specified with a falloff greater than the G-R *b*-value (Kagan, 1997; Kijko and Graham, 1998; Kijko, 2004); (3) a global modified G-R relationship keyed only to tectonic boundary type (Bird and Kagan, 2004).

An implication of the characteristic model (1) is that earthquake ruptures rarely, if ever, rupture through segment boundaries. These boundaries are usually geologically defined based on the structure of the forearc region in subduction zones or on topographic features of the downgoing plate. The characteristic model is also used in combination with a time-dependent earthquake occurrence probability model, resulting in what is commonly known as "seismic gap hypothesis" (McCann *et al.*, 1979; Nishenko, 1991). If indeed the characteristic rupture model is correct, then it is fairly straightforward to determine the probability of future earthquakes using, for example, a log-normal probability distribution (Nishenko and Buland, 1987), if a sufficient history of past events is known. However, a series of studies (Kagan and Jackson, 1991, 1995; Rong *et al.*, 2003) has indicated that the seismic gap hypothesis is not statistically valid in comparison to a Poissonian (time-independent) null hypothesis. In addition, it has been shown by Okal *et al.* (2006) that what have been thought of as segment boundaries, have been ruptured by past earthquakes.

These studies lead to option (2), where broadly distributed earthquakes

are assumed to follow a modified G-R distribution with regionally dependent parameters based on a particular zonation scheme. The various forms of the G-R tails presented by Kagan (2002) are parameterized by a corner moment, past which the frequency-magnitude distribution falls off sharply. (It should be noted that Kagan (2002) presents a continuous "characteristic" distribution that is different than the discontinuous characteristic distribution presented by Wesnousky (1994) discussed above.) The different zonation schemes include those presented in the "seismic gap" papers and the Flinn-Engdahl regions (Flinn *et al.*, 1974) currently used to locate earthquakes. Whereas regionally dependent modified G-R distributions are defined according to the specific tectonic and stress regime of the zonation scheme used, there is some concern that there are not enough earthquakes in the historic catalog with which to reliably estimate the distributions' parameters. For this reason, Bird and Kagan (2004) provide global modified G-R distributions based only on type of tectonic boundary. Importantly, for subduction boundaries, the corner moment magnitude is quite high ($M_c = 9.58^{+0.48}_{-0.46}$), suggesting that if a subduction zone is long enough, one should assume that M > 9 earthquakes can occur unless proven otherwise. Bird and Kagan (2004) also specify a corner moment for oceanic convergent boundaries ($M_c = 8.04^{+0.52}_{-0.22}$).

***4.1.3.2 Fault geometry.*** For historic cases, the rupture width and length can be estimated from the distribution of aftershocks or inversion of seismic and geodetic data. For potential future rupture zones, the dimensions approximately scale with seismic moment. Past a certain magnitude, however, the width of the rupture zone saturates and cannot get any larger. The saturation width depends on frictional stability conditions that vary with depth as described by Scholz (1990). Rupture length and average slip can continue to increase resulting in an increase to large seismic moment (Scholz, 1982, 1994; Yin and Rogers, 1996; Zeng *et al.*, 2005). General scaling relationships for rupture dimension are given by Geller (1976), Kanamori and Anderson (1975), and Wyss (1979). Scaling relationships derived for intra-plate thrust faults (Wells and Coppersmith, 1994) are not necessarily applicable to inter-plate subduction thrusts.

Fault dip is generally determined from controlled-source geophysical studies and/or analysis of past seismicity and focal mechanisms. For thrust faults, Geist (1999) indicates that dip angles common for interplate thrust (20–30°) result in maximum tsunami efficiency, if all other source parameters are held constant.

***4.1.3.3 Slip vector.*** The orientation of relative plate convergence at subduction zones can attain any value between 0–90°, termed the angle of obliquity. Even for a single subduction zone, such as the Aleutian or Sunda, there can be a great deal of along-strike variation in relative plate convergence because of the motion of plates in a spherical geometry. The orientation of the slip vector along the interplate thrust, however, also depends on the amount of slip partitioning in subduction zones. As explained by Fitch (1972) and McCaffery (1992), for oblique subduction zones some of the strike-parallel or transcurrent motion is taken up on arc-parallel strike slip faults. For a fully slip-partitioned subduction zone, interplate thrust

earthquakes would have a pure thrust mechanism (maximum tsunami efficiency), even for highly oblique relative convergence directions. Other cases, such as the north Hispaniola subduction zone, do not exhibit slip partitioning under oblique convergence conditions (ten Brink and Lin, 2004).

***4.1.3.4 Slip distribution.*** For local tsunamis, slip models that account for heterogeneity (Somerville *et al.*, 1999) are based on self-affine properties of rupture dynamics (Hanks, 1979; Andrews, 1980; Frankel, 1991; Herrero and Bernard, 1994; Hisada, 2000; Mai and Beroza, 2000; Hisada, 2001; Mai and Beroza, 2002) that in part are constrained by the seismic source spectrum (Hartzell and Heaton, 1985; Tsai, 1997; Polet and Kanamori, 2000). In this case the average slip is given by the overall seismic moment of the scenario earthquake, and the fall-off of the seismic source wavenumber spectrum is linked to the fall-off of far-field displacement spectrum observed from seismograms (Tsai, 1997; Mai and Beroza, 2000, 2002) or following the canonical $\omega^{-2}$ model of Aki (1967). This standard slip model results in a suite of slip distribution patterns for a given seismic moment and have been used in strong-ground motion studies (e.g., Berge *et al.*, 1998; Somerville *et al.*, 1999) and can be used in tsunami source models. Recent research from onland earthquakes (Lavallée and Archuleta, 2003; Lavallée *et al.*, 2006) and from the 2004 Sumatra-Andaman earthquake indicate that slip can exhibit larger fluctuations than predicted from the standard self-affine model of Andrews (1980). Lavallée *et al.* (2006) proposes that random variables based on Lévy law distributions be used for these cases. Maximum tsunami efficiency is for those cases where slip is concentrated near the sea floor (usually associated with sea floor rupture), as in the case of tsunami earthquakes (Kanamori and Kikuchi, 1993; Satake and Tanioka, 1999).

***4.1.3.5 Shear modulus.*** Because of the diversity of rock types at subduction zones, there is a large variation in elastic moduli, including shear modulus (rigidity). Elastic moduli are either measured in the laboratory (Gregory, 1976; Thomson, 1985; Saffer *et al.*, 2001) or deduced from earthquake source-time functions (Bilek and Lay, 1999, 2000). For tsunami generation models based on moment (rather than slip) distributions, depth-dependent variations in shear modulus have a large effect in determining the initial tsunami wave height (Fig. 4.1-3). A theoretical study by Okal (1988) indicates that if only $\frac{1}{10}$ of the seismic moment of an earthquake is located in the low-rigidity sedimentary rocks of subduction zones, initial tsunami amplitudes would increase by an order of magnitude.

This leads to an explanation of tsunami earthquake, defined as tsunamigenic earthquakes with anomalously high tsunami severity relative to earthquake magnitude (Kanamori, 1972; Kanamori and Kikuchi, 1993; Polet and Kanamori, 2000). These earthquakes are located farther updip near the trench (perhaps along the structurally defined décollement) than typical interplate thrust earthquakes. This results in four changes that are favorable toward increased tsunami excitation: (1) moment release in low rigidity rocks increases slip, for a given magnitude; (2) shallow rupture initiation increases likelihood for seafloor rupture that also increases slip (i.e., traction-free boundary condition at seafloor) (Rudnicki and Wu, 1995); (3) shallower focal depth increases coseismic vertical displacement for a given amount of

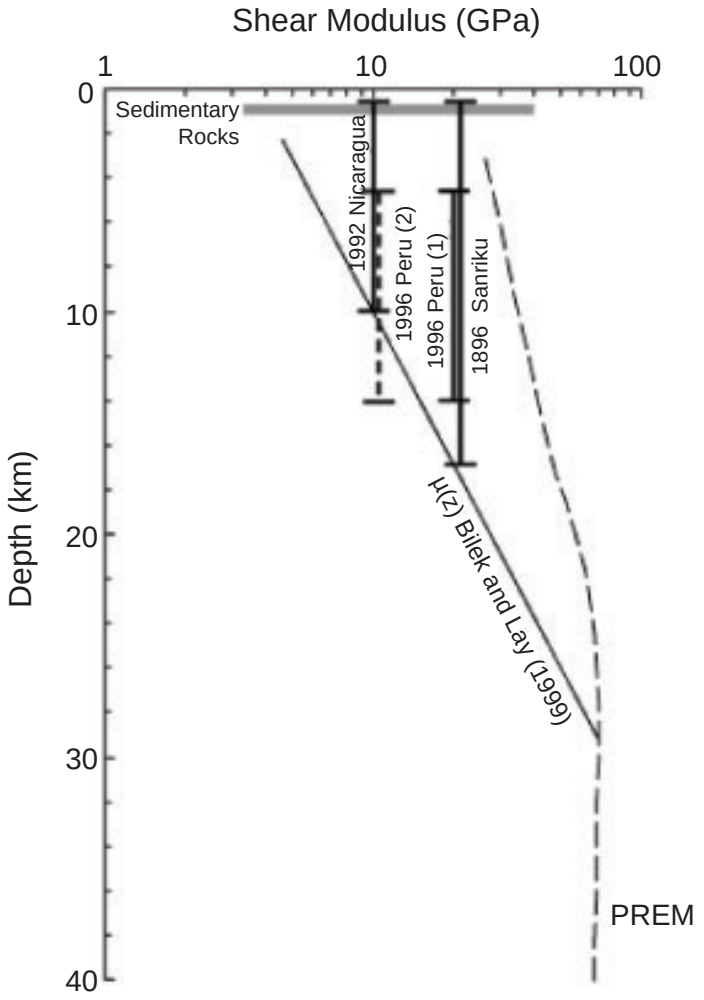


**Figure 4.1-3:** Comparison of shear modulus estimates as a function of depth in subduction zones. Dashed line is the standard Preliminary Reference Earth Model (Dziewonski and Anderson, 1981), solid line is estimate from source-time functions of historic earthquakes (Bilek and Lay, 1999), bars with constant value are estimates from source studies of tsunami earthquakes, and gray bar is range from laboratory studies.

slip; and (4) increased water depth above source region increases amplification during tsunami shoaling according to Green's Law (Satake, 2002).

## 4.2 Submarine and Subaerial Landslides

### *4.2.1 Source types and environment of occurrence*

Submarine and subaerial landslides occur in many types, depending on geologic composition, slope steepness, triggering mechanism, and pore pressure. Following the classification scheme described by Varnes (1978), there are five primary types of slope movements: (1) falls, (2) topples, (3) slides (rotational and translational), (4) lateral spreads, and (5) flows (Fig. 4.2-1). In

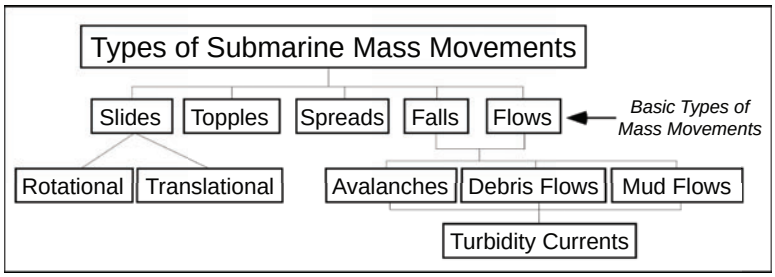


**Figure 4.2-1:** Classification of submarine mass movements adapted from sub-aerial classification proposed by the ISSMGE Technical Committee on Landslides (TC-11).

some cases, a specific event will involve a combination of these types and be termed a complex slope movement. Because tsunami generation is sensitive to the style and time history of slope movement, it is important to accurately assess the dominant type in a given area. In a given region, there can be a variety of slope movements. For example, in Alaska, both sub-aerial rock falls (1958 Lituya Bay) and landslides in Valdez Arm triggered by the 1964 Great Alaska earthquake have been known to generate destructive local tsunamis. Also, in Southern California, both submarine mud flows (Santa Barbara Channel) and debris avalanches (Palos Verdes) have occurred in the geologic past that may have been tsunamigenic (Lee *et al.*, 2003). On the passive margin of the U.S. east coast, the transition from a clastic-dominated offshore environment in the north to a carbonate-dominated environment in the south is a key factor in determining the type of slope movements that are found. Several publications (Schwab *et al.*, 1993; McAdoo *et al.*, 2000; Locat and Mienert, 2003; Lee, 2005) describe regional differences in landslides around the world and along the U.S. continental margin.

***4.2.1.1 Guidelines for investigating submarine mass movements.*** The following aims at establishing some guidelines leading to the demonstration of the potential for tsunamigenic landslides. From known cases of major submarine mass movements, the investigation may initially have to be conducted over a very large area (e.g., in a radius of about 1000 km). These areas may be identified as a result of the initial inventory effort. Then a larger scale can be considered for detailed analysis to first establish the mass movement history, the remaining hazards, and their potential to generate significant tsunamigenic landslides. The steps are as follows:

1. Identification of areas of interest (if possible at the beginning).

2. Literature review of existing documentation in areas of interest.

3. Compilation of existing seafloor and coastal data (e.g., multibeam, seismic, cores, etc.). Actual Geologic Long-Range Inclined Asdic (GLORIA) images may be an excellent starting point in the U.S. Exclusive Economic Zone (EEZ) area (Schwab *et al.*, 1993) (`http://coastalmap.marine.usgs.gov/gloria/`).

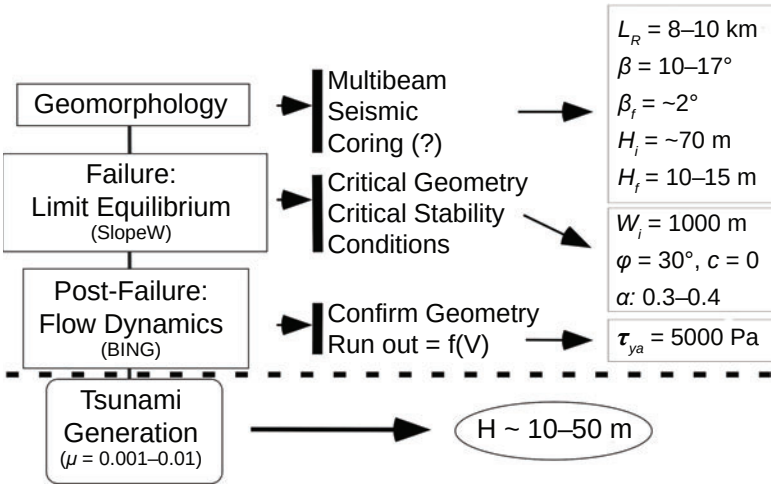


**Figure 4.2-2:** Approach used for estimating the generation of tsunami for the Palos Verdes debris avalanche. Values given here are provided only for illustration purposes and were taken from the case of Palos Verdes (Locat *et al.* 2004).

4. Primary inventory of mass movements to establish the hazard in terms of the slide inventory (volume, geometry, material, type of failure, date, etc.).

5. Identification of potential source area.

6. Detailed investigation of characteristic slides and potential slide areas using existing techniques such as multibeam surveys, high-resolution seismic surveys, coring and dating (e.g., $^{14}C$ or sedimentation rate). In coastal areas, it may require the study of the groundwater system bridging onshore and offshore sediments.

7. Carry out advanced geotechnical testing (both in situ and in the laboratory) to determine the geotechnical parameters (e.g., Table 4.2-1) used in the detailed analysis outlined in Fig. 4.2-2. If gas (hydrate gas, or even high pore pressure) are expected, the detailed slope stability analysis will require in situ measurements (e.g., CPT: cone penetrometer tests).

8. Retro-analysis of old landslides to estimate their tsunamigenic potential using the approach outlined in Fig. 4.2-2). This can be used to calibrate the models and provide field-controlled physical parameters (e.g., geometry, flow characteristics, etc.).

9. Identify potential sources and carry out a detailed analysis following the outline in Fig. 4.2-2.

10. Provide a map of tsunamigenic submarine landslide sources and a table of characteristic parameters.

**Table 4.2-1:** Parameters required in various slope failure and post-failure analyses (X: primary; x: secondary relevance; RO: run out analysis; Tur: turbidity currents; source: Locat and Lee, 2005).

| | | Slab failure (infinite) | | Circular failure | | | | |
|---|---|---|---|---|---|---|---|---|
| **Parameters** | **Symbol** | **D** | **U** | **D** | **U** | **Retrogressive Failure** | **RO** | **Tur** |
| Slope angle, degrees | $\beta$ | X | X | X | X | X | X | x |
| Slope height (m) | H | X | X | X | X | X | X | x |
| Geotech. stratigraphy | — | X | X | X | X | X | x | — |
| Seafloor morphology | | x | x | x | x | x | X | X |
| Water content (%) | w | X | X | X | X | X | X | — |
| Plastic limit (%) | $w_P$ | X | X | X | X | X | X | — |
| Liquid limit (%) | $w_L$ | X | X | X | X | X | X | — |
| Liquidity index | $I_L$ | X | X | X | X | X | X | — |
| Undrained strength, kPa | Cu | x | X | x | X | X | x | — |
| Remolded undrained strength, kPa | $Cu_r$ | — | X | — | X | X | X | — |
| Sensitivity | $S_t$ | X | X | X | X | X | X | |
| In situ effective stress, kPa | $\sigma'_v$ | X | — | X | — | x | — | — |
| Pre-consolidaiton pressure, kPa | $\sigma'_p$ | X | X | X | X | X | — | — |
| Overconsolidation ratio | OCR | X | X | X | X | X | — | — |
| Sensitivity | $S_t$ | X | X | X | X | X | X | — |
| Friction angle, degrees | $\phi'$ | X | — | X | — | — | x | |
| Cohesion, kPa | c′ | X | — | X | — | — | — | |
| Pore pressure, kPa | u | X | — | X | — | X | x | — |
| Excess pore pressure, kPA | $u_e$ | X | — | X | — | X | x | — |
| Gas pressure (hydrates), kPa | $u_g$ | X | x | X | x | X | x | — |
| Pore pressure ratio | $r_u$ | X | x | X | | | X | |
| Earthquake acceleration | $\alpha$ | X | X | X | X | — | — | — |
| Viscosity, Pa·s | $\mu$ | — | — | — | — | x | X | x |
| Yield strength, Pa | $\tau_c$ | — | — | — | — | x | X | x |
| External loads, kN | Q | X | X | X | X | x | | |
| Hydraulic conductivity, cm/s | k | x | — | x | — | — | x | — |

### *4.2.2 Generation mechanism and methodology—submarine landslides*

Ideally, tsunami generation from submarine landslides would involve modeling of slide physics coupled with the overlying water column, similar to earthquake tsunami generation modeling. This has been done for the specific case of submarine mud flows in a series of papers by Jiang and LeBlond (1992, 1993, 1994) in which different constitutive rheologies were used (see also Rubino *et al.*, 1998; Mariotti and Heinrich, 1999; Fine *et al.*, 2005; Locat and Lee, 2005). In other studies, granular models were used to simulate slide movement (Heinrich *et al.*, 2001).

It is often useful to first assess the limit equilibrium state of the slope under ambient and seismic loading (Lee *et al.*, 1999). The material failure behavior is assumed to follow a Mohr-Coulomb failure criterion such as:

$$\tau = c' + (\sigma - u)tan\phi' \ , \tag{4.1}$$

where $\tau$ = the shear strength mobilized along the failure plane, $c'$ = the cohesion, $\sigma$ = the total stress, $u$ = the pore pressure, and $\phi'$ = the friction angle.

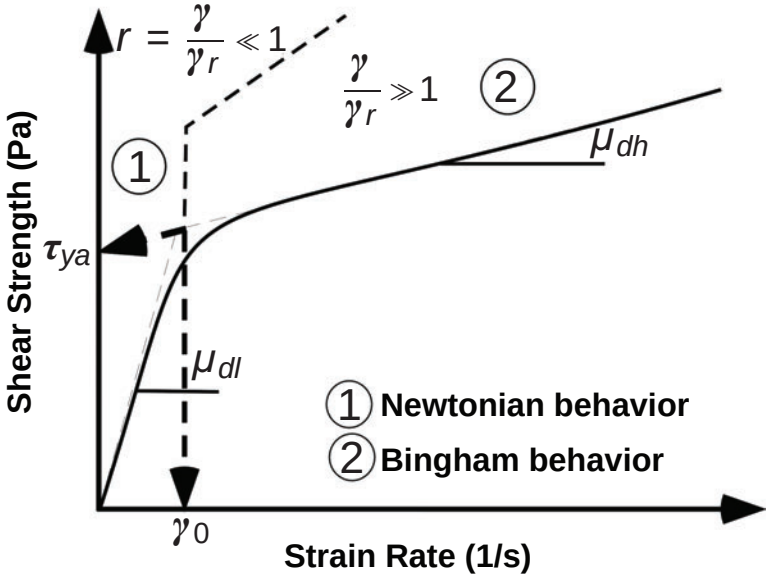


**Figure 4.2-3:** Bi-linear model of Locat (1997) with the boundary conditions used in the 1D numerical model BING (Imran *et al.*, 2001); see the text for explanation of symbols.

For post-failure analysis of the failed mass, Locat *et al.* (2004) proposed a simple 1D-flow dynamics model, BING, presented by Imran *et al.* (2001), which has been developed for the study of debris flows. BING can be used with various rheological models: Bingham, Herschel-Bulkley and bi-linear. The bi-linear model used in the case of the Palos Verdes rock avalanche (Locat *et al.*, 2004) has been proposed by Locat (1997) to best describe the rheology of clayey silt or silt mixtures, which often present a pseudo-plastic behavior. A similar proposal was made by O'Brien and Julien (1988), also for coarse silt mixtures. In our analysis (Locat *et al.*, 2004), we assumed that the rheological properties of the Palos Verdes debris avalanche could be described by a bi-linear rheological model. The bi-linear model assumes that the initial phase of the flow is Newtonian (1 in Fig. 4.2-3) and evolves, after reaching a threshold shear rate value ($\gamma_0$), into a Bingham type flow (2 in Fig. 4.2-3). The constitutive equation proposed by Locat (1997) for bi-linear flow is expressed by:

$$\tau = \tau_{ya} + \mu_{dh}\gamma - \frac{\tau_{ya}\gamma_0}{\gamma + \gamma_0} \ , \tag{4.2}$$

where $\tau$ is the flow resistance, $\tau_{ya}$ the yield strength, $\mu_{dh}$ the viscosity, $\gamma$ the shear rate, and $\gamma_o$ the shear rate at the transition from a Newtonian to a Bingham behavior.

In BING (Imran *et al.*, 2001), equation 4.2 is re-written

$$\frac{\tau}{\tau_{ya}} = 1 + \frac{\gamma}{\gamma_r} - \frac{1}{1 + r\frac{\gamma}{\gamma_r}} \ , \tag{4.3}$$

where $\gamma_r$ is the strain rate defined as

$$\gamma_r = \frac{\tau_{ya}}{\mu_{dh}} \ , \tag{4.4}$$

and $r$ the ratio of the strain rates,

$$r = \frac{\gamma_r}{\gamma_0} \ . \tag{4.5}$$

One of the main parameters used in this analysis, the yield strength $\tau_{ya}$, is estimated from field observations of the failed mass in the accumulation zone. The values related to the viscosity, i.e., the strain rate, $\gamma_r$, and the ratio of strain rates, $r$, will be estimated from a parametric analysis to find the best values which can fit the observed geometric characteristics in the runout zone.

In most cases, kinematic descriptions of landslide movement have been used to model tsunami generation. So-called "hot start" models in which wave propagation from landslide sources is specified by static initial conditions is less preferred than a completely coupled system (e.g., Jiang and Leblond, 1994) or kinematic models, because the time-dependent source effects are not explicitly accounted for. One of the more realistic kinematic landslide models is incorporated into Cornell University Long and Intermediate Wave Modeling Package (COULWAVE) described by Lynett and Liu (2002). In this model, landslides are described by a smooth time function (parameterized by the duration of slide movement and necessary for numerical stability) in which regions of progressive excavation (depletion) and down-slope deposition (accumulation) are coupled with the overlying water column. The effect of spreading in the down-slope during slide movement is discussed by Trifunac *et al.* (2003). Non-linearity and dispersive wave propagation are also incorporated into COULWAVE, which are relatively more important for landslide-generated tsunamis in comparison to seismogenic tsunamis. Finally, while single-rigid block slides are rare in nature, they are useful in the laboratory setting to compare numerical wave results with physical modeling (e.g., Liu *et al.*, 2005).

***4.2.2.1 Initial wave characteristics.*** One of the essential differences between tsunamis generated by landslides and earthquakes is the strong directivity of tsunami waves in the direction of slide movement (down slope). In contrast, for earthquake tsunamis, because of the faster process speeds, there is only a weak directivity effect in the direction of rupture propagation (Geist, 1999). The higher amplitude outgoing wave generated in the direction of slide movement is characterized by a leading-elevation polarity with amplitude controlled by the terminal velocity of the slide (Trifunac *et al.*, 2003). The backgoing wave is dependent on the initial time history (namely, acceleration) of slope failure—it is typically characterized by a leading, and sometimes solitary, depression wave approaching shore.

The other primary difference between landslide- and earthquake-generated tsunamis is related to attenuation in the far-field. Whereas locally, landslide tsunamis can have potentially dramatic effects broadside from the source (Okal and Synolakis, 2004), because landslides deform a

much smaller area of the sea floor in comparison to earthquakes they attenuate more rapidly away from the source than seismogenic tsunamis (e.g., Gisler *et al.*, 2006). For the largest slides (e.g., Storegga), evidence of tsunamis occurs at distances of more than 1000 km (Bondavik *et al.*, 2005).

### *4.2.3 Source parameters—submarine landslides*

Unlike seismogenic tsunamis where the key source parameter related to tsunami severity is seismic moment, there are two primary parameters that influence tsunami generation: landslide volume and time history (slide acceleration and speed). These and other landslide tsunami source parameters are described below.

***4.2.3.1 Volume distribution.*** It has recently been determined that the volume distribution for submarine landslides follows a power-law with similar exponent to on-land cases (Issler *et al.*, 2005; ten Brink *et al.*, 2006a). Determination of the volume distribution is of particular importance in estimating the largest failures. It should be emphasized that care must be taken in identifying individual failures. In some cases, what looks like a single failure is actually a complex of individual failures (e.g., Lee *et al.*, 2004), perhaps spaced closely in geologic time such as a retrogressive failure in which the head wall becomes destabilized. These types of complexes may appear to be a large-scale feature, but in fact are composed of individual, smaller events, each hypothetically creating a separate tsunami. In some cases, large-scale geomorphic amphitheaters have been misinterpreted in the marine environment as being caused by a single failure. As illustrated by the Palos Verdes slide (Locat *et al.*, 2004), it is important to be able to evaluate how the slide mass was displaced. Was it more or less moving as a coherent mass, or much like a retrogressive failure, i.e., only one piece at a time? Also, care must be taken so as not to misinterpret apparent landslide features just from seismic profile records, which may in fact be sediment waves (Lee *et al.*, 2002).

Like the modified Gutenberg-Richter distribution for earthquakes, the tail of the landslide volume distribution follows the general upper-truncated power-law distribution (cf., Burroughs and Tebbens, 2005). In calculating landslide volume, assumptions often have to be made in converting mapped area to volume (McAdoo *et al.*, 2000; ten Brink *et al.*, 2006b). For cases such as north Puerto Rico (ten Brink *et al.*, 2006b), it is unclear if the fall-off at high volumes is caused by a physical restriction in the maximum size of the failure or from under-sampling (i.e., the largest events have not occurred yet). It is evident, however, that there are factors such as down slope length of the continental margin that limit the size of the maximum event.

Locat and Lee (2002) have presented a worldwide compilation of known submarine mass volume and run out distance (Fig. 4.2-4) which enlarged the data base provided by Hampton *et al.* (1996) and by Edgers and Karlsrud (1982). Figure 4.2-4 presents a large range in term of both size (up to 3500 $km^3$) and run out distances (up to 1000 km for channelized flows).

***4.2.3.2 Slide acceleration and speed.*** Tsunami generation from landslides is critically dependent on the time history of movement. In partic-

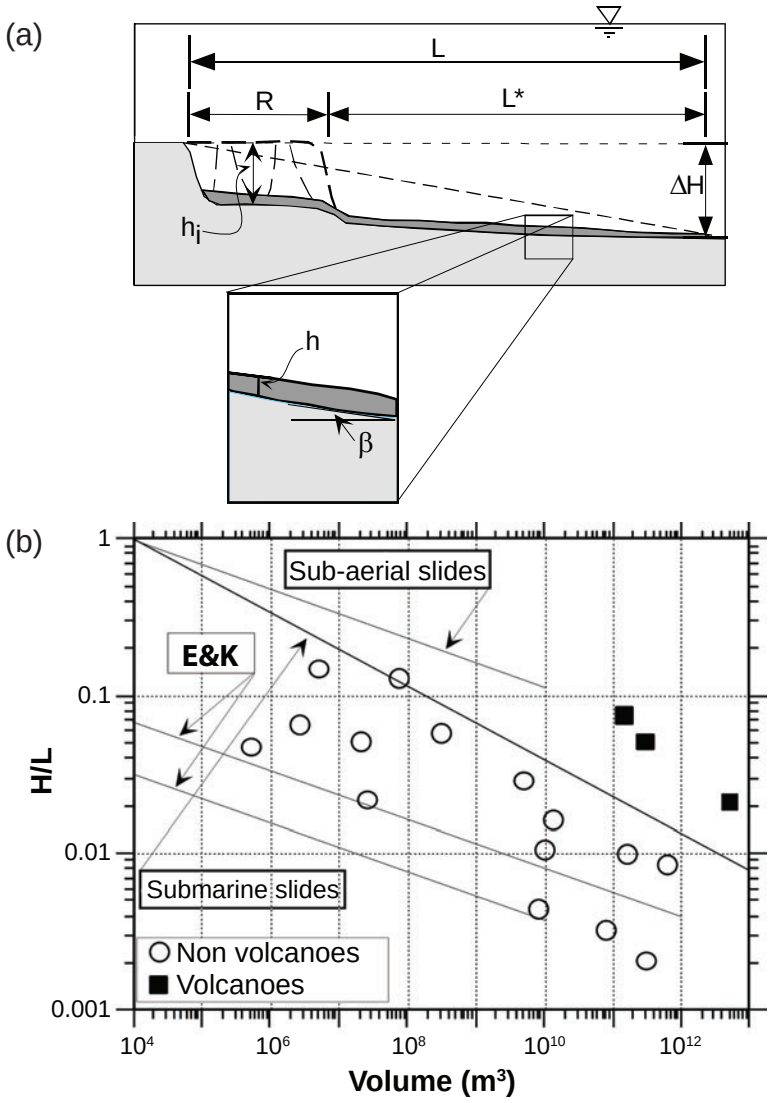


**Figure 4.2-4:** (a) Geometrical description of mobility ($h_i$: initial height, h: flow thickness). (b) Relationship between the run out ratio (height of the slide/travel distance) as a function of the initial volume (Locat and Lee, 2002).

ular, the near-field tsunami is sensitive to the initial acceleration of the slide, whereas the far-field (outgoing) tsunami is sensitive to the maximum velocity (Trifunac *et al.*, 2002, 2003). To some extent, the initial wave height can be influenced by the depth of the center of mass of the sliding mass (Murty, 1979). However, unlike earthquakes where rupture dynamics can be accurately reconstructed from seismograms, there is a lack of any direct observations of submarine landslide dynamics. Some direct measurements of turbidity currents have been made, most recently by Xu *et al.* (2004), but few, if any, of the initial tsunamigenic stages of failure. As discussed below, the use of turbidity current may provide a lower bound value for speed but

one must remember that at that point, the submarine mass movement has evolved significantly from its initial conditions so that its actual potential for maintaining a tsunami at that stage may be quite limited. As mentioned previously, landslide speed (or more properly, the time history of slide movement) can be determined from physical modeling of landslide dynamics, such as in the study of Locat *et al.* (2004). In fact, a single landslide speed parameter may inaccurately describe the dynamics of failure, since the region of excavation may fail at different rates than the rate of deposition down slope (Trifunac *et al.*, 2002, 2003). Nonetheless, in the absence of physical modeling of the landslide, the lack of direct observations often constrains tsunami models to be based on a single dynamic parameter (landslide speed or duration). Indirect evidence from runout distance and elevation can yield clues of landslide speed (Ward, 2001). Most likely, bathymetric slope and basal friction are key parameters that dictate landslide speed. Most modeling studies have used speeds in the 20–75 m/s range (see supplementary material, ten Brink *et al.*, 2006b). The case of maximum tsunami generation efficiency (outgoing wave) occurs when the terminal landslide speed matches that phase speed of tsunami waves ($c = \sqrt{gh}$). Landslide speeds less and greater than this value will result in smaller outgoing wave amplitudes.

***4.2.3.3 Cohesiveness/fluidity.*** Tsunami generation will also be affected by how rigid the slide mass is during failure, in terms of how quickly it disintegrates and/or fluidizes into a turbidity flow. Rigid slides that behave like a single mass will be more efficient in tsunami generation than a disintegrative slide. Turbidity flows are primarily a bottom-boundary layer phenomenon and are unlikely to generate significant tsunami waves. Geomorphological analysis is an important tool that bears also on the identification of the type of initial failure: fall, topple, slide, spreads, and flow (Fig. 4.2-1). Geomorphological analysis should be followed by seismic and multibeam surveys and coring cruises. Cores are taken for further analysis in the laboratory to determine the physical and geotechnical properties of the material involved in the mass movement (Table 4.2-1).

***4.2.3.4 Triggering mechanism.*** There are a variety of triggering mechanisms for tsunamigenic submarine landslides. The most common of these mechanisms is earthquakes, such as for the 1929 Grand Banks (Fine *et al.*, 2005), 1946 Aleutian (López and Okal, 2006), the 1964 Valdez (Lee *et al.*, 2003), and the 1998 Papua New Guinea (Satake and Tanioka, 2003) tsunamis. Several studies have described the link between strong-ground motion in destabilizing regions toward slope failure (Biscontin *et al.*, 2004; Biscontin and Pestana, 2006). As such, the seismic-induced landslides occur nearly at the same time as the earthquake, such that the tsunami is a composite of both earthquake and tsunamigenic sources (Johnson and Satake, 1997; Satake and Tanioka, 2003; López and Okal, 2006). Many of the events listed in the NGDC tsunami catalog as having a landslide component are triggered by earthquakes and thus are likely to have a composite source (e.g., López and Okal, 2006). Still, in some cases, the development of a failure plane, caused by an earthquake, may take up to many hours (Seed *et al.*, 1975), so that a significant delay may take place between the earthquake and the occurrence of the tsunami. In these cases, other triggering mechanisms such as

extreme tidal excursions for shallow-seated submarine landslides and simply accumulated sediment deposition or tectonic tilting (ten Brink, 2005) are the cause of the events. The occurrence of gas hydrates has also been linked to seafloor failures (Kayen and Lee, 1991; Schwab *et al.*, 1993).

### *4.2.4 Generation mechanism and methodology—Subaerial landslides*

Tsunamis generated by subaerial landslides occur in a more geographically restrictive area compared to submarine landslides—namely in regions where there is steep coastal topography such as fjords. Even though the impact velocity of subaerial landslides can be significantly greater than for the submarine case, because they displace less water in the near shore region than submarine slides in deeper water, for example, along the continental slope, the geographic extent of damaging wave activity is typically less for subaerial slides compared to submarine slides. Many of the largest tsunamigenic subaerial landslides, excluding those associated with active volcanism (described in Section 5.3), have been triggered by earthquakes (e.g., 1958 Lituya Bay).

Walder *et al.* (2003) make an important distinction between subaerial slides that (a) start near shore and that have a substantial proportion of their runout under water (termed release-at-shore cases) and (b) those slides starting at considerable elevation and having a substantial proportion of their runout above water (termed initial-velocity cases). The relevant parameter that distinguishes these cases is the slide impact Froude number, which is the ratio of inertial forces to gravitational forces. In the case of landslides, it is a measure of the slide velocity upon entry relative to the long-wave phase speed of tsunamis. The tsunami generation mechanism for the release-at-shore cases is very similar to that for submarine landslides (Section 5.1.2). In contrast, for the initial-velocity cases, wave generation occurs primarily from impact of the slide upon contact with the water, and has a very different character from submarine or release-from-shore cases (Heinrich, 1992).

The hydrodynamics of a fast moving body (higher Froude number) impacting water is complex. Near the site of impact, laboratory studies (Fritz *et al.*, 2003a; 2003b; 2004) and fully 3-D Navier Stokes hydrodynamic modeling (Mader and Gittings, 2002) indicate that complex flow separation and crater formation occurs. In particular, Fritz *et al.* (2004) indicates the near-field wave characteristics for these strongly non-linear waves. For fully 3-D modeling of release-from-shore subaerial-slide generated waves (lower Froude number), Lynett and Liu (2006) indicate modifications to standard hydrodynamic theory must be made for cases in which the slide is not completely submerged. Due to the complexity and turbulent nature of this flow, Walder *et al.* (2003) considers the splash zone a "black box" and derives scaling relations to estimate the near-field hydrodynamic response.

### *4.2.5 Source parameters—subaerial landslides*

The primary source parameters that determine the severity of subaerial landslide tsunamis, are the impact Froude number (linked to the coastal topo-

graphic slope), density, and geometric dimensions of the slide. Heinrich (1998) indicates that the shape of the frontal portion of the subaerial slide also has a significant effect on wave generation. It is likely too, that the cohesiveness of the slide also has an effect.

#### *4.2.6 Ice falls*

Although research on waves generated by ice falls is limited, it is likely that this process shares many characteristics with sub-aerial landslides described in 4.2.4–5. An overview of types of glacial processes that can result in large masses entering the water is given in Richardson and Reynolds (2000). These include snow and ice avalanches, with the former broken down into frontal block failure (calving, when the terminus of a glacier is in the water), ice slab detachment and ice-bedrock failure in which part of the underlying rocks are included in the failure (see also Salzmann *et al.*, 2004). Ice avalanches down a slope will behave similar to the impact wave generator and associated wave characteristics described by Fritz *et al.* (2004). Again, the primary source parameters are likely the volume and impact Froude number of the avalanche. Maximum volumes of ice avalanches in the European Alps are given in Huggel *et al.* (2004). Calving, in contrast, will often behave as a topple (Fig. 4.2-1) entering the water. A historic example of waves generated by a frontal block failure is described by Tinti *et al.* (1999) where a 7,000–16,000 $m^3$ frontal block failure in the western Italian Alps generated a damaging ∼2 m wave in a lake.

### 4.3 Volcanoes

#### *4.3.1 Source types and environment of occurrence*

A variety of mechanisms associated with active and Holocene-age volcanoes has been known to generate tsunamis. These mechanisms can occur at any volcano located in or near the world's oceans or other large bodies of water. The global distribution of Holocene volcanoes is described by Siebert and Simkin (2002). The following are general source types described by Begét (2000) and Newhall (in prep.): (1) pyroclastic flows into the ocean; (2) submarine caldera collapse; (3) submarine explosion; (4) debris avalanches and flank failures (Masson *et al.*, 1998; Urgeles *et al.*, 1999). Other papers describe less common mechanisms, including rapid inflation or bulging of the seafloor due to injection of magma at depth (e.g., Satake and Kanamori, 1991; Kanamori *et al.*, 1993) and coupling of the ocean with atmospheric shock waves (Begét, 2000). In many cases such as the 1883 Krakatau and mid-17th century BC Santorini events, a combination of source types is ascribed to tsunami generation. As with landslides, it is recommended that detailed geologic studies be conducted at potential tsunamigenic volcanoes to determine evidence and possible mechanisms of tsunami generation. It is worth noting that no submarine volcano is continuously monitored by a volcano observatory (Begét, 2000).

### 4.3.2 Generation mechanism by type of volcanogenic source

In this section, we describe the generation mechanism for each of the source types listed above where they differ from the previous discussion of landslides and earthquakes. We also indicate relevant source parameters and historical examples.

***4.3.2.1 Pyroclastic flows.*** Pyroclastic flows are debris flows and avalanches of hot, gas-rich material flowing quickly downslope and are products of explosive eruptions. If pyroclastic flows reach the ocean, the hot material separates into a "dust cloud" of hot ash and gas, and denser material that potentially can generate a tsunami (Legros and Druitt, 2000; Watts and Waythomas, 2003). Of the several mechanisms investigated by Watts and Waythomas (2003), including steam explosion and excitation of pressure waves, the pyroclastic debris flow is thought to be the most efficient at generating tsunami waves. The mechanism of tsunami generation, therefore, is similar to that for subaerial landslides and avalanches. Case histories include the 1997 Montserrat (Lesser Antilles) event (Heinrich *et al.*, 1998) and the 3500 y.b.p Aniakchak events (Waythomas and Neal, 1998; Watts and Waythomas, 2003). As with subaerial landslides, the primary source parameters are the impact Froude number, density, and dimensions of the tsunamigenic portion of the mass flow.

***4.3.2.2 Submarine caldera collapses.*** For caldera collapses that occur beneath the water, sudden down-dropping of the caldera floor can potentially generate a tsunami. The initial one-side displacement hydrodynamically evolves into a train of both positive and negative waves (Momoi, 1964). The mechanism of wave generation by caldera collapse is thoroughly investigated by Gray and Monaghan (2003) from both laboratory experiments and numerical modeling. From this study, the primary source parameters are the dimensions of the caldera (diameter) and the fixed wall height and the height of the down-dropped caldera floor, relative to the water surface. It is thought that both the 1883 Krakatau and mid-17th century BC Santorini tsunamis may have had a significant component of generation from caldera collapse (Gray and Monaghan, 2003; Newhall, in prep.), although this may not have been the only tsunami source mechanism.

***4.3.2.3 Submarine explosions.*** Waves induced by submarine volcanic activity can range between being very localized, as in the case of excitation from large steam bubbles such as Kick 'em Jenny in the Caribbean (Begét, 2000), to regionally destructive waves caused by violent explosions, such as the case of the initial stages of the 1883 Krakatau eruption (Nomanbhoy and Satake, 1995). Belousov *et al.* (2000) indicate a rapid decay of waves generated by volcanic explosions and provide a case history for a 4-km diameter lake. A parameter describing source potency that can be linked to tsunami generation is the Volcanic Explosivity Index (VEI) (Siebert and Simkin, 2002). Increased hydrostatic pressure on volcanoes at significant water depths tends to inhibit large hydromagmatic explosions (Begét, 2000).

***4.3.2.4 Debris avalanches and flank failures.*** Some of the largest volume debris avalanches are associated with volcanoes (Siebert, 1996; Locat and Lee, 2002) and as such, they have the potential to generate the

most severe volcanogenic tsunamis. Debris avalanches can be triggered by volcanic activity or occur during the late-stage erosional phase of volcanoes. Most commonly, large-scale debris avalanches evolve from sector collapses or large flank collapses (Ui *et al.*, 2000). In addition, because the avalanches are composed of volcanic rocks with high cohesion, they are more likely to be tsunamigenic than avalanches composed of dominantly clastic material, such as mud slides. Tsunami generation from debris avalanches follows the tsunami mechanism as that for submarine and subaerial landslides. Notable historical examples include the 1741 Oshima, Japan, (Satake and Kato, 2001), 1782 Unzen, Japan, 1883 Augustine, 1888 Ritter Island (Ward and Day, 2003), and the prehistoric Nuuanu and Wailau landslides off the Hawaiian Islands (Satake *et al.*, 2002), and off Stromboli (Tinti *et al.*, 2000).

Flank failures induce tsunamis through a combination of mechanisms. Typically, volcanic spreading will result in overthrusting along a décollement on the edge of a volcanic flank (Lipman *et al.*, 2002, 2003; Morgan *et al.*, 2003). The result is a very shallow thrust fault, similar to subduction thrusts in terms of earthquake mechanism but resulting from very different geologic processes. Using the south flank of Hawaii as an example, a large earthquake on the basal décollement can also trigger large-scale slumping along normal faults in the hanging wall (e.g., the Hilina fault system) (Cannon *et al.*, 2001) and debris avalanches that can involve large slide blocks. It is often difficult distinguishing large-scale debris avalanches from flank failures—one way is to note that the latter involves deep-seated rotational slumping and overthrusting above a basal décollement. In an examination of the tsunami from the M = 7.5 1975 Kalapana flank earthquake, Ma *et al.* (1999) indicates that most of the far-field tsunami energy resulted from the earthquake, whereas regionally, the concomitant landslide also added to the tsunami. Klein *et al.* (2001) indicates that the volcanic flank regions are the most seismically active in Hawaii. The even larger M = 7.9 (Klein *et al.*, 2001) 1868 Kau earthquake that occurred along the southern flank of Hawaii also generated a far-field tsunami. The method with which to model the tsunami source from these complex events would be to combine individual tsunami generation displacement fields from the décollement earthquake, movement along the normal faults resulting from the rotational failure, and possible debris avalanches (cf., Ma *et al.*, 1999).

## 4.4 Recommendations

Here we provide recommendations specific to the task of specifying potential tsunami source parameters.

A. Specify conservative values and ranges for parameters of all potential tsunami sources, as indicated for the case of seismic source parameters by NUREG-0800 (pg. 2.4.6-2).

B. Identify and include as potential tsunami sources those events in the historical and pre-historic record deemed capable of tsunami generation, but for which no tsunami evidence, per se, can be found. This is because tsunami observations along some coastlines are very sparse,

and geologic evidence may not be well preserved, but there are often multiple sources of data indicating the presence of a possible tsunami source region. For historic earthquakes, this would include seismograms and macroseismic observations. For landslides, this would include seafloor mapping and age-dating of deposits. Deterministic hydrodynamic modeling can then assess the tsunami potential from these sources.

C. Conduct slope-stability and post-failure analyses for landslide sources, using the morphological and geotechnical parameters for a potential source region to better assess potential tsunami generation effectiveness.

# 5. Tsunami Dynamics

*by Vasily Titov*

The evolution of earthquake-generated tsunami waves has three distinctive stages: generation, propagation, and inundation (Fig. 5-1).

## 5.1 Generation

The generation stage of tsunami evolution includes the formation of the initial disturbance of the ocean surface due to a geophysical source. This initial water-surface disturbance evolves into a long gravity wave radiating from the source. The modeling of the initial stage of tsunami generation is closely linked to studies of the various source mechanisms. The hydrodynamic part of the tsunami generation process is usually studied with linear models, since the formation of the gravity wave from the initial water disturbance is a fairly slow process that takes tens of seconds to minutes. Therefore, wave generation is driven primarily by hydrostatic forces, and non-linear effects are negligible.

### *5.1.1 Co-seismic deformation sources*

When an earthquake source is located beneath the seabed, part of the earthquake energy is transmitted into the water body. If the amount of this energy is large enough, the earthquake can generate long gravity waves on the surface of the water, i.e., tsunami waves. Studies show that the amount of energy transferred into tsunami wave generation is not more then 10% of the total energy released by the earthquake (Iida, 1956; Gusiakov, 1976; Gusiakov, 1978). The amount of energy transmitted is highly dependent on the earthquake source mechanism; for typical tsunamigenic earthquakes, only about 1% of the total released energy is contributed to tsunami wave gen-

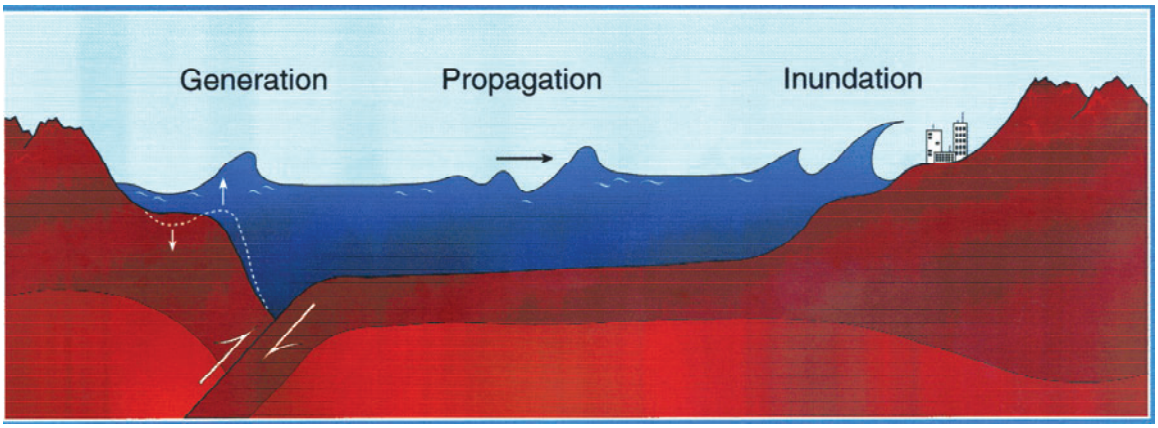


**Figure 5-1:** Schematic representation of three stages of tsunami evolution.

eration, which implies that only strong earthquakes with $M_w$ greater than 6.8–7.0 can generate a significant tsunami.

A typical model of the tsunami generation process is based on an elastic model of the earthquake source (e.g., Gusiakov, 1972). The model assumes compressibility of a liquid layer (the ocean) and elasticity of the underlying layer (earth crust). Poddyapolsky (1968) first applied the elastic model to the tsunami generation problem. Assuming compressible fluid, he was able to find approximate solutions for the far-field displacement due to a point source. A similar approach was later developed by Gusiakov (1972), Yamashita and Sato (1974), and Ward (1980). These authors investigated the dependence of tsunami generation on basic source parameters such as depth, source mechanism, rupture velocity, and duration of the displacement. The very general conclusions based on this theory were that (1) large tsunami waves are produced by earthquakes with a shallow, thrust-type source mechanism with low-angle fault plane and that (2) the duration of the source motion affects tsunami wave generation only if the motion persists for more than several minutes. The latter implies that the tsunami source can be considered in most cases to be an instantaneous movement of the seafloor without introducing substantial error into the tsunami evolution model.

One of the basic limitations of the elastic model is the assumption of a flat bottom; this assumption is made because the solution of a fully coupled system with variable interface between the ocean and earth crustal layers becomes very complex. On the other hand, ocean depth variation is a major factor in tsunami wave propagation. To overcome this limitation, the following approach is used. The elastic model is used only as the first step in tsunami wave modeling, to provide either the initial water-wave field displacement or the ocean bottom deformation due to the earthquake. Since the duration of the source movement is very short compared to the periods of long gravity water waves, the ground motion during an earthquake does not significantly affect the evolution of the tsunami wave. Then, tsunami wave evolution can be modeled separately from the seismic process. Thus, tsunami wave simulation is split into two parts:

1. Calculation of the static bottom displacement for an elastic half-space with an inner seismic source,

2. Calculation by a hydrodynamic model of tsunami wave propagation for an incompressible inviscid ocean.

The results of the first part of the modeling are thus used as initial conditions for hydrodynamic modeling. The static bottom displacement is usually calculated using the elastic model without consideration of the ocean layer. This approach has become a standard technique since Mansinha and Smylie (1971) published a formula for the surface deformation calculation; the formulation was later improved by Okada (1985).

Section 4 describes the state of the science in modeling earthquake-generated deformations. These deformations can be used as initial conditions for tsunami propagation models. Since the nonlinear and non-hydrostatic effects during the earthquake do not contribute to generation of the long

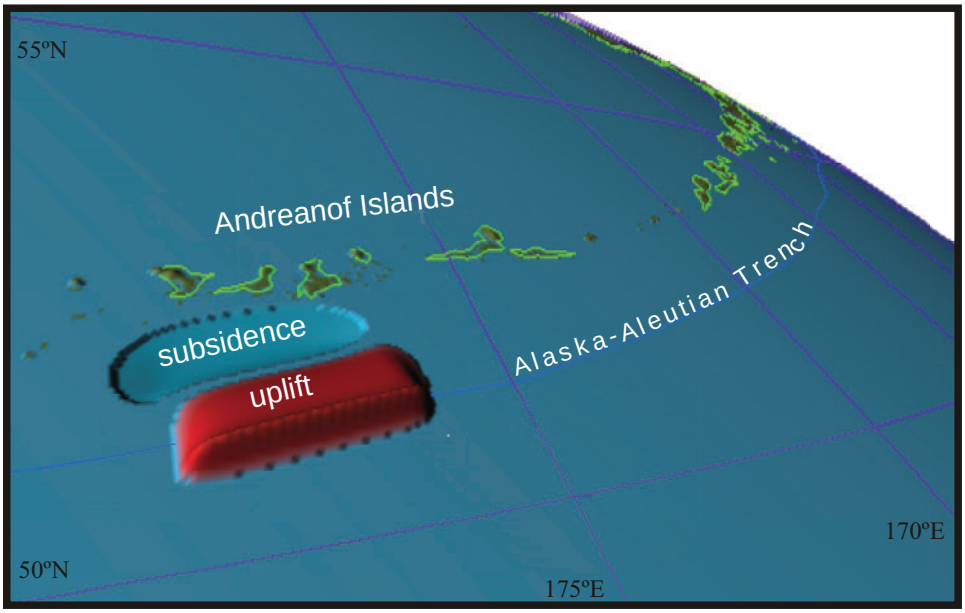


**Figure 5-2:** Model of the 10 June 1996 Andreanov tsunami source, in which the typical ocean bottom deformation pattern is simulated by the elastic model. The initial conditions for the subsequent propagation simulation (shown on the figure) repeats the pattern of the instantaneous bottom displacement.

gravity wave that constitutes a tsunami, the bottom deformation is translated unchanged into the initial water surface displacement for tsunami generation. Because the strongest earthquakes occur on large faults between tectonic plates along the subduction zones, these areas generate most of the tsunamigenic earthquakes (see Section 4.1.1 for a more detailed discussion). Typical large earthquakes at a subduction zone deform the ocean bottom in a dipole-type pattern, in which coastal areas subside and the offshore ocean floor is uplifted (Fig. 5-2).

***5.1.1.1 The NCTR propagation database.*** The exact shape of the deformation depends on the details of the earthquake mechanism, but general patterns persist for all large earthquakes on subduction zones. Moreover, source sensitivity studies (Titov *et al.*, 1999; Gica *et al.*, 2006b) have established that far-field tsunami characteristics are dependent on only a few critical source parameters, namely the location and the magnitude (assuming some typical mechanism for the displacement). For a given fault plane geometry, the magnitude of the corresponding earthquake is linearly dependent on the magnitude of the slip parameter, and the deep water propagation equations are linear to a very good approximation. Therefore, a discrete set of propagation solutions corresponding to unit sources, i.e., fault plane sources with a slip value of 1 m, can provide the basis for constructing a tsunami propagation scenario (see Section 5.2). That is, numerical solutions of tsunami propagation from these unit sources, when linearly combined, can simulate an arbitrary tsunami. This principle is used to construct a tsunami forecast database of pre-computed propagation solutions for unit

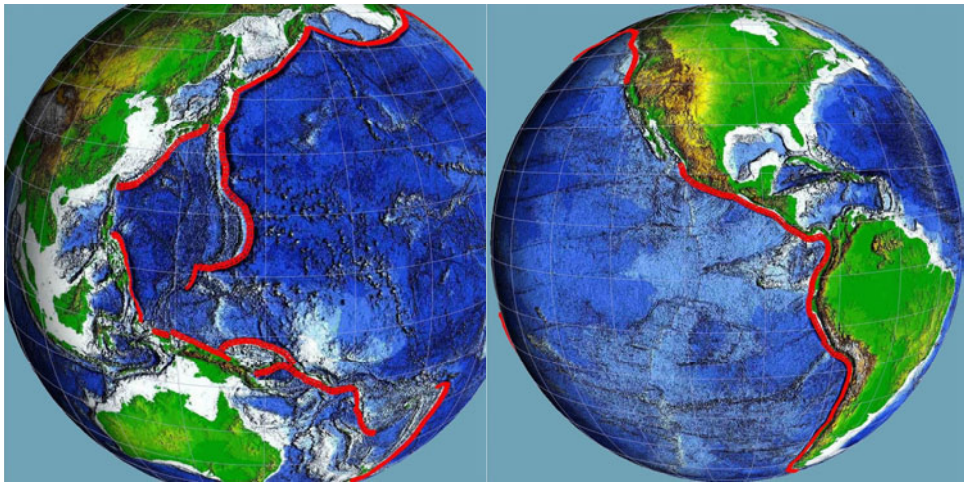

**Figure 5-3:** Schematic locations of unit sources for the forecast tsunami propagation database in the Pacific.

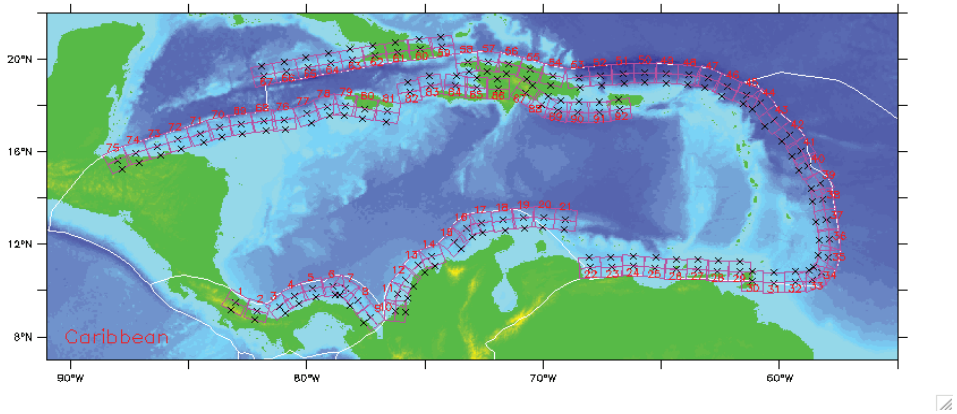


**Figure 5-4:** Locations of unit sources for the forecast tsunami propagation database in the Atlantic Ocean.

sources around the Pacific (Fig. 5-3) and provides preliminary source coverage in the Atlantic (Fig. 5-4). Details of defining the unit sources and use of the propagation database are described by Titov *et al.* (1999), Titov *et al.* (2005), and Gica *et al.* (2006a). The source parameters for the database runs are assembled using the latest estimates of the typical subduction source parameters in the corresponding subduction zone (Kirby *et al.*, 2006). Therefore, the propagation scenarios assembled from the database data provide robust and verified estimates of tsunami propagation (Section 5.2). One use of this database, developed by the NCTR, is to provide boundary conditions for inundation models applied to forecasting and tsunami hazard assessment studies (see Section 5.4.3, below).

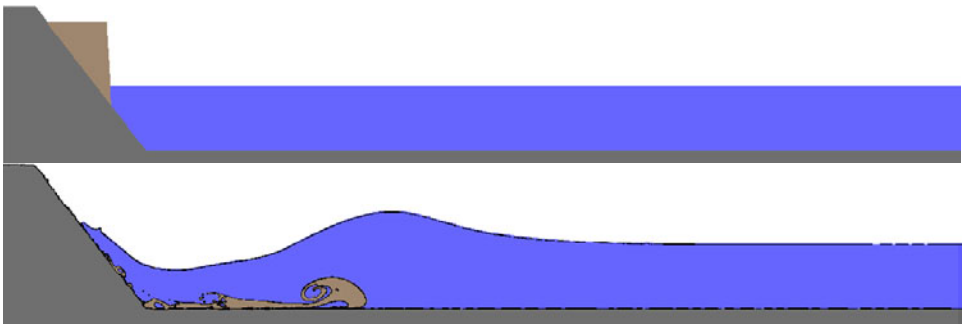

**Figure 5-5:** Example of tsunami generation by a landslide.

### *5.1.2 Landslide tsunami source*

The landslide generation mechanism is fundamentally different from that of seismic sources. Once the main shock occurs, co-seismic deformation of the ocean floor is considered to occur so rapidly that the duration does not affect the dynamics of the ocean surface waves; consequently, tsunami generation by an earthquake can be considered as a classic Cauchy-Poisson problem with initial conditions. In contrast, a landslide can occur hours after destabilization by an earthquake, and have much longer duration than that of an earthquake. Because landslide duration can be significant, the dynamics of landslide/water-wave interaction must be taken into account (Fig. 5-5); this coupling of the moving underwater landslide with water surface gravity waves is much more complex. Furthermore, additional complexity is introduced because the term "landslide tsunami generation" includes a wide range of mass movement that generates long gravity water waves in a way that is dependent on the rigidity of the moving mass and can include processes as disparate, for example, as turbidity flows, rock slides, and ice falls.

Figure 5-6 presents the evolution of a tsunami generated by a landslide off the coast of Papua New Guinea, simulated by Titov and González (2001) with the Method of Splitting Tsunamis (MOST) model and tsunami generation dynamics provided by the landslide model of Jiang and Leblond (1992) and Jiang and Leblond (1994). This event, in which an underwater landslide is suspected of playing a major role, has motivated an increase in studies of landslide tsunami generation. Nonetheless, this topic has been studied much less than earthquake tsunami generation and most studies consider either idealized slide parameters or one-dimensional dynamics. Some results and overviews of existing models can be found in Jiang and LeBlond (1992), Watts (1998), and Fine *et al.* (1999). Section 4.2 provides additional discussion of landslide dynamics and descriptions of landslide models and associated source parameters.

## 5.2 Propagation

Tsunamis are long gravity waves that are generated in water bodies by abrupt geophysical events such as earthquakes, landslides, or volcanic erup-

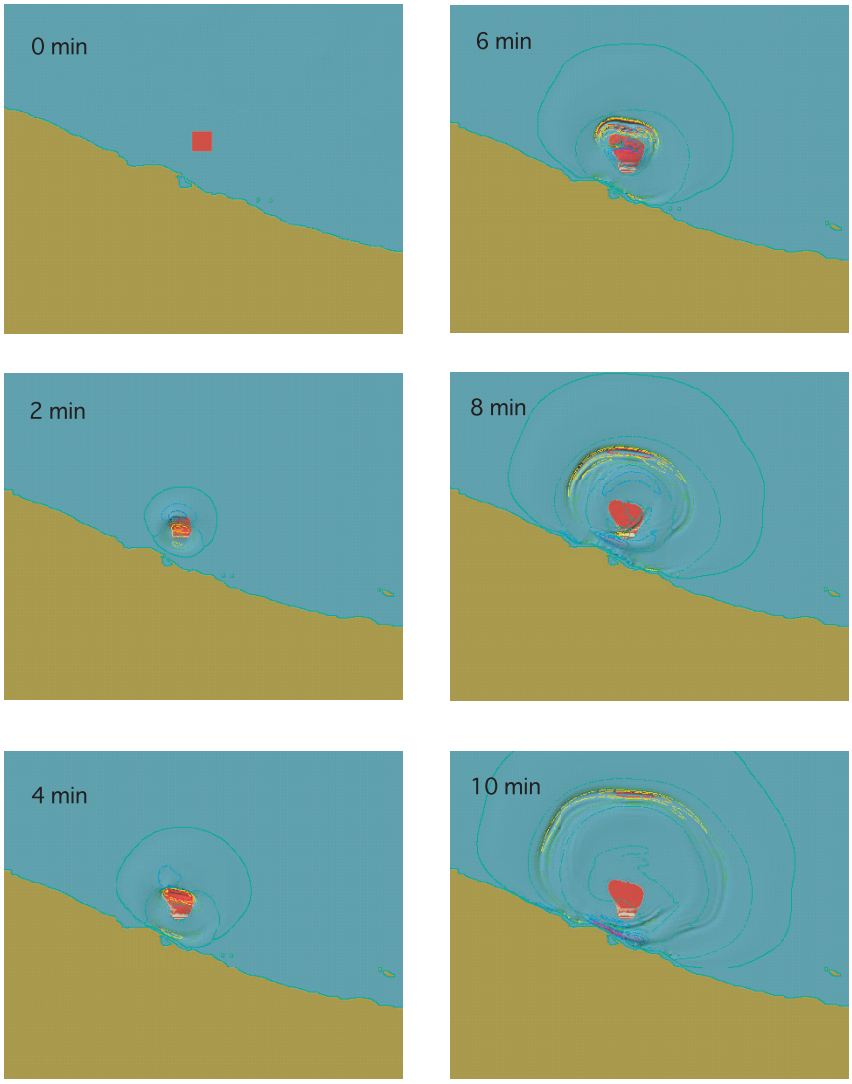


**Figure 5-6:** Example of tsunami generation by a landslide. One of several models of the 17 July 1998 Papua New Guinea tsunami considered by Titov and González (2001).

tions. Sometimes these processes work in conjunction to enhance the amplitudes of the tsunamis. There is also evidence that huge tsunamis have occurred in the geological past when asteroids struck the earth. Tsunamis are called long waves because their wavelengths (the distances between successive wave crests) are much longer than the water depth.

Tsunamis have such long wavelengths (tens to hundreds of kilometers in the deep ocean) because the abrupt bottom movements that generated them have large horizontal scales. Smaller source events tend to have smaller spatial scales, and the tsunamis generated are usually significant only near such sources. However, the ground movements associated with major subduction earthquakes can have finer scale structure. Localized areas of stronger

**Table 5-1:** Representative tsunami phase speed $c = \sqrt{gd}$ based on long gravity waves, where $g$ is the acceleration of gravity ($g = 9.8$ m/s$^2$) and $d$ is the local water depth in meters.

| Depth (m) | Phase Speed (m/s) | (km/hr) |
|---|---|---|
| 50 | 22 | 80 |
| 100 | 31 | 113 |
| 500 | 70 | 252 |
| 1000 | 99 | 356 |
| 2000 | 140 | 504 |
| 3000 | 171 | 617 |
| 4000 | 198 | 713 |
| 5000 | 221 | 797 |
| 6000 | 242 | 873 |

ground movement, called asperities, often occur. Indeed, model simulations of tsunamis are used to estimate finer scale details of the source by tuning the simulation source to tsunami observations from coastal tide gages and offshore pressure gages.

Multiple reflections and partial wave trapping, especially near the source, produce an extended wave train of many waves, even though the original source was a single impulse. Trapped waves are produced by refraction and reflection of the outgoing wave back to the coast due to the sloping bottom profile and, therefore, slower wave propagation speeds near the coast. The later waves of a tsunami form very complicated patterns in which it is difficult to determine the relationship of a later wave to the initial source.

The speed at which tsunami waves propagate is given by the long wave formula (Table 5-1). As indicated in Table 5-1, the speed of these waves depends only on the depth, not on the period of the wave—i.e., these waves are non-dispersive—and they travel across the deep ocean at hundreds of kilometers per hour. Hence, it takes a number of hours for a tsunami to traverse a major ocean, whereas the same tsunami impacts the local coast within a few minutes. The period $T$ of a tsunami (the time elapsed between the passage of two successive wave crests) is determined by the wavelength $\lambda$ and the phase speed $c$ through the relationship $\lambda = cT$. Typical periods of trans-oceanic tsunamis range from about 2 to 90 min.

If the oceans were of constant depth, the first waves of trans-oceanic tsunamis would arrive at an impact site by a great circle route on the globe. However, broad scale variations of the water depth cause the tsunami waves to refract with a tendency for the wave crests to turn toward shallower water. Using wave ray-tracing methods and coarse bathymetric grids, travel time maps were constructed by tsunami warning centers to predict when tsunamis would arrive at impact sites from the major source areas around the Pacific Ocean that have a history of producing dangerous tsunamis (Murty, 1997; Shokin *et al.*, 1987).

In the late 1980s and 1990s, high-resolution bathymetric grids became available that enabled the models to simulate trans-Pacific tsunamis much more accurately as they propagated across the Pacific. Using the MOST finite difference model developed by Vasily Titov, he and co-workers in the NOAA Tsunami Research Program began to simulate and analyze numerous tsunamis in the 1990s soon after they occurred. The model used the high-resolution Smith/Sandwell bathymetric grid (Smith and Sandwell, 1997) developed from a combination of altimetric data from satellites and ship-track observations. This bathymetry data (a.k.a. ETOPO2) is available from the National Geophysical Data Center web site, `http://www.ngdc.noaa.gov/mgg/bathymetry/relief.html`.

The model simulations made it immediately apparent that small-scale topographic features in the open ocean were having a major effect on tsunamis as they propagate across some regions of the Pacific. Figure 5-7 shows an example of tsunami wave scattering in the North Pacific that occurred in the model waves from the 1996 Andreanov Islands Earthquake in the western Aleutians after they propagated southward and struck the Emperor Seamount Chain, the Northwest Hawaiian Ridge and the Hawaiian Islands. Also contributing to the scattering are the Musician Seamounts and Hess Rise northwest of Hawaii, and probably the Shatsky Rise to the west of the Emperor Seamount Chain. In simulations of several trans-Pacific tsunamis, concentric rings of tsunami waves emanated from Kinmei Seamount (Fig. 5-7) at the southern end of the Emperor Seamount Chain. Apparently a very effective scatterer, the seamount has a broad shallow top. Scattering by mid-ocean topographic features affects not only the amplitudes of tsunamis that have passed through the scattering regions but also the directionality of the tsunamis and the duration of the tsunami wavetrain in time.

Dispersion may be important during propagation of the tsunami wave from the source to the inundation area. This effect changes the wave shape due to the slightly different propagation speed of waves with different frequencies. Dispersive effects may become pronounced if the wave propagates over a distance of three or more wavelengths, as in trans-oceanic tsunami propagation. Such cases are studied with dispersive models such as the Boussinesq model. Near-field or local tsunamis, i.e., those for which the source of the tsunami is within 1000 km of the area of interest, have a very short travel time, 30 min or less, while mid-field or regional tsunami waves have travel times on the order of 30 min to 2 hr. Local tsunamis are not significantly affected by dispersion because the propagation distances are often less than one wavelength. Even in the case of long travel times, dispersion can be taken into account without the use of dispersive terms in the governing equations. Thus, Shuto (1991) suggested that the numerical dispersion of finite-difference algorithms could be used to simulate the dispersive effects of wave propagation. This method allows the use of non-dispersive linear or non-linear equations for wave propagation modeling, that still accounts for dispersive effects.

Simulations of historical events with shallow water-wave approximation using the non-dispersive models show very good comparisons with measurements (Fig. 5-8), suggesting that the process of tsunami propagation is

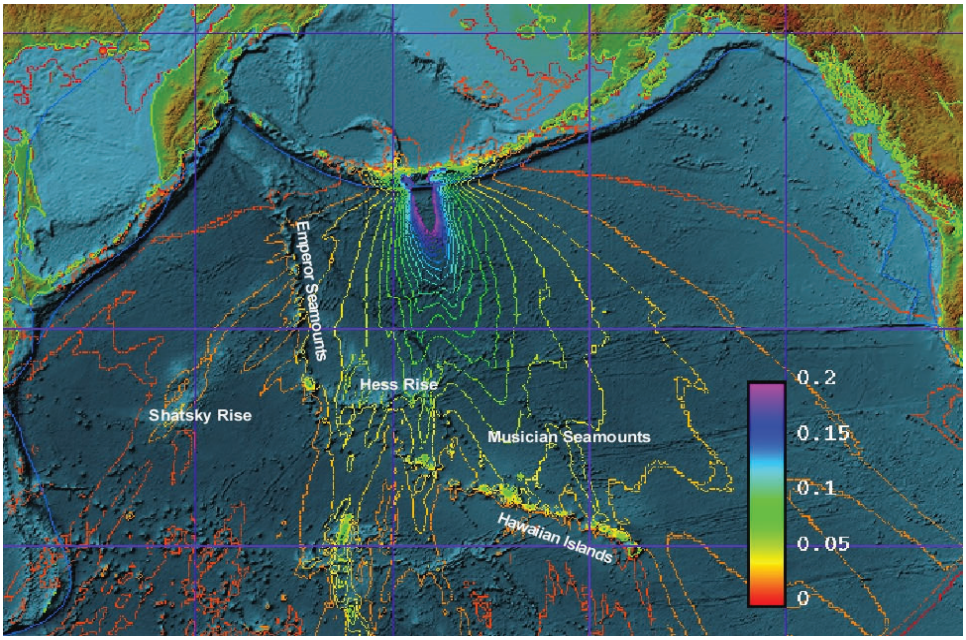


**Figure 5-7:** Maximum computed tsunami amplitudes in the open ocean for the 1996 Andreanov Island tsunami (wave heights in meters).

mostly linear. This linearity of tsunami propagation dynamics can be used to construct an arbitrary tsunami propagation scenario from a set of pre-computed propagation solutions for tsunamis generated by unit sources. A database of such propagation runs for unit sources along potential tsunamigenic areas (see discussion in Section 5.1) has been assembled for the new NOAA Tsunami Forecast System that is now being implemented and tested at U.S. Tsunami Warning Centers. Currently, the tsunami propagation model area includes most of the Pacific and Atlantic coasts, including all U.S. coastlines. In the future, global coverage is planned for the forecast database. This approach allows data assimilation during a real-time forecast without additional, time-consuming model runs. It also provides an offshore forecast of tsunami amplitudes and all other wave parameters around the North Pacific immediately after the data assimilation is completed. The pre-computed propagation scenarios from the database can also be used for tsunami hazard assessment of any location included in the computational area. Appendix D provides an example of the use of this database for tsunami hazard assessment.

The database stores all simulation data for each unit solution, including amplitudes and velocities for each offshore location around the North Pacific. This model output can then drive the high-resolution site-specific inundation model to assess the near-coast dynamics of the wave from the far-field sources. Figure 5-8 presents a model propagation scenario obtained as a combination of two unit-source scenarios from the forecast propagation database. Site-specific tsunami hazard assessment should include inundation modeling to account for local effects.

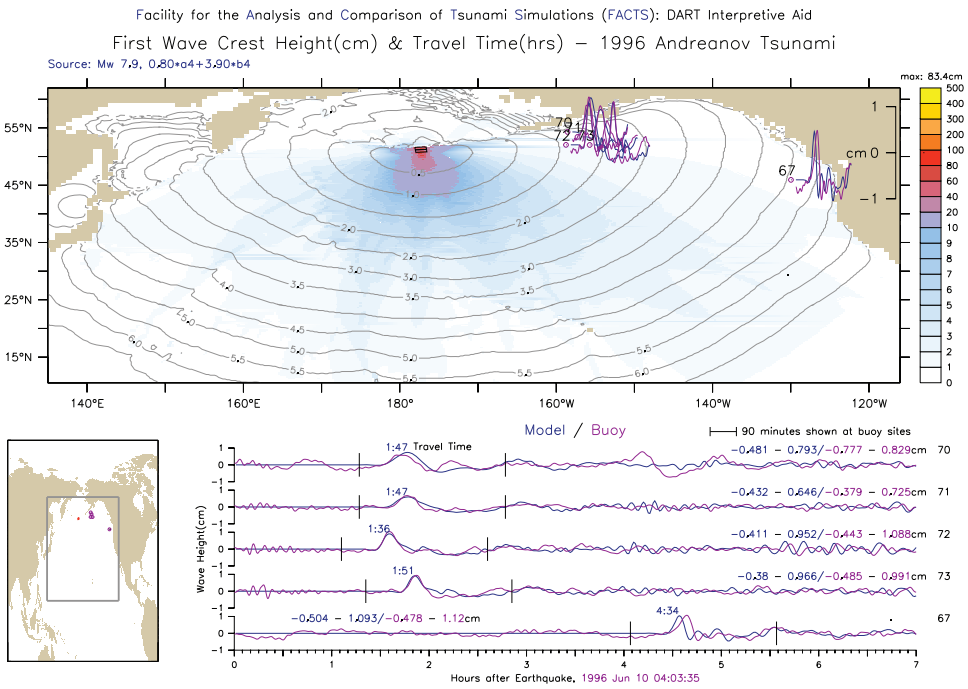


**Figure 5-8:** Comparison of the 1996 Andreanov Island tsunami propagation model (blue line) with deep-ocean bottom pressure recorder (BPR) data (magenta line). Top frame shows the source inferred by the inversion (black rectangles indicate fault planes of the unit sources), maximum computed amplitudes of the tsunami (filled colored contours), travel time contours in hours after the earthquake (solid lines) and locations of the BPRs. Bottom frame shows reference map (left) and comparison of the model (blue) and BPR data (magenta).

## 5.3 Inundation

Models that explicitly include inundation dynamics of tsunami waves near the coast by tracking the instantaneous shoreline during wave interaction with the coast are referred to as *inundation models*. High-resolution inundation modeling is a critical component of a tsunami hazard assessment. Without including inundation (and drawdown) dynamics, the model estimates can be significantly in error.

Inundation modeling is probably the most underdeveloped part of tsunami modeling technology. Until recently, there was a lack of high quality experimental and field data for the long wave runup process to test the performance of models, especially for cases in which the geometry is strongly three-dimensional. This obstacle has been significantly reduced by a series of large-scale runup experiments conducted at the Corps of Engineers Research Center (CERC) (Briggs *et al.*, 1995; Liu *et al.*, 1995; Kânoğlu and Synolakis, 1998) and several post-tsunami field surveys that have provided high quality field data (Satake *et al.*, 1993; Yeh *et al.*, 1993; Imamura *et al.*, 1995; Yeh *et al.*, 1995; Borrero *et al.*, 1997).

### *5.3.1 Runup*

It has been common practice to estimate tsunami runup heights by modeling wave propagation up to the 10 m depth contour and then use the wave height at that depth to infer the maximum runup. These models are referred to as *threshold models*. Field surveys of the 1992–1996 tsunamis demonstrated that these models produce predictions that differ with field observations by a factor ranging from three to ten; this has raised concern because of their ubiquitous use in civil defense planning, and has fueled controversy as to whether the poor predictions were due to inadequacy of the shallow water-wave approximation now used by most hydrodynamic inundation models. New data from laboratory experiments and the field suggest that the evolution of the wave during the last stage of propagation is substantial, and that the wave height can change significantly from 10 m depth to the coastline.

In addition, the runup height itself might not be an accurate indicator of the severity of the wave impact. The magnitude of currents during wave runup determine the scale of coastal destruction due to a tsunami attack. Since the inundation flow is non-linear, flow velocities do not necessarily correlate with the height of the wave. In fact, some preliminary evidence suggests that during overland flow the maximum flow velocities occur when the flow depth is at a minimum. Flow velocity estimates during tsunami evolution are completely missing from "inundation" modeling without runup computations. Tsunami waves are long waves (small depth-over-length ratio) during their entire propagation and even during the runup phase, making the long-wave approximation an attractive and popular method for modeling tsunami generation and propagation. However, the runup process often involves wave breaking, supercritical currents, and overland flows, all complicating the modeling of the process; furthermore, the complexity of the flow near the tip of the climbing or receding wave has raised questions about the applicability of the depth-averaged approximation for runup modeling.

Recent advances in hydrodynamics through validation of model results with large-scale laboratory experiments (Titov and Synolakis, 1993; Yeh *et al.*, 1994; Liu *et al.*, 1995; Briggs *et al.*, 1995) have demonstrated the excellent predictive capabilities of state-of-the-art inundation algorithms, yet the extrapolation of these results to the modeling of actual tsunamis is not unequivocal. In physical models, idealized and well-defined solitary waves evolve over constant depth and then over idealized bathymetry, while in nature the initial wave profile is never known in detail, and the wave propagates over complex bathymetry and climbs topography known only to finite resolution. The latter was not believed to be an important constraint, given that typical tsunami wave scales are larger than microtopographic features, until recent field data demonstrated otherwise (Yeh *et al.*, 1993; Synolakis *et al.*, 1995).

The $M_w = 7.8$ Hokkaido-Nansei-Oki, Japan, earthquake of 12 July 1993 was a fortuitous large-scale experiment which allowed the measurement of high-quality runup data and the inference of fairly unambiguous ground deformation contours due to its proximity to seismic instrument arrays in a locale where high-resolution bathymetry and topography data exist. Hydro-

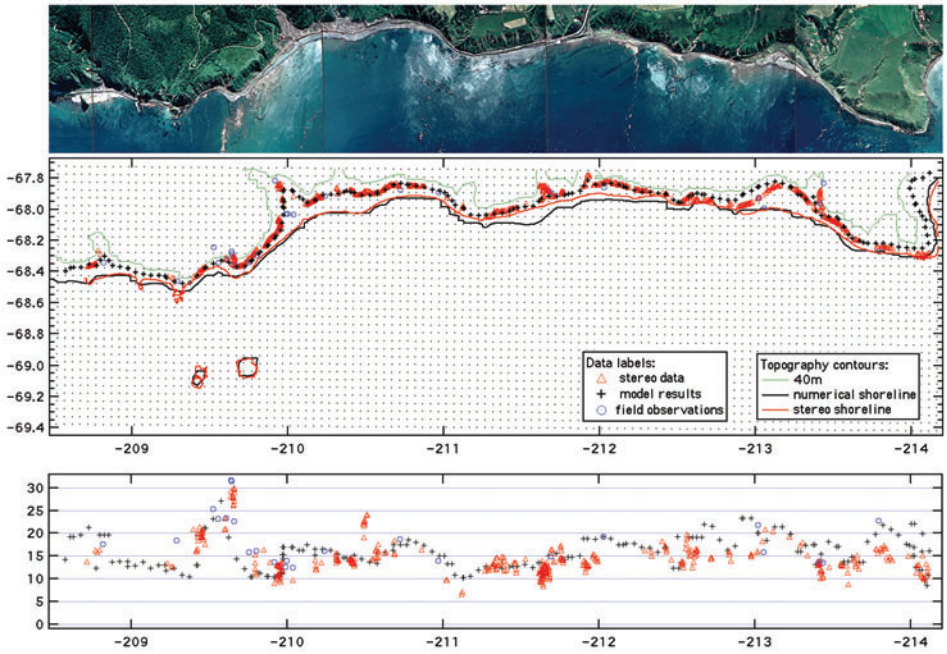


**Figure 5-9:** Comparison of the 1993 Hokkaido-Nansei-Oki, Japan, tsunami inundation model (crosses) with field observations (circles) and stereo photo data (triangles). Top frame shows aerial photo of the modeled area used for stereo analysis of the inundation data. Middle frame illustrates the numerical grid used for the simulation in the same area (dots are computational nodes, contours show topography data) and compares inundation distances. Bottom frame compares maximum vertical runup for the same shoreline locations.

dynamic computations reported to date (Myers and Baptista, 1995; Satake and Tanioka, 1995; Takahashi *et al.*, 1995) using the shallow water-wave approximation (SW) have reproduced the general runup height distribution along the coast of Hokkaido and, to some extent, around Okushiri, but neither the wave current velocities nor the extreme runup values observed in the front of the island; at best (Takahashi *et al.*, 1995), predictions for the extreme measurements have differed by a factor of two from the field data. Furthermore, the region of most extensive devastation did not correlate well with the highest measured runup. Given that the Hokkaido-Nansei-Oki event was not a tsunami earthquake (Schindelé *et al.*, 1995), i.e., an earthquake that produces a tsunami disproportionately large for its size, these differences are intriguing, and they have implications in planning for large tsunami disasters.

Figure 5-10 presents results from numerical experiments that compare the predictions of models with 10 m-contour calculation thresholds for the area shown in Fig. 5-9. For identical grid resolutions, the results show that interrupting the computation at the 10 m depth, a step essentially equivalent to placing reflective "wall"-type boundaries at that depth, underpredicts the runup by a factor of two, as compared with the inundation computations.

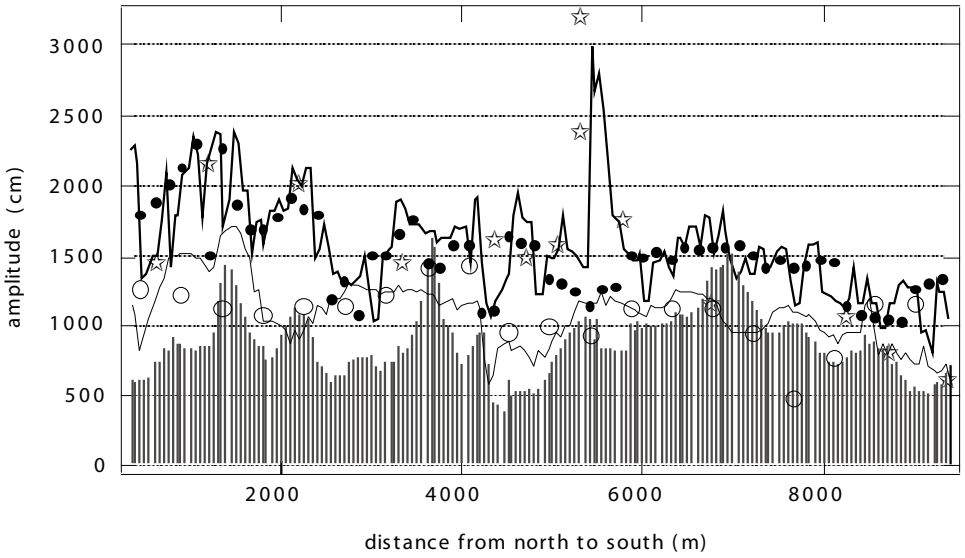


**Figure 5-10:** Comparison of computed runup heights by computations using different grid resolutions and different types of computation thresholds for the 1993 Hokkaido-Nansei-Oki, Japan, tsunami. The heavy line, solid circles and empty circles are model predictions of inundation computed with a 50 m, 150 m, and a 450 m grid, respectively. Vertical bars are inferred runup heights using a 10 m-depth threshold in the 50 m grid calculation, i.e., the wave height assuming the existence of a vertical wall along the 10 m depth contour. The thin line is the maximum wave height at the 10 m-depth contour for the 50 m grid inundation computations. Stars are runup measurements (Shuto and Matsutomi, 1995).

Even the computed maxima at the 10 m contour from the full inundation calculation differ substantially from the computed maxima from the 10 m-threshold "wall" calculations, suggesting that the practice of using the wave-height at the 10 m depth to infer the runup to first order produces substantial errors. Clearly the wave evolves substantially as it propagates from the 10 m depth up the beach to its maximum runup.

These and other published results show that the shallow water-wave approximation and current state-of-the-art solution methods are capable of correctly modeling quantitative tsunami inundation, including extreme runup heights and inundation velocities. It is also clear that even small local bathymetric structures affect amplitude and distribution of the tsunami runup values. Hence, the resolution of the bathymetric data may be more important than the grid resolution. During overland flow, coastal devastation correlates stronger with inundation velocities than inundation heights. This difference, along with the often-substantial wave evolution from the 10 m depth to the maximum runup, suggests caution in interpreting threshold-depth type calculations, as they may miss extreme runup heights.

**Figure 5-11:** Withdrawal of water at Tenacatita Bay before the tsunami inundation during the 9 October 1995 Manzanillo tsunami. The photo was taken 15 min after this local earthquake with epicenter right offshore of this location. The normal water depth at far left of this frame is 5–6 m (Borrero *et al.*, 1997).

### *5.3.2 Drawdown*

In the numerical modeling sense, it is somewhat artificial to treat drawdown separately from runup, since both are part of the inundation process and the same physics apply. Thus, in this sense, much of the preceding discussion on runup modeling applies to drawdown as well. There are significant differences, however.

First, as difficult as it is to obtain accurate runup field measurements for testing and improving models, it is clearly more difficult to acquire reliable drawdown field measurements. The runup phenomena can leave signature effects—marks on buildings, debris lines, etc.—that can be measured after the event. In contrast, drawdown estimates must normally rely on real-time observations and eye-witness reports of questionable accuracy or photos such as that shown in Fig. 5-11 or, rarely, satellite imagery of drawdown, such as that acquired during the 26 December 2004 Indonesian tsunami. Second, the impact of drawdown is clearly very different than that of runup. Drawdown endangers ships in shallow water, causing vessels to ground and even capsize. More importantly for this review, however, is the possibility that drawdown can expose critical water intakes that cool a nuclear power plant.

It is thus critical that inundation computations be an integral part of any THA of a potential NPP site. Without inundation computations, runup is treated inadequately (if at all), and the drawdown effect is ignored al-

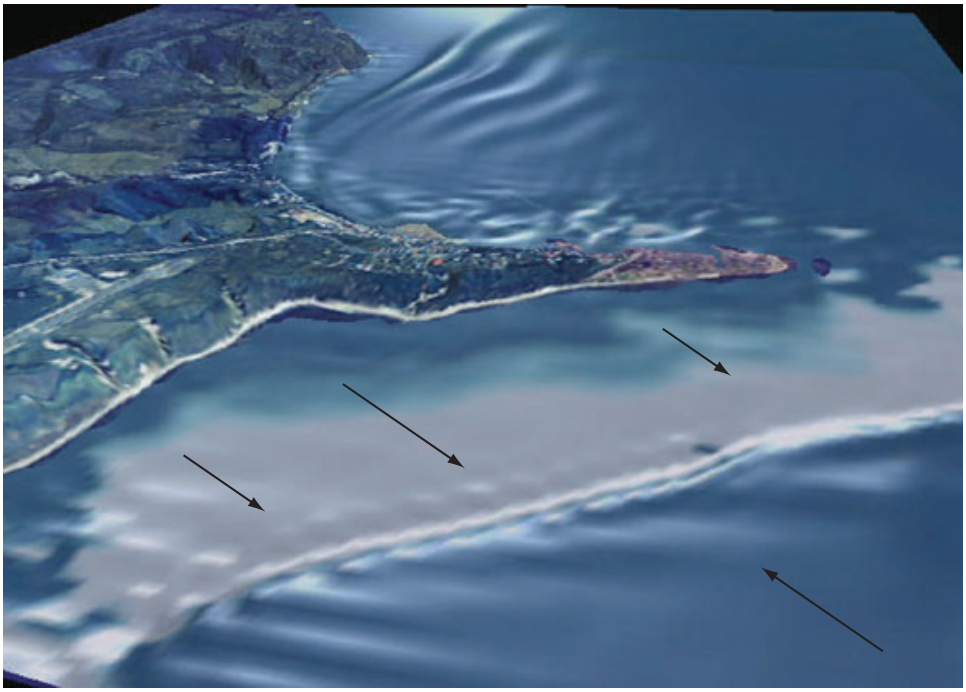

**Figure 5-12:** Draw-down at Aonae penisula during the 12 July 1993 Hokkaido-Nansei-Oki tsunami, as simulated by the MOST inundation model. Frame is at 8 min 30 sec after the earthquake.

together, since it is not included in propagation models, i.e., those models with fixed boundaries. Figure 5-12 is an example of drawdown modeled by the MOST model. The arrows show the direction of the water flow during withdrawal before the second wave attack on the Aonae peninsula. The backflow of a large mass of water forms a hydraulic shock (or standing bore) that is clearly seen forming parallel to the coastline that will then propagate shoreward. Factors affecting the duration of drawdown are discussed in the next section.

### *5.3.3 Duration of inundation*

Duration of the drawdown and runup is related to the tsunami wavelength and, therefore, to the tsunami period. While the wavelength of tsunamis is changing dramatically during propagation from the deep ocean to the coastal area (from hundreds of kilometers in the deep water to just a few kilometers near the shoreline), the tsunami period stays approximately the same.

The drawdown duration is directly proportional to the tsunami period. The water will withdraw from the coastline until the next positive wavefront arrives. Therefore, the duration of the drawdown is roughly equal to half of the tsunami period (see Fig. 5-13), so the withdrawal of the water can continue from 2 to 30 min (see Table 1-2).

The duration of the tsunami flooding, on the other hand, will depend not only on tsunami period, but also on the local coastal topography. A flat

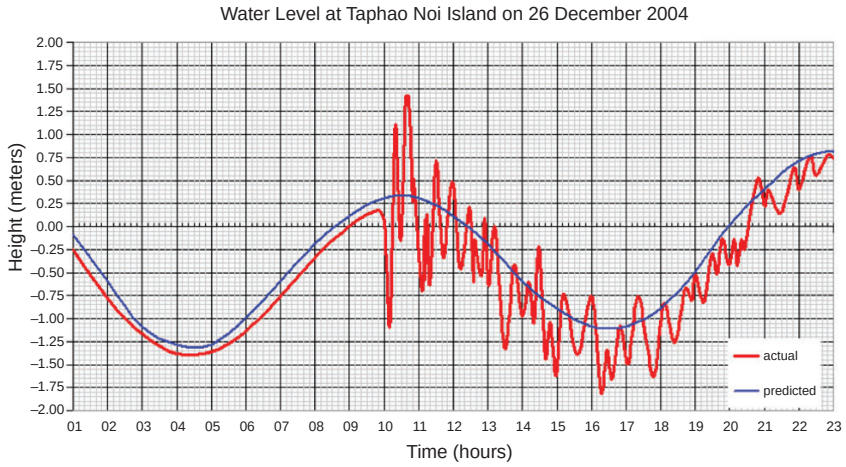


**Figure 5-13:** Tide gage record of the 26 December 2004 Sumatra tsunami near Phuket Island in Thailand. Red line is measurement, blue line is predicted tides at the location. The leading depression wave caused substantial (about 20-min) drawdown at the coasts of Thailand.

topography (common for coastal population centers), if inundated, will drain the water back to the ocean very slowly. Flat coastal plains may not drain all the water from the previous tsunami wave before the next wave transports additional water onto the coast. Local lows of the topography will be flooded by ocean water but would not be able to drain back to the ocean. The scouring effects of the tsunami may create new low topographical features that guide the water withdrawal into narrow channels, which will prolong the drainage of tsunami water. Therefore, the duration of the tsunami flooding may be much longer than the tsunami period on coastlines with flat profiles, and substantial tsunami floods may persist for hours.

### *5.3.4 Bores*

When a tsunami is incident on a river mouth or estuary, the wave often forms a tsunami bore—a steep, turbulent, rapidly moving tsunami wave front. The tsunami bore is formed after tsunami wave breaking, due to nonlinear dynamics of the tsunami front in shallow water near the coast. The nonlinear shallow water-wave theory predicts that a wave will eventually break due to the difference of the propagation speed at the front of the wave ($\sqrt{gd}$, $g$ is acceleration of gravity, $d$ is local depth) and the wave crest ($\sqrt{g(d+\eta)}$, $\eta$ is wave amplitude). Breaking occurs faster in shallow water for large tsunamis, when this difference becomes substantial, and almost certainly occurs as sizable tsunamis propagate up rivers (Fig. 5-14). The same mechanism forms so-called tidal bores at some rivers during the highest tides of the year (some famous tidal bores include Qiantang River, China; Turnagain Arm, Alaska;

Amazon River, Brazil; Severn, Wales). The tsunami (and tidal) bores form a stable wave structure that can propagate long distances upriver (several kilometers), often developing an undular bore structure when the initial wave front separates into a train of smooth or breaking fronts (Fig. 5-15). Similar dynamics are observed for large tsunamis near coasts with a shallow shelf.

## 5.4 Theory and Implementation of Long-Wave Models

Tsunami models often and successfully use the long wave approximation, which assumes that the ratio of depth over the wavelength is small. Long-wave processes such as tides and even near-shore wind waves have also been modeled successfully using the shallow water-wave equations. Tsunami inundation studies can be grouped into two-dimensional models (2-D) and three-dimensional models (3-D). A few different approaches have been used for runup studies of both 2-D and 3-D long-wave inundation problems.

### *5.4.1 Mathematical formulation*

We use the two-dimensional shallow water-wave equations (SW) to model this phenomenon. Despite certain limitations (Liu *et al.*, 1991), these equations have proven capable of modeling many important physical characteristics of tsunami propagation, including wave breaking and bore runup on mild and steep beaches (Peregrine, 1966; Kobayashi *et al.*, 1987). Recent studies (Titov and Synolakis, 1995) have shown that this approximation works reasonably well even in the case of relatively short (length to depth ratio less then 10) breaking waves. Although the equations cannot resolve the specific pattern of the breaking front, they adequately model the overall wave behavior and give an accurate estimation of runup values over a wide range of wave parameters. The shallow water-wave equations are

$$\begin{aligned} h_t + (uh)_x + (vh)_y &= 0 \ , \\ u_t + uu_x + vu_y + gh_x &= gd_x \ , \\ v_t + uv_x + vv_y + gh_y &= gd_y \ , \end{aligned} \tag{5.1}$$

where $h = \eta(x, y, t) + d(x, y, t)$, $\eta(x, y, t)$ is the amplitude, $d(x, y, t)$ is the undisturbed water depth, and $u(x, y, t)$, $v(x, y, t)$ are the depth-averaged current speeds in the $x$ and $y$ directions, respectively.

We do not include bottom friction terms in the model. Although the bottom friction does affect the dynamic of the runup process in the surf zone, we considered several reasons for not using friction terms in this model. The commonly used bottom friction model for shallow water-wave approximation is the Chézy formula with different types of roughness coefficient (see, for example, Packwood and Peregrine, 1981; Ramming and Kowalik, 1980; Kobayashi *et al.*, 1987, Liu *et al.*, 1995). This formula is an empirical relationship developed from steady channel flows, so it might not adequately reflect the dynamics of a rapidly changing runup process. Also, there is no consensus on a proper form of the roughness coefficient in the formula. A number of studies have been devoted to designing a proper roughness coefficient to replace the commonly used Manning's coefficient (Fujima and

**Figure 5-14:** Tsunami bore forming at the Wailua River, Hawaii, during the 1946 Unimak tsunami.


**Figure 5-15:** Tsunami bore propagating along a river in Japan after the 25 September 2003 Hokkaido tsunami.

Shuto, 1989). On the other hand, several studies show that an unsteady flow during runup is not very sensitive to changes in the roughness coefficient value (Packwood and Peregrine, 1981; Kobayashi *et al.*, 1987). Any moving boundary numerical algorithm for wave runup induces a numerical friction near the tip of the climbing wave (except, perhaps, in a Lagrangian formulation), a fact that further complicates the proper choice of the friction coefficient for a numerical model. An argument could be made that the roughness coefficient in the numerical model at the present stage of the science is a quite arbitrary parameter which, even though it can be adjusted to fit given experimental data, is very difficult to determine a priori; this reduces the overall credibility of results for problems other than those in which the model is validated. Since our goal is an estimate of the upper limit of the runup level, and since friction can only reduce this maximum in some cases, we decided not to complicate the model with an additional adjustable parameter.

A variety of boundary and initial conditions can be specified for these equations. To solve the problem of tsunami generation due to bottom displacement, we specify the following initial conditions

$$\begin{aligned} d(x,y,t) &= d_0(x,y,t), t \le t_0 \ , \\ d(x,y,t) &= d_0(x,y,t_0), t > t_0 \ . \end{aligned} \tag{5.2}$$

Usually, $t_0$ is assumed to be small, so that the bottom movement is an almost instantaneous vertical displacement.

To model the wave entering into the computational area through the boundary $y = y_b$, one should specify the following conditions on the boundary

$$\begin{aligned} u(x,y_b,t) &= u_0(x,y_b,t) \ , \\ v(x,y_b,t) &= v_0(x,y_b,t) \ , \\ h(x,y_b,t) &= h_0(x,y_b,t_0) \ . \end{aligned} \tag{5.3}$$

The proper boundary conditions should be specified for open-sea boundary and for land boundary. These boundary conditions depend on the specific numerical or analytical methods applied for the solution of the equations.

### *5.4.2 Moving boundary condition*

To calculate wave evolution on a dry bed, it is necessary to use moving boundary conditions. The Froude number, $u/(gh)^2$, may be greater than 1 near the shoreline point, implying that all characteristic families have the same inclination in this region (Titov and Synolakis, 1995). Hence, it is impossible to use the direct analytical relationships near the tip of the wave as boundary conditions. Therefore, approximations of the boundary values from previous space nodes are usually used. One of the methods is described in Fig. 5-16.

The shoreline algorithm uses a time-dependent space step $\Delta x(t)$ of the last node of the computational area. The objective is to maintain the shoreline boundary point (represented consecutively by A, B, or C on Fig. 5-16)

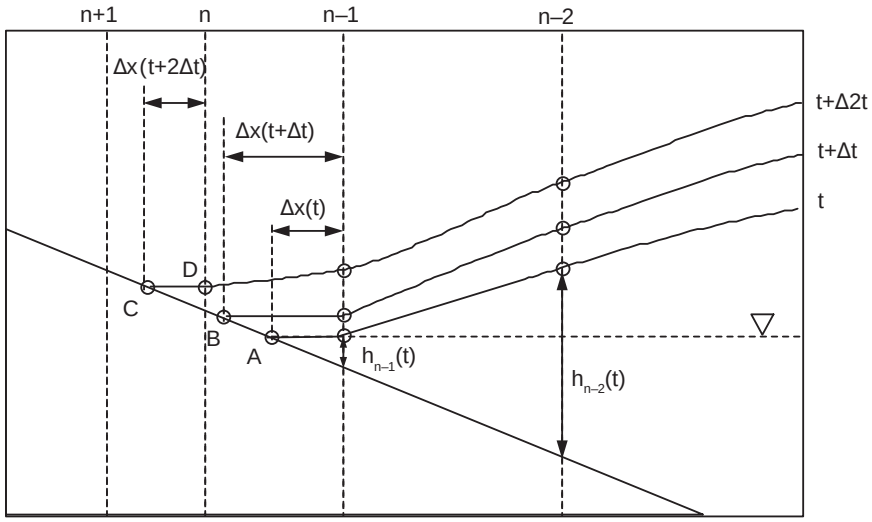


**Figure 5-16:** Definition sketch for the shoreline boundary computation.

on the surface of the beach during the computation. We therefore adjust the length of the last space step $\Delta x(t)$ every time step, so that the shoreline point (A) is at the intersection of the beach with the horizontal projection of the last "wet" point, for example $n-1$ node on Fig. 5-16. The value of the velocity on the shoreline node is equal to the velocity on the previous "wet" point.

We introduce additional grid points as follows. Referring to Fig. 5-16, at the time interval between times $t$ and $t+\Delta t$, there are $n$ grid points $(n-1)$ fixed grid points and the instantaneous shoreline, points A or B, in the computation. At time $t+2\Delta t$, when the shoreline point (C) reaches beyond the next fixed grid point ($n$-th fixed node of the constant bed grid), this $n$-th fixed point is introduced between the shoreline point (C) and the previous internal fixed node $(n-1)$ and $\eta(D)=\eta(C)$. Now, there are $n+1$ grid points in the computational area and we repeat the process. During rundown, we reduce the number of dry grid points sequentially in an analogous manner.

Other implementations of moving boundary conditions for long wave approximations can be found in Yeh *et al.* (1996).

### *5.4.3 Solution methods*

The majority of numerical models for three-dimensional tsunami inundation use the long-wave approximation. The linear shallow water-wave equations can provide analytical results for the runup height of plane waves for simple and complicated 1-D beach profiles (Synolakis, 1986, 1987; Tadepalli and Synolakis, 1994, 1996; Kânoğlu and Synolakis, 1998; Kânoğlu, 1998) and even for 2-D piecewise-linear beaches (Kânoğlu and Synolakis, 1998; Kânoğlu, 1998). Nevertheless, to model the flow evolution on a dry bed (depth below zero) with complicated 2-D topography, where the waves experience breaking and overflow, non-linear equations are essential for modeling.

Most long-wave inundation models utilize classic non-linear shallow water-wave equations (NSW), which may include bottom friction terms and/or viscosity terms. The major difference between the models is the method of numerical solution of the equations.

The finite-difference method has been widely used for tsunami propagation modeling and it has become a natural choice for several tsunami inundation models. Shuto (1991) used the staggered explicit leap-frog finite-difference scheme to simulate the inundation of the 1983 Japan Sea tsunami. This model has been refined by Imamura *et al.* (1995) and Takahashi *et al.* (1995) to develop what is now the most widely used model for tsunami inundation. Several numerical runup models were produced based on the same technique (Liu *et al.*, 1991). Takahashi presented the model at the 2004 International Long-Wave Runup Workshop to simulate the Hokkaido-Nansei-Oki tsunami, which was one of the four benchmark problems. The inundation calculations produced fairly correct results in the lee of the island, but at the front, they differed by a factor of two from the field data.

The other often-used method to solve the shallow water-wave equations is the finite-element technique. The advantage of this method is the usage of an adaptive non-structured numerical grid for the computations, which makes possible the resolution of the changing wavelength of the tsunami with enough grid points throughout the computational domain. The disadvantage is a rather complex and computationally expensive way of solving the discretized equations, as compared with the finite-difference method. Myers and Baptista (1995) used the finite-element method to model the benchmark problem of solitary wave runup on a conical island. The results show that the method appears to be very sensitive to changing the model parameters. The model has to be calibrated before the results fit well to the laboratory data. Another finite-element inundation model presented recently is that of Takagi (1996) to solve the same benchmark problem. The model showed a good agreement with the laboratory data.

Bottom friction is often used in the models to account for sub grid roughness of digital bathymetry and topography. This formula is an empirical relationship developed from steady channel flows, so it might not reflect the dynamic of the rapid runup process adequately. Also, there is no consensus on a proper form of the roughness coefficient in the formula. A number of studies are devoted to designing a proper roughness coefficient instead of the commonly used Manning's coefficient (Fujima and Shuto, 1989). On the other hand, several studies show that an unsteady flow during runup is not very sensitive to changes in the roughness coefficient value (Packwood and Peregrine, 1981; Kobayashi *et al.*, 1987). Any numerical algorithm with a moving boundary for the wave runup induces a numerical friction near the tip of the climbing wave (except, perhaps, a Lagrangian formulation). This complicates the proper choice of the friction coefficient for any numerical model. As discussed above, however, the roughness coefficient in the numerical model at present appears to be a quite arbitrary parameter that is adjusted to fit a given experimental data, but is very difficult to be determined a priori. Given that extrapolation is always risky, this dramatically reduces the predictive ability of a numerical model with ad-hoc parameters.

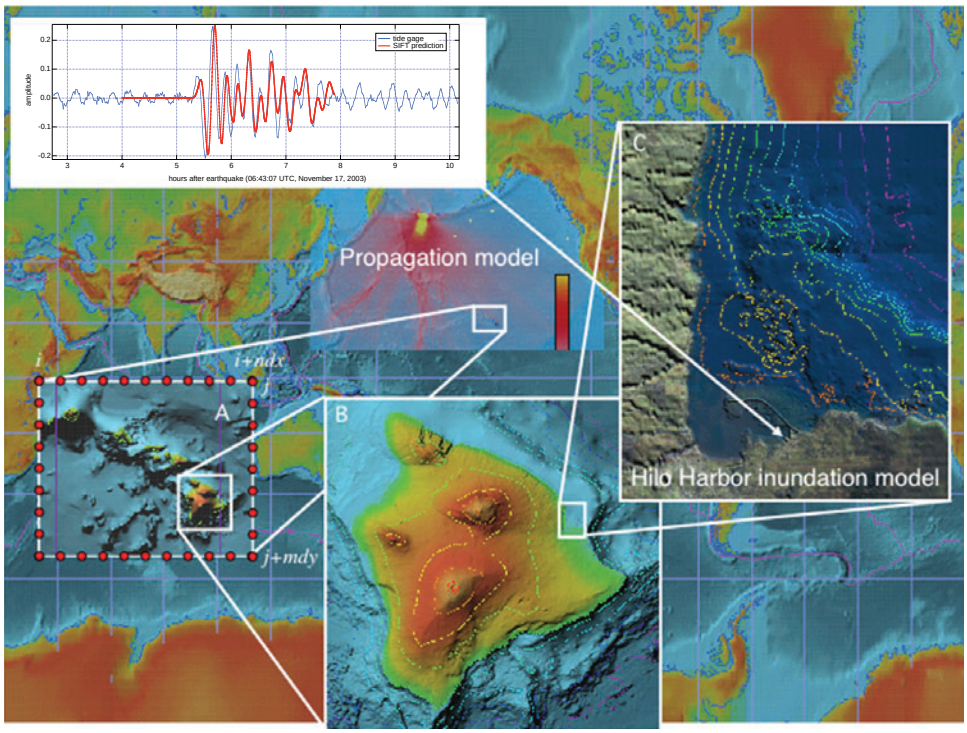


**Figure 5-17:** Example of model setup for tsunami inundation model of Hilo Harbor using propagation and inundation models. Model results of the 2003 Rat Island tsunami simulation obtained from a pre-computed database of propagation scenarios and inundation models with telescoping grids are shown. Comparison of the model results (red line) and measured signal (blue line) at Hilo gage are shown in the inset graph. The red dots on Grid A are locations where the boundary conditions are provided by the Propagation Model grid solution; these boundary conditions are required for computations in the nested grid system (grids A, B, and C, in this figure) that carry the tsunami waves onto the coast where inundation occurs (see Table 5-2 and discussion of boundary conditions).

Since the goal is the evaluation of the maximum runup level and the maximum inundation velocities, which the friction can only reduce, it may be practical not to complicate the model with additional, adjustable parameters. Therefore, using the least possible friction coefficients (or no-friction depth-averaged approximation) may be a conservative way to use tsunami inundation models for the tsunami hazard analysis.

Tsunami generation, propagation and inundation models can be combined for simulation of tsunami dynamics from generation to inundation. If a finite-difference method on a structured grid is used, several nested numerical grids would allow one to "telescope" from a coarse-resolution propagation model (resolution of about 4 nautical miles) to a high-resolution inundation model with a model grid of at least 50 m resolution (Fig. 5-17). This method decouples the propagation modeling and the high-resolution inundation simulation. It provides flexibility to use input from one propagation model for

**Table 5-2:** List of variables for boundary conditions along the nested grid boundaries required for continuing the simulation of tsunami dynamics into the higher resolution rectangular area. Here, $i, j$ are indices along longitude and latitude; $\Delta x$, $\Delta y$ are space steps along longitude and latitude of the outside (propagation) computational grid; $n, m$ are dimensions of the area of interest of the outside (propagation) grid.

| | | | |
|---|---|---|---|
| top | $u_{i,j}, v_{i,j}, h_{i,j}$ | ... | $u_{i+n\Delta x,j}, v_{i+n\Delta x,j}, h_{i+n\Delta x,j}$ |
| left | $u_{i,j}, v_{i,j}, h_{i,j}$ | ... | $u_{i,j+m\Delta y}, v_{i,j+m\Delta y}, h_{i,j+m\Delta y}$ |
| right | $u_{i+n\Delta x,j}, v_{i+n\Delta x,j}, h_{i+n\Delta x,j}$ | ... | $u_{i+n\Delta x,j+m\Delta y}, v_{i+n\Delta x,j+m\Delta y}, h_{i+n\Delta x,j+m\Delta y}$ |
| bottom | $u_{i,j+m\Delta y}, v_{i,j+m\Delta y}, h_{i,j+m\Delta y}$ | ... | $u_{i+n\Delta x,j+m\Delta y}, v_{i+n\Delta x,j+m\Delta y}, h_{i+n\Delta x,j+m\Delta y}$ |

several inundation coastal sites, or several propagation scenarios from precomputed database for an inundation model of a particular coastal location.

The interaction between the propagation and the higher resolution inundation models is performed at the grid boundaries. The values of $u$, $v$, and $h$ from the previous computation grid are interpolated into the finer resolution grid and applied as boundary conditions for computation of the tsunami in the interior of the grid.

The values of computed variables from the propagation run listed in Table 5-2 will define the solution inside the grid A (Fig. 5-17). Those values need to be interpolated into the higher resolution grid along the corresponding boundary. This set of values defines the input wave from the outside (propagation) grid. The higher resolution model inside the grid will simulate the tsunami dynamics with the resolution needed to account for shorter wavelength near the target coastline.

### *5.4.4 Tsunami/current interactions*

All waves, including tsunamis, are transformed by propagation through a non-uniform medium. Thus, just as changes in water depth and land height induce changes in the amplitude and direction of tsunami waves, so, too, do changes in currents. As might be expected on physical grounds, the degree of tsunami wave transformation by currents is governed primarily by the relative speed of each. Thus, since tsunami speed increases with depth and current speed decreases with depth, wave transformation is generally larger in shallow coastal areas and inlets than in the deep ocean.

For insight into the effect of currents on tsunami wave height, simple one-dimensional linear theory can provide estimates of the amplification. Peregrine (1976), reviews the detailed physics and mathematics of wave-current interaction theory. González (1984) provides a brief summary of the most important concepts that lead to the wave height transfer function in one dimension:

$$T\left(U,d,\sigma\right)=\frac{\eta}{\eta_0}=\left(\frac{U_0+c_{g0}\cos\theta_0}{U+c_g\cos\theta}\right)^{1/2}\left(\frac{\sigma}{\sigma_0}\right)^{1/2}\quad,\tag{5.4}$$

where $U(x)$ is the current speed, $c_g(x)$ is the wave group speed, $\theta$ is the angle

between the current and wave directions, $\sigma$ is the wave frequency, and the subscript zero indicates initial conditions at some point $x = x_0$.

To estimate the maximum effects, we assume that tsunami propagation and current flow are both in the $x$-direction, so that $\theta = \theta_0 = 0$. We also note that, to a good approximation, tsunami frequency is constant, i.e., $\sigma = \sigma_0$, and the group speed is equal to the long wave phase speed, i.e., $c_g = c = (gd)^{1/2}$. Equation 5.4 then simplifies to

$$T\left(U, d; U_0, d_0\right) = \frac{\eta}{\eta_0} = \left(\frac{U_0 + \sqrt{gd_0}}{U + \sqrt{gd}}\right)^{1/2} , \tag{5.5}$$

where we formally identify $U_0$ and $d_0$ as parameters. Note that negative or positive values of $U$ indicate an opposing or following current, respectively. This means that the denominator can become zero when the speed of a tsunami is equal to that of an opposing current; the location of this occurrence is known as a *stopping point* (Peregrine, 1976; González, 1984). Note also that in the absence of currents, i.e., when $U_0 = U = 0$, this expression reduces to

$$T_d = \frac{\eta}{\eta_0} = \left(\frac{d_0}{d}\right)^{1/4} , \tag{5.6}$$

which governs the effect of shoaling, and is known as Green's Law.

Table 5-3 evaluates equation 5.5 for the parameter values $U_0 = 0$ and $d_0 = 5000$ m and an illustrative range of $U$ and $d$ values; the table also isolates the effects of currents by subtracting the shoaling component to form $T_U = T - T_d$. We see that $T_U$ is positive or negative for a negative or positive current, respectively, so that an opposing current increases the tsunami height, while a following current decreases the tsunami height. For deep ocean and offshore locations deeper than 300 m, the effect is less than 3%, even for an improbably high current speed of 3 m/s. In shallower coastal waters, where it is possible for tidal currents to attain 2–3 m/s, especially near coastal inlets, the effect of such currents on the amplification factor can approach 7%. The table does not extend to water depths less than 50 m because nonlinear effects may begin to be important at this point.

At this time, the MOST model does not include tsunami/current interactions, and the author is unaware of other existing tsunami models that do include these effects. Future research is needed to include tsunami/current interaction, especially for those models applied to shallow coastal regions with strong currents, where the effects are greatest.

## 5.5 Recommendations

Tsunami modeling technology includes many technical and scientific issues that continue to be addressed and improved. An effort to systematically document these issues and provide guidance on standards and procedures for assessing the accuracy and reliability of individual numerical models is presented by Synolakis *et al.* (2006). The number of specific scientific and technical recommendations provided in that report are too numerous

**Table 5-3:** Tsunami amplification factors $T$, $T_d$, and $T_U$ as a function of depth $d$ and current speed $U$, for initial current and depth values set to $U_0 = 0$ and $d_0 = 5000$ m. See text for discussion.

| **Opposing current $U$, with $U_0 = 0$ and $d_0 = 5000$ m** | | | | | | | | |
|---|---|---|---|---|---|---|---|---|
| | **$U = -1$ m/s** | | | | **$U = -3$ m/s** | | | |
| **$d$** | **$T$** | **$T_d$** | **$T_U$** | **$\%T_U$** | **$T$** | **$T_d$** | **$T_U$** | **$\%T_U$** |
| **5000** | 1.0 | 1.0 | 0.00 | 0.2% | 1.0 | 1.0 | 0.01 | 0.7% |
| **3000** | 1.1 | 1.1 | 0.00 | 0.3% | 1.1 | 1.1 | 0.01 | 0.9% |
| **1000** | 1.5 | 1.5 | 0.01 | 0.5% | 1.5 | 1.5 | 0.02 | 1.5% |
| **500** | 1.8 | 1.8 | 0.01 | 0.7% | 1.8 | 1.8 | 0.04 | 2.2% |
| **300** | 2.0 | 2.0 | 0.02 | 0.9% | 2.1 | 2.0 | 0.06 | 2.8% |
| **100** | 2.7 | 2.7 | 0.04 | 1.6% | 2.8 | 2.7 | 0.14 | 4.9% |
| **50** | 3.2 | 3.2 | 0.07 | 2.3% | 3.4 | 3.2 | 0.24 | 7.0% |

| **Following current $U$, with $U_0 = 0$ and $d_0 = 5000$ m** | | | | | | | | |
|---|---|---|---|---|---|---|---|---|
| | **$U = 1$ m/s** | | | | **$U = 3$ m/s** | | | |
| **$d$** | **$T$** | **$T_d$** | **$T_U$** | **$\%T_U$** | **$T$** | **$T_d$** | **$T_U$** | **$\%T_U$** |
| **5000** | 1.0 | 1.0 | 0.00 | −0.2% | 1.0 | 1.0 | −0.01 | −0.7% |
| **3000** | 1.1 | 1.1 | 0.00 | −0.3% | 1.1 | 1.1 | −0.01 | −0.9% |
| **1000** | 1.5 | 1.5 | −0.01 | −0.5% | 1.5 | 1.5 | −0.02 | −1.5% |
| **500** | 1.8 | 1.8 | −0.01 | −0.7% | 1.7 | 1.8 | −0.04 | −2.1% |
| **300** | 2.0 | 2.0 | −0.02 | −0.9% | 2.0 | 2.0 | −0.05 | −2.7% |
| **100** | 2.6 | 2.7 | −0.04 | −1.6% | 2.5 | 2.7 | −0.12 | −4.7% |
| **50** | 3.1 | 3.2 | −0.07 | −2.2% | 3.0 | 3.2 | −0.19 | −6.6% |

to include here, but the report is provided as Appendix C, for convenient reference.

In addition to the recommendations in Synolakis *et al.* (2006), we make the following recommendations that are specific to assessment of a particular NPP site,

A. Require that the tsunami model use boundary conditions provided by the NCTR database in cases where it is possible and appropriate. This approach takes advantage of the well-tested accuracy and reliability of the NCTR computations, and eliminates the additional effort required to develop a basin-wide model. But more importantly, some measure of consistency with official NOAA products is achieved, since these are the same boundary conditions used by NOAA tsunami models for both real-time forecasting and THA studies (see the discussion of real-time THA for NPPs, Section 8.4).

B. Require that tsunami models demonstrate acceptable accuracy and reliability for application to the general region of the NPP site by documented testing against all available historic and prehistoric tsunami data for the region.

# 6. Tsunami Impact Forces

*by Utku Kânoğlu and Costas Synolakis*

Tsunamis can generate large onshore currents that can cause dramatic damage to structures and even move large objects far inland. The 26 December 2004 megatsunami demonstrated tsunami impact on structures in a rather dramatic fashion. However, it does not require a large tsunami to move large objects around. During the 1994 Mindoro Philippines tsunami, in an area where the vertical inundation heights did not exceed 3 m (10 ft), the tsunami floated a 6000 ton generating barge, broke its mooring lines and carried it 1 mile inland down the Baryan River.

## 6.1 Currents and Wave Heights

The evolution of two different waveforms over a simple geometry of sloping beach are shown in Fig. 6-1 (Kânoğlu and Synolakis, 2006). As shown in Fig. 6-1, even for propagation over a simple geometry of sloping beach, the highest velocity does not occur close to the highest inundation depth location. Furthermore, the location of the region of highest velocity depends on the incoming waveform, hence on the particular scenario under study. Therefore, currents cannot be neglected in tsunami hazard assessments, because the associated kinetic energy can be the most destructive aspect of a tsunami and very high currents can be associated with relatively modest wave height. In particular, note that, for certain locales, regions of high currents frequently do not correspond to regions of high wave heights. This frequently occurs in river entrances and adjacent bay areas (see Fig. 27 in Appendix D.) The lack of correspondence between maximum wave heights and currents means that inundation maps of maximum wave height could be dangerously misleading, i.e., the overall tsunami hazard and destructive potential could be seriously underestimated in areas of modest wave height because destructively high currents were not taken into account. A more complete hazard assessment must employ "impact indices" or "impact metrics" that take account of both potential and kinetic energy, i.e., both wave height and current. Therefore, in addition to inundation zones, different impact metrics need to be evaluated in an effort to determine a single hazard zone that best describes tsunami impact on structures for use in evaluating structural safety. This topic is explored in detail in the section "Evaluating Tsunami Impact Metrics" of the report by the Tsunami Pilot Study Working Group (2006). Here, we will present a brief explanation of the background theory that helped motivate the choice of combination of flow parameters, i.e., acceleration, velocity, depth, amplitude, and wave front velocity.

## 6.2 Theoretical Framework

The estimation of impact forces and currents is still far less understood than hydrodynamic evolution and inundation computations. In what follows, different methods and formulae in the literature are described, although

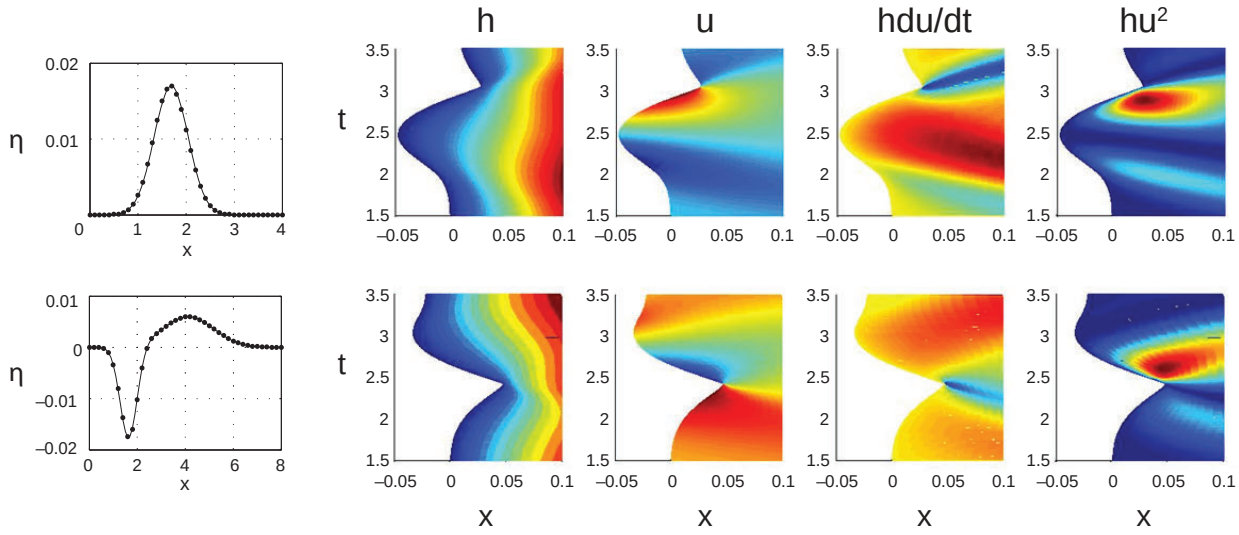


**Figure 6-1:** Evolution over time, $t$, of the total water height ($h$), velocity ($u$), $hdu/dt$, and $hu^2$ as a function of the onshore variable $x$ of a simple sloping beach, as evaluated by Kânoğlu and Synolakis (2006) for two different initial waveforms, i.e., Gaussian and leading-depression Gaussian. The color scale is relative, with blue representing relatively small values and red representing relatively large values.

none has been truly validated by comparisons with field data. In principle, the calculation of wave forces on structures involves the integration of the pressure and of the shear force over the exposed area of the structure during the wave motion. To understand the development of the damage metrics, two of the simplest possible geometries are considered for the calculation of the instantaneous wave force at time $t$.

The first geometry is a cylindrical pile of radius $R$. The force on a cylinder due to shallow water-waves is given by

$$\vec{F}_T(t) = \pi C_M \rho R^2 \frac{d\vec{V}}{dt}(\eta_p + d) + C_D \rho R \vec{V}|\vec{V}|(\eta_p + d) \ , \qquad (6.1)$$

where both $\vec{V}$ and $d\vec{V}/dt$ are depth-independent. Here $\vec{V}$ is the instantaneous horizontal velocity in the direction of wave motion, while $d\vec{V}/dt$ is the instantaneous water particle acceleration. Also, $\eta_p$ and $d$ are the local amplitude and undisturbed water depth at the pile, respectively, with the assumption that they do not vary significantly over the pile diameter. Once the accelerations and current velocities are known, drag $C_D$ and inertial mass $C_M$ coefficients can be determined for the specific shapes of the structures under consideration. Note that if these coefficients cannot be found for transient flows, the equivalent coefficients for steady flows can be used. (In the more general case of objects that do not possess central symmetry, these coefficients depend on the Reynolds number, Re, and the angle of attack. In such cases, the values of Re and the angle of attack that provide the worst credible scenario should be used.) The second geometry considered is

a vertical wall. Hughes (2004) proposed the momentum flux parameter

$$M_t(x,t) = \int_0^{d+\eta(x)} (p_d + \rho u^2) dz \ , \tag{6.2}$$

as a better characterization of the flow kinematics than other formulations. Here $p_d$ is the pressure, $u$ is the horizontal particle velocity, and $\frac{1}{2}\rho u^2$ is the dynamic pressure. Hughes (2004) noted that at the front surface of a perfectly reflecting seawall, $M_t$ is the instantaneous dynamic force. Note that, by performing the integration in the previous equation, the momentum flux parameter $M_t(x,t)$ for shallow water-waves can be rewritten as

$$M_t(x,t) = p_d(\eta_p + d) + \rho u^2(\eta_p + d) \ . \tag{6.3}$$

Here, again, $\eta_p$ and $d$ are the local amplitude and undisturbed water depth at the wall, respectively. Observing that the instantaneous dynamic pressure gradient in $z$ reflects the instantaneous fluid acceleration in $z$, this equation is reminiscent of the force equation for the total force on a pile, equation 6.1.

## 6.3 Impact Metrics

For the purpose of determining tsunami impact zones consistent with both force on a pile and a wall, it is conjectured that tsunami forces can be thought of as consisting of two parts, an inertial component (proportional to depth times acceleration) and another due to the dynamic effects of the moving flow (proportional to depth times velocity squared). Damage metrics of use in planning, and possibly zoning, must identify areas of exceptional force and reflect the distribution of the force over the entire impacted area. Therefore, the following parameters are of interest in assessing tsunami impact:

- $h = \eta_p + d$, the entire water depth, (6.4a)
- $V^2 = u^2 + v^2$, the current speed, (6.4b)
- $d\vec{V}/dt$, the acceleration in the flow direction, (6.4c)
- $hd\vec{V}/dt$, a coefficient for calculation of the inertial component, (6.4d)
- $hV^2$, the momentum flux. (6.4e)

Again, while one might have expected that regions of large flow depths might correlate with regions of large velocities, this is not always the case. For example, as a tsunami evolves over dry land, the flow depth decreases up to the point of maximum runup, and the velocity of the shoreline tip becomes zero. Here, both $h$ and $|\vec{V}|$ are small. During rundown, the flow depth remains small, but the velocity can be substantial, leading to higher $hV^2$ values in regions of the flow field that are unexpected, as suggested in a simple one dimensional setting by Kânoğlu and Synolakis (2006). The acceleration $d\vec{V}/dt$ may diminish during wave run-up, but may be substantial during run-down.

The Tsunami Pilot Study Working Group (2006) report, reproduced here as Appendix D, used detailed inundation computations for both near-field

and far-field scenario events to calculate and compare the distributions of four different damage metrics—$V^2$, $d\vec{V}/dt$, $hd\vec{V}/dt$, and $hV^2$—over the entire Seaside, Oregon, region. Careful examination of these distributions suggests that, while individual differences exist among the different scenarios, the momentum flux represents the most suitable damage indicator for both near-field and far-field events. In contrast to what one might have expected based on 1-dimensional considerations, flow velocities appear to correlate well with inundation depths over the two sand-spits in Seaside, Oregon. Hence, the momentum flux shows a similar distribution as the inundation depths and currents. Overall, while small-scale differences exist, the inertial component appears to have a similar geographical distribution as the momentum flux. Therefore, the momentum flux is recommended for use as a determinant of tsunami impact.

In addition to the tsunami metrics suggested by the Tsunami Pilot Study Working Group (2006), the minimum run-down location and event duration need to be added as tsunami impact metrics. As shown in Fig. 6-1, maximum momentum fluxes occur around the minimum run-down locations. Minimum run-down location might therefore be an important design consideration for nuclear reactor water intake structures. Event duration estimates are also crucial, as discussed in Appendix D and Section 8, below. Tsunamis are a series of waves and often get trapped in closed bays or on the continental shelf, resulting in sea level oscillations that may persist for several hours. During the 1993 Okushiri inundation, bay oscillations at Aonae trapped the tsunami for over 30 min, and a large portion of Aonae remained submerged for a substantial percentage of this time. In the 15 November 2006 Kuril Island event, harbor oscillations lasted for about 5 hr in Crescent City, California. The 7th wave was the largest, and damage is currently estimated to be $700,000 from the 2-m wave. Forecasting the event duration is thus essential to safe planning of nuclear power plant operation during emergencies.

## 6.4 Recommendations

The following recommendations are based on the reality that tsunami impact dynamics is an active area of research that continues to evolve and mature, and that impact analyses are only as good as the model results on which they are based. In that context, we make the following recommendations.

A. Develop and analyze multiple impact metrics needed to address individual NPP site impact issues, including total water depth, current speed, acceleration, inertia, momentum flux, drawdown, and duration.

B. Require that modeling tools meet adequate quality and reliability standards, such as those adopted by NOAA for evaluation of tsunami numerical models (Synolakis *et al.*, 2007).

C. When calculating forces, avoid creation of an extremely fine grid simply by interpolation of existing bathymetry and topography data that is too coarse to justify such a process, a common error in the application

of tsunami models. This practice may increase the formal accuracy of the numerical solution of the dynamic equations, but the proper and accurate site-specific solution is strongly dependent on the quality and resolution of the bathymetric and topographic data actually available, and the interpolated-grid result may be misleading.

# 7. Poorly Understood Hazards

This section deals with two topics that are exceedingly complex and poorly understood—the dynamics of flow with a debris load, and sedimentation and deposition. As a result, the associated hazards are also poorly modeled, although first-order approximations do exist for the underlying physical processes. Consequently, the use of such results to model these hazards must be carefully interpreted and must be viewed as tentative and subject to potentially large errors.

## 7.1 Debris and Projectiles

*by Utku Kânoğlu and Costas Synolakis*

Debris loads are a significant hazard during a tsunami attack. The 1946 Alaskan tsunami carried logs from a nearby lumber plant and deposited them to elevations up to 42 m in the most highly affected area on Unimak and Senak Islands. Also, a substantial number of videos exist showing enormous debris flow during the 26 December 2004 Boxing Day tsunami. Contrary to intuition, it does not take a large tsunami to transport large objects. A tsunami approximately 3 m high carried a recreational vehicle more than 100 m inland during the 1995 Manzanillo, Mexico tsunami. Current knowledge of debris flows and methods for calculating the force of debris flow on structures is very limited and approximate. The Coastal Construction Manual (CCM) (Federal Emergency Management Agency, 2003) recommends

$$F = wV/(gt) \ , \tag{7.1}$$

where $w$ is the weight of the object impacting the structure, $V$ is its speed, $t$ is the duration of the impact, and $g$ is the gravitational acceleration. In the absence of any specific information as to the size of debris, the CCM further recommends the use of $w = 1000$ lb and $V = (gh)^{1/2}$ for tsunamis; here, $h$ is the total depth. For the duration, $t$, the CCM recommends a range of 0.7–1.1 sec for wood walls, 0.5–1.0 sec for wood piles, 0.2–0.4 sec for reinforced concrete walls, 0.3–0.6 sec for concrete piles, and 0.3–0.6 sec for reinforced concrete piles, concrete masonry walls and pipes. This relationship is believed to provide conservative estimates, since large objects are not carried at the same speed as the tsunami current.

## 7.2 Erosion and Sedimentation

*by Robert Weiss*

Tsunamis cause sediment movement when they approach a coastal area. When entrainment of grains into the water column creates saturated conditions—i.e., no more sediment can be carried by the flow—an increase of the net density by up to 30% can occur; this increased density must be accounted for in estimates of the tsunami forces on buildings and other objects.

**Table 7-1:** Load conditions and the corresponding force equation (FEMA, 2003).

| Load | Formula |
|---|---|
| Breaking wave load on vertical piles | $F_{brkp} = (1/2)C_{db}\gamma D H_b^2$ |
| Breaking wave load on vertical wall, for an enclosed dry space behind the wall | $f_{brkw} = 1.1C_p\gamma d_s^2 + 2.41\gamma d_s^2$ |
| Breaking wave load on vertical wall, for equal stillwater level on both sides of wall | $f_{brkw} = 1.1C_p\gamma d_s^2 + 1.91\gamma d_s^2$ |
| Hydrodynamic load for flow <10 ft/sec | $d_{dyn} = (1/2)C_d V^2/g$<br>$f_{dyn} = \gamma d_s d_{dyn}$<br>$F_{dyn} = f_{dyn}(w)$ |
| Hydrodynamic load for flow >10 ft/sec | $F_{dyn} = (1/2)C_d\rho_f V^2 A$ |

**Table 7-2:** Localized scour depth vs. soil type (Dames and Moore, 1980).

| Soil Type | Expected Depth (% of $d_s$) |
|---|---|
| Loose sand | 80 |
| Dense sand | 50 |
| Soft silt | 50 |
| Stiff silt | 25 |
| Soft clay | 25 |
| Stiff clay | 10 |

### *7.2.1 Float load and scour erosion*

Scour erosion can frequently be extensive. The CCM suggests different formulae for different load conditions (Table 7-1).

The parameters used in these equations are: $d_s$—design stillwater depth, $V$—design flood velocity (corresponding to $U$), $C_{db}$—breaking wave drag coefficient (2.25 for square or rectangular piles, 1.75 for round piles), $C_p$—dynamic pressure coefficient, $C_d$—drag coefficient, $\gamma$—specific weight of water, $f_{dyn}$—equivalent hydrostatic force per unit area, $d_{dyn}$—equivalent additional flood depth, $H_b$—breaking wave height, $D$—pile diameter, $\rho_f$—mass density of fluid, $A$—surface area of obstruction normal to flow.

Scouring due to dynamic interaction of the tsunami waves with coastal geometries can be severe and have effects up to 300 ft from the shoreline (Dames and Moore, 1980). The CCM does not provide a formula to compute the effect, but does provide the guidance presented in Table 7-2, on expected scour depth for different soil types.

### *7.2.2 Grain entrainment on sloping beaches and sedimentation*

The dynamics of tsunami sediment transport are poorly understood. Here we use linear wave theory and basic physical concepts to explore this topic, which continues to be the subject of cutting-edge research.

Figure 6-1 presents the evolution of two different waveforms propagating over the simple geometry of a sloping beach. This figure illustrates how sensitive the distribution of velocity is to the shape of an incoming wave.

The results are crucial to an understanding of the sediment dynamics as well, because it is common sense to expect that higher velocities are associated with erosion, while lower velocities allow sedimentation.

Shields (1936) carried out the first parametric study on grain entrainment and found critical conditions for setting grains in motion; a result of his work became famous as the Shields curve. Many subsequent researchers continued to carry out similar experiments with many different materials and grain sizes, using the scaling derived by Shields.

The data in Fig. 7-1a are fit with the equation

$$Y_{cr} = aX_{cr}^{b} + ce^{(dX_{cr}^{e})} \ , \tag{7.2a}$$

where the five parameters $a$–$e$ are varied to best fit the data, and where the classical scaling is given by

$$X_{cr} = u_* D_g / \upsilon \ , \tag{7.2b}$$

$$Y_{cr} = \rho_f u_*^2 / (\gamma D_g) \ , \tag{7.2c}$$

and where $\upsilon$ is the kinematic viscosity, $D_g$ the grain size, and $\gamma = g[\rho_s - \rho_f]$ with $\rho_s$ the density of the sediment grains and $\rho_f$ the density of the fluid. The shear velocity $u_*$ is given by

$$u_* = \sqrt{\tau_0 / \rho_f} \ , \tag{7.2d}$$

where $\tau_0$ is the shear stress. There is also an empirical relationship between the shear velocity and the flow velocity

$$U \approx \sqrt{8/f} u_* \ , \tag{7.3}$$

where $f$ is the Darcy-Weissbach roughness estimator (Yalin, 1977). It has been experimentally determined that variations of the dimensionless Darcy-Weissbach number from 0.04 to 0.5 correspond to a broad range of grain sizes, from fine sand to medium gravel.

Figure 7-1b presents the critical water depth, $d_c$, at which grains of size $D_g$ begin to move, for the case of a wave of amplitude $A_0$ in water depth $d_0$ that is incident on an idealized 1-dimensional beach, i.e., a beach with bathymetric variations only in the offshore direction. Each line in the figure is associated with a different value of the amplitude, $A_0$. To construct the figure, linear theory was used to provide estimates for shoaling, known as Green's Law,

$$A(d) = A_0 (d_0/d)^{1/4} \ , \tag{7.4}$$

that describes the amplitude $A$ as a function of the water depth $d$ based upon a one-dimensionally varying beach geometry. The critical depth of initial grain movement

$$d_c = L/(2\pi) log \left( 2\pi A/(TU) + \sqrt{1 + [2\pi A/(TU)]^2} \right) \ , \tag{7.5}$$

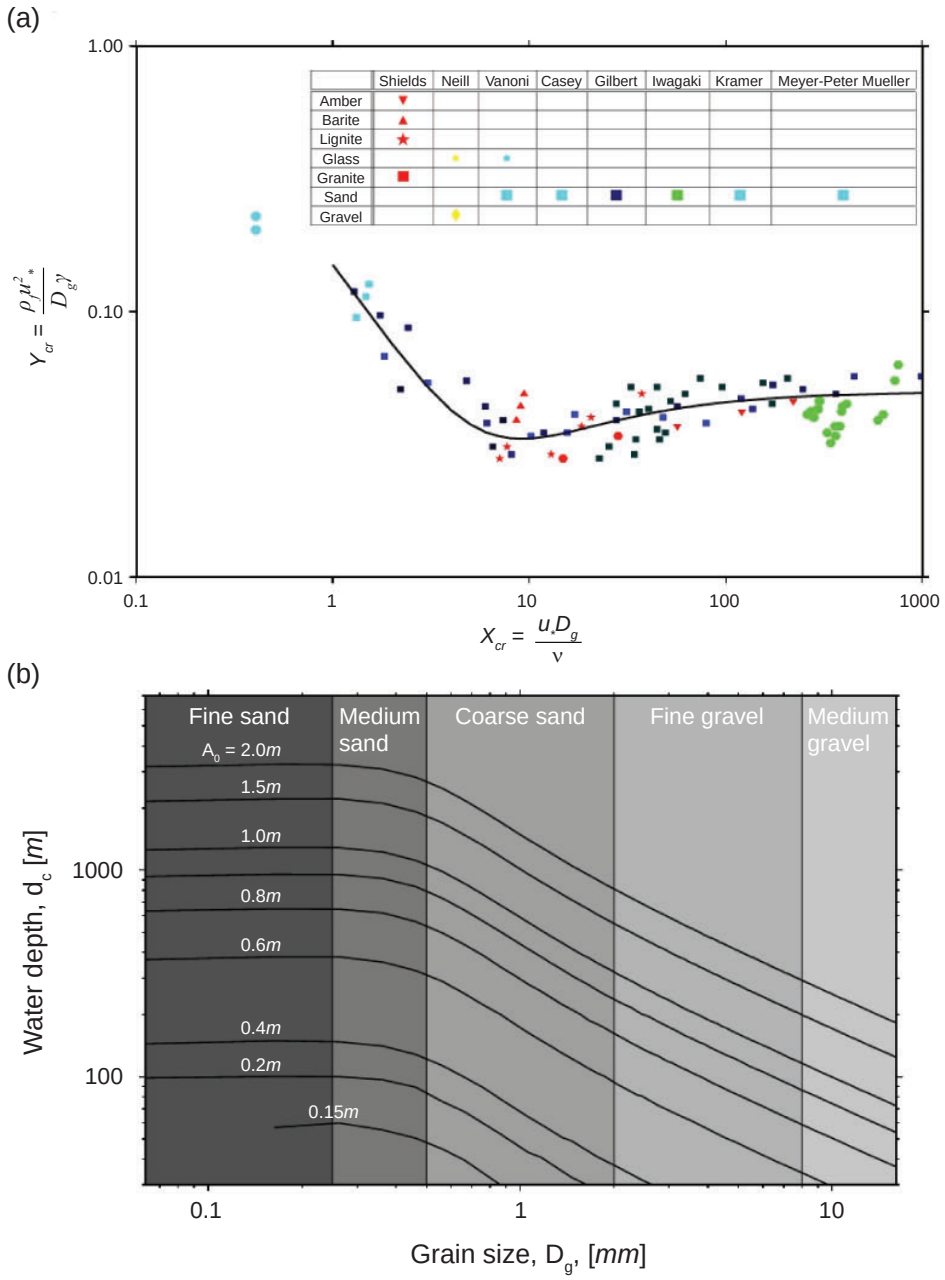


**Figure 7-1:** (a) Shields diagram from Yalin (1977). The solid line represents the best fit of equation 7.2 (see text). (b) Critical water depth $d_c$ on a 1-dimensional beach for which grains first move, as a function of grain size, parameterized by offshore wave amplitude $A_0$ (equation 7.4).

is a function of $A$, $T$, $L$, and $U$, the wave amplitude, period, length, and flow velocity, respectively. A derivation of equation 7.5 and a comprehensive description of the iterative scheme to solve equations 7.1–7.5 for construction of Fig. 7-1b are provided by Weiss (2007). Of course, this diagram has a severe drawback, since linear wave theory is used in a domain where non-linear elements cannot be neglected; however, this approach appears to provide a reasonable first order approximation to the dynamics of grain entrainment by tsunami waves.

### *7.2.3 Boundary layer development and density increase by grain entrainment*

The boundary layer is a physical concept that simplifies discussion of near-bottom fluid dynamics, including that of tsunamis, by treating the flow as two separate fluid layers with different physical behavior—an upper layer characterized by a simple flow structure and a lower layer (the boundary layer) characterized by more complex flow structure (Fig. 7-2). For tsunamis, the velocity $u$ at the top of the boundary layer can be assumed to be the depth-integrated velocity $U$ of the main flow. Depending on the velocity profile assumed, the velocity at the bottom of the boundary layer or surface of the sediment is zero for a laminar structure of the flow within the boundary layer and values of $0 \leq u \ll U$ for the turbulent boundary layer. Sediment can be suspended and transported only within the boundary layer; therefore, the thickness $\delta$ of the boundary layer is an important parameter.

There are different ways to specify the boundary layer; that chosen here is one of the simplest, and often used in numerical models. This approach assumes a turbulent flow within the boundary layer with a logarithmic velocity profile

$$u = [u_*/\kappa] ln(y/k_*) \ ,$$

where $\kappa$ is Karman's constant ($\kappa = 0.41$), and $k_* = k_n/30$ with $k_n$ being Nikuradse's equivalent roughness (Yalin, 1977). Due to the non-zero velocity directly at the bottom, computing the boundary layer thickness must start with the physical assumption that the thickness depends on the upper layer velocity $U$ and the roughness of the sediment bed. Fredsøe (1984) defined the variable $z = \kappa U/u_* \approx \kappa\sqrt{8/f}$. As already mentioned, the velocity at the top of the boundary layer must match $U$. In the logarithmic velocity profile, $y$ can be defined as $y = \delta + k_*$, which leads to

$$\delta = k_*(e^z - 1) \ .$$

Figure 7-3a depicts the thickness of the boundary layer $\delta$ as a function of roughness height. The roughness can vary from that of grains to sedimentary structures, and can, therefore, vary from a few millimeters to a few decimeters. The different lines represent variations of the Darcy-Weissbach number $f$. In this theoretical model of the boundary layer, it is possible that $\delta$ is larger than the water depth, which physically means that the entire water column is a sediment-laden boundary layer. Video footage from the Boxing

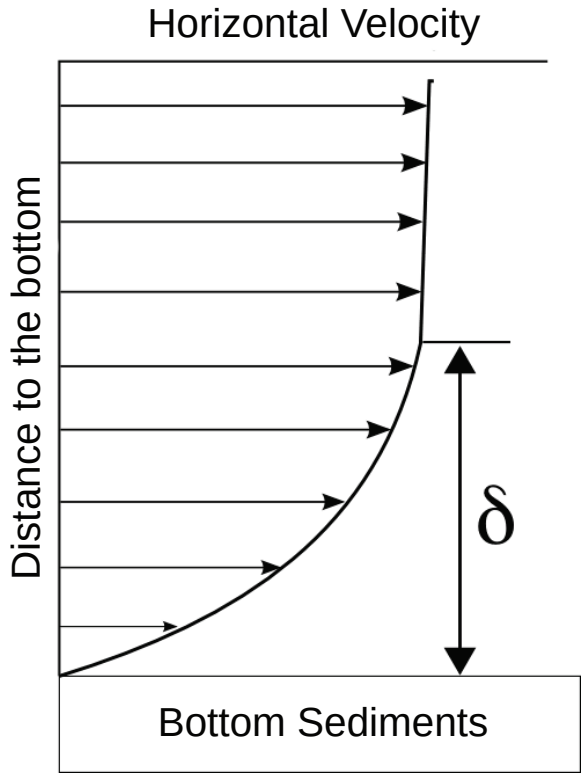


**Figure 7-2:** The concept of a boundary layer of thickness $\delta$.

Day Tsunami in 2004 clearly showed such conditions in the form of brownish colored water inundating land. When computing the hydrodynamic forces, this sediment content must be taken into account, since the net density of the fluid is increased. A mixture of water and non-cohesive sediment reaches saturation at 30% sediment content distributed through the water column (Allen, 1985). An intuitive mixing law can be given by $\rho_f = (1-c_s)\rho_w + c_s\rho_s$, where $\rho_w$ is the density of water. Figure 7-3b illustrates the density of the fluid $\rho_f$ as a function of sediment concentration $c_s$.

## 7.3 Recommendations

The theoretical considerations presented here are first-order approximations. From a physical point of view, there is coupled, dynamic interaction between the thickness of the boundary layer, the grain entrainment, and mixing within the boundary layer. Such an internal dynamic is nonlinear and is not taken into account in the equations presented in this section. The relevant research is cutting-edge and far from being applicable for engineering use. Four-dimensional models (three space and one time variable) that include boundary layer dynamics are needed to gain more detailed insight into sedimentation and erosion by tsunami waves; such models could also be used for more realistic estimates of tsunami impact on structures. We therefore recommend:

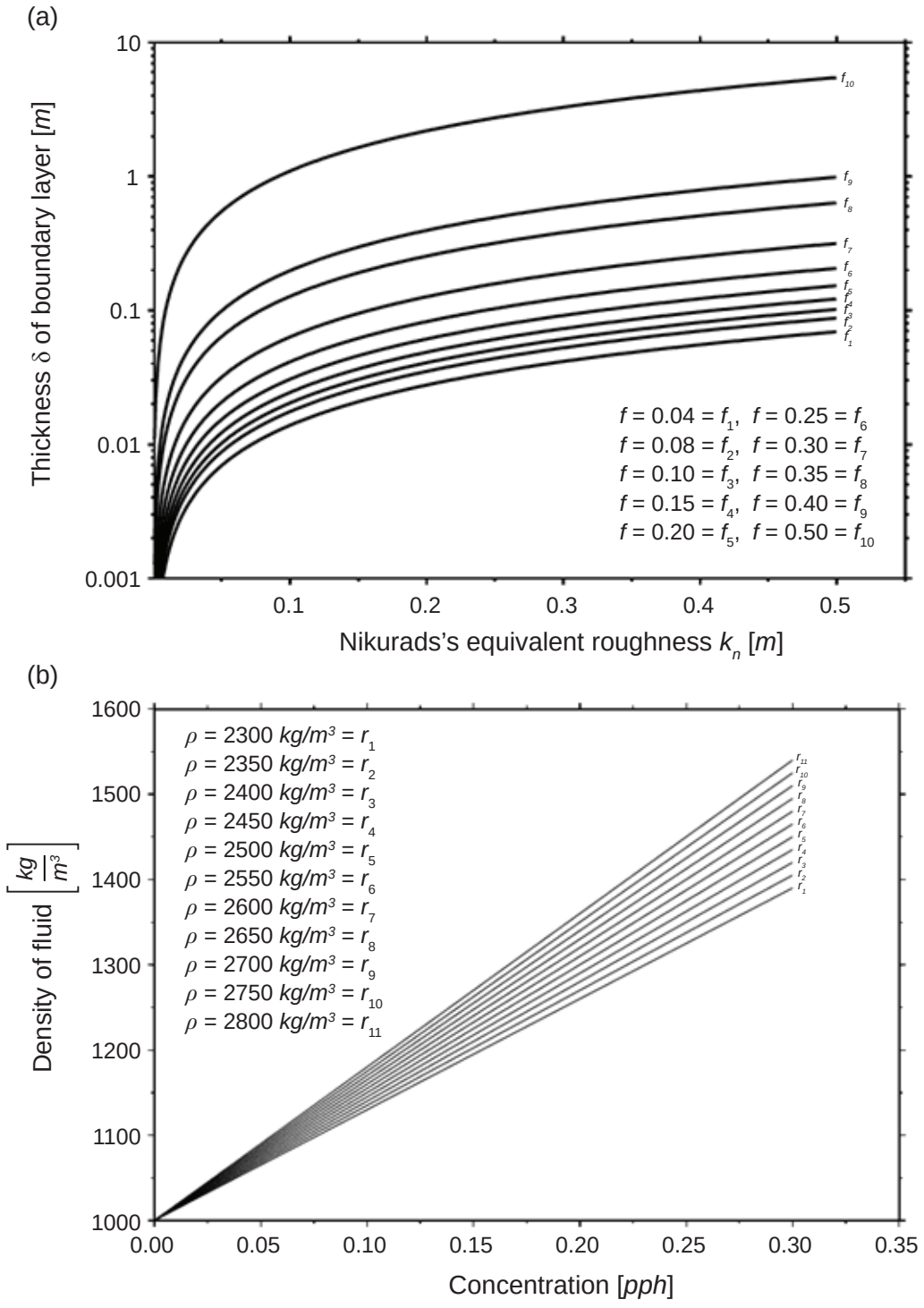


**Figure 7-3:** (a) The thickness $\delta$ of the boundary layer as a function of the roughness height (Nikuradse's equivalent roughness for different Darcy-Weissbach coefficients). (b) The density $\rho_f$ of the fluid as a function of the concentration ($pph$ = parts per hundred) for different grain densities.

- Development of a tsunami propagation and inundation model with dynamic coupling to a four-dimensional boundary-layer model. This is necessary because standard tsunami models with a depth-integrated velocity field violate the condition $\delta \ll d$ and fail to account for the increase in water column density induced by the sediment load.

# 8. Template THA

*by Frank González and Eric Geist*

This section draws on the preceding content of this report to develop a general template for THA that provides a starting point for the development of detailed procedures to guide NRC reviews. As useful background, we first provide a brief description of the Japanese THA methodology, as presented by the Japan Society of Civil Engineers (2002), and an analysis of the methodology in the context of THA for U.S. sites. This is followed by presentation and discussion of individual components of a Template THA for U.S. NPP, including an initial screening study, development of scenarios known as Probable Maximum Tsunamis (PMTs) and associated assessment metrics, and the issue of real-time tsunami hazard assessment capabilities.

## 8.1 Japanese Approach

For brevity, we here refer to the report by the Japan Society of Civil Engineers (2002) as JSCE02.

### *8.1.1 Basic methodology*

Essentially, the Japanese methodology is a deterministic, parametric study that includes the following components:

- *Scenario Earthquakes* are determined, each with a "reasonable range" of nine fault parameters.
- Parametric tsunami modeling is conducted, based on *Scenario Earthquake* sources for which the nine fault parameters are systematically varied.
- *Scenario Tsunamis* are identified as that subset of modeled tsunami cases that " ... exceed historical and calculated heights."
- *Design Tsunamis* are developed by adding and subtracting the means of the high and low background water levels, respectively, to the *Scenario Tsunamis*.
- Harbor Response to *Design Tsunamis* are modeled and studied, including the impact on water intake.

We also note several important features of this approach:

- Earthquakes are the only source mechanism considered.
- Water level is the only tsunami parameter considered.
- Historical tsunami information, which is much more plentiful in Japan than the U.S., is used to test and verify earthquake and tsunami models.

### *8.1.2 Analysis in the context of U.S. THA*

Further analysis of JSCE02 suggests certain issues should be more closely examined and modified for U.S. applications:

(1) ***Source Specification***: In contrast to Japan, the U.S. must supplement historic sources with the use of regional or global earthquake size distributions based on a seismic moment balance (see Section 4.1.3 of this report). This is because the U.S. does not have a long historic record of tsunamis, as in Japan, and thus the scenario source, in many cases, cannot be strictly based on a historic source. An informative analog would be application of the Japanese approach to the northern Bay of Bengal before 2004. Here, the historic and scenario sources would have been based on a maximum moment magnitude ($M_{max}$) of 7.7–7.9, which would have severely underestimated the tsunami hazard. (Note that the Japanese report was written in 2002, before the disastrous 24 December 2004 earthquake and tsunami.)

(2) ***Maximum Moment Magnitude Specification***:

(a) *Plate boundary earthquakes.* The best U.S. option is to determine $M_{max}$ through the USGS Seismic Hazard Mapping Program (SHMP). This is in contrast to Japanese reliance on historic sources to define $M_{max}$ (JSCE02, Section 4.3.2). Full documentation for U.S plate boundary faults (Alaska, Cascadia, Puerto Rico) can be found at `http://earthquake.usgs.gov/research/hazmaps/`. The Japan Report correctly indicates that the design tsunami may be from a far-field source. For other subduction zones not encompassed by the USGS/SHMP, the global or regional determination of magnitude distribution described in Section 4.1.3 in our report can be used.

(b) *Back-arc fault systems.* These are generally not significant sources of tsunamis for U.S. shorelines; exceptions include Puerto Rico/U.S. Virgin Islands, western Pacific territories, and the Bering Sea shoreline of Alaska. These systems are analogous to the eastern margin of the Japan Sea (JSCE02, Section 4.3.3).

(c) *Near-shoreline fault systems.* The USGS/SHMP has systematically determined $M_{max}$ for other fault systems or "floating" sources near U.S. shorelines, including Hawaii and Puerto Rico. In most cases, the onland determination for a floating source can be extended offshore a limited distance—especially along passive margins. These near-shoreline fault systems are termed submarine active faults in Section 4.3.4 of JSCE02.

(3) ***Standard Fault Model***. (See Appendices 1–4 of JSCE02.) U.S. studies should base the geometry for Standard Fault Models on the NCTR database that is part of the Facility for the Analysis and Comparison of Tsunami Simulation (FACTS), which includes most plate-boundary faults of relevance and other offshore, active intra-plate faults. The

geometry for the plate-boundary faults is based on the recent compilation of Bird (2003), along with regionally specific studies to establish fault dip. Other source parameters that scale with moment magnitude (average slip, fault length, and fault width up to saturation) can be established by a methodology similar to that described in JSCE02. For faults not included in the FACTS database, other sources such as the USGS/SHMP (primarily near-shore and on land) and previous geophysical surveys should be used.

(4) ***Rigidity of Medium Near the Fault***. (See Section 4.1.4 of JSCE02.) The elastic properties of rocks in the shallow part of the subduction zone are quite depth dependent and, in particular, the shear modulus near the sea floor is likely significantly lower than indicated by JSCE02 (see Fig. 4.1-3 of this report). This will have the effect of increasing the slip for a given moment magnitude in the shallow part of the subduction zone (see Okal, 1988).

(5) ***Parametric Studies***. (See Section 4.3.5 of JSCE02):

(a) *Parameter limits*. U.S. coastlines currently lack parameter limits for specific fault zones, such as those provided for the Nankai and eastern margin of Japan Sea in Table 4-3 of JSCE02. The entry "Along the Japan Trench" in JSCE02 Table 4.3 could apply to most subduction zones of interest. The framework of the parametric study laid out in the Japan Report is very good.

(b) *Slip distribution*. This is an additional parameter that should be included for near-field tsunamis. Standard slip models are discussed in Section 4.1.3 of this report and can be implemented in a manner similar to strong-ground motion hazard assessments (Somerville *et al.*, 1999). Small-scale variations in slip distribution are less important for far-field tsunami amplitude determination, and the FACTS database could be used for such cases. Variations in slip distribution are also less important for steeply dipping faults.

(6) ***Landslides***. The maximum volume ($V_{max}$) of recent landslides would optimally be determined from seafloor mapping and geologic age dating in a given region. As indicated in the report, slope-stability and post-failure analyses using the morphological and geotechnical parameters for a potential source region (e.g., Locat *et al.*, 2004) should be performed to better assess potential tsunami generation efficiency.

(7) ***Tsunami Models***. U.S. tsunami hazard assessment of existing and candidate nuclear power plant sites should be conducted with models that have demonstrated that they meet standards now being adopted by NOAA and the international modeling community (Appendix C). Sections 5.1–5.3.2, 5.3.4, and 5.3.5 of JSCE02 provide a good discussion of the theory and numerical simulation of tsunami dynamics that is consistent with current modeling practices, including general statements regarding the desirability of accuracy. However, JSCE02 does

not discuss specific national standards for candidate models, such as formal, peer-reviewed documentation of theory and numerics, and successful application of the model to benchmark tests and historical hindcasts.

(8) ***Bathymetry and Topography***. (See Sections 5.3.3, JSCE02). U.S. responsibility for the acquisition and quality assurance of bathymetric and topographic data lies primarily with NOAA and the USGS, respectively. Such data are also acquired by other Federal agencies, such as the U.S. Army Corps of Engineers (USACE), State and local agencies, academia, and private contractors. Within NOAA, the National Geophysical Data Center bears responsibility for the gathering, archiving, and distribution of all available bathymetric and topographic data (see Appendix A). This repository of quality-assured data should be the primary source for development of numerical computational grids used for tsunami modeling.

(9) ***Computational Grid Development***. (Not discussed in JSCE02.) Within NOAA, the NGDC and PMEL are currently the primary developers of computational grids for tsunami modeling. Each continues to actively develop new grid-development methodologies and incorporate those developed by others. Accurate computational grids, especially for shallow areas nearshore, are essential to reliable THA model simulations. As such, the development of such model computation grids for THA of NPP sites should follow published NOAA guidelines and be well-documented.

## 8.2 Initial Screening Study

The concept of an initial screening study was discussed at a joint NOAA/NRC workshop held at Oregon State University on 24 July 2006. The rationale given for such a study was the following hierarchical procedure that governs an NRC review of tsunami hazard at a given NPP site:

(a) If the site can be determined to be safe from tsunamis, then no further tsunami assessment is needed. Otherwise,

(b) Conduct a tsunami hazard assessment study based on the concept of PMT.

The initial screening study conducted to determine whether or not tsunami hazards exist at an NPP site should be characterized by elements that include:

A. The *goal* of conclusively establishing the existence or absence of a tsunami hazard.

B. An *inventory* of existing information that bears on the goal, including: databases of historic and pre-historic tsunami occurrences; published analyses of these data, such as regional tsunami hazard assessments;

physical setting and characteristics of the proposed NPP site; tsunami-relevant design features of the NPP itself, including the cooling water intake system.

C. An *analysis* that provides interpretation of the existing information based on best available science.

D. A *conclusion*, based on the analysis in C, that either (a) the tsunami hazard is absent or negligible, or (b) a tsunami hazard exists, or (c) the existing information is inadequate to determine (a) or (b).

Note that steps C and D avoid placing the applicant in the untenable position of having to prove a negative proposition—i.e., that no tsunami hazard exists. Rather, C and D refer to a process of establishing "best available science" as it bears on the hazard, i.e., documentation of expert scientific consensus that the conclusions in D are justified by the analysis of C.

The Pacific Northwest National Laboratory (2006) has proposed a screening rule based on three siting metrics: D, distance from the coast; L, distance upriver; Z, height above mean water level (Fig. 8-1). A trivial example in which a tsunami hazard might be declared absent is an upriver site located hundreds of miles inland. In general, however, NPP designs require a water cooling system that extends from the NPP proper to a water cooling intake located somewhere in a significant body of water. Consequently, if the water source is large enough to accommodate the generation and propagation of a tsunami, it is clear that further study must be conducted.

Sections that follow discuss individual aspects of the subsequent study. The first step of the study would seek evidence of past tsunamis. Whether or not evidence of past tsunamis is found, the study would also seek to identify all potential tsunami sources that might threaten the site. If the study finds no evidence of past tsunamis *and* also concludes that no potential tsunami sources exist, the tsunami hazard may be assessed as absent or negligible. If the study finds evidence of past tsunamis or identifies potential tsunami sources, then the next step in the tsunami hazard assessment must be taken—a study of the potential impact on the NPP, including the water intake system, of tsunamis generated by the identified sources. Essentially, this second step would establish acceptable values for D, L, and Z. Furthermore, if we interpret these parameters more generally, to include constraints on the cooling water system, for example, then the intake might be required to be at least $L_I$ kilometers upriver or $D_I$ kilometers offshore, in water depth of at least $Z_I$ meters, a location deep enough to avoid intake exposure by a tsunami trough.

We note that the DLZ concept is useful and the apparent simplicity of the rule is appealing; as usual, however, application of such a rule is more complex in actual practice. This is because, in principle, each of these parameters are clearly a function of the NPP design itself. For example, the thickness and strength of concrete walls will determine the maximum tsunami forces safely sustainable and, therefore, acceptable values of the distances D and L; similarly, acceptable current speeds, and therefore the

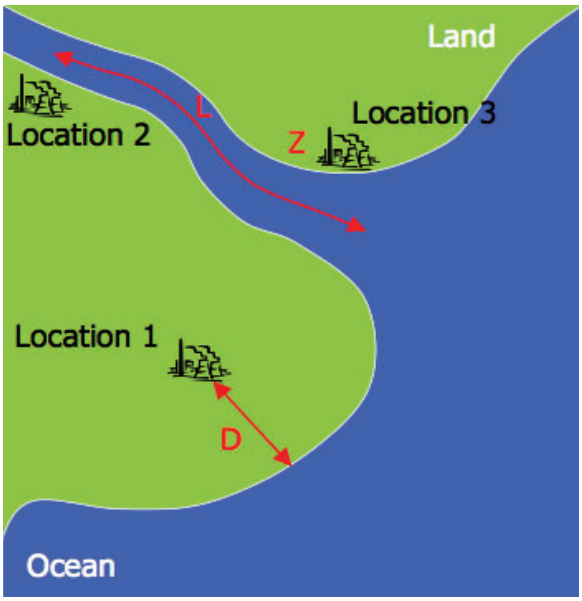


**Figure 8-1:** Physical setting of three hypothetical nuclear power plant locations, each illustrative of one of three siting metrics, D, L, and Z (from Pacific Northwest National Laboratory, 2006). It is important to note that, although not shown here, a cooling water intake will likely extend from each NPP to a point offshore or upriver.

water depth Z, will clearly depend on the design details of the cooling water system and intake.

## 8.3 Probable Maximum Tsunami Study

The terminology "Probable Maximum Tsunami" (PMT) has been used by NRC since at least 1975, in Version 0 of NUREG-0800 (U.S. NRC, 1996), also known as the Standard Review Plan (SRP). The latest version of the SRP includes a history of revisions to each section and is available at `http://www.nrc.gov/reading-rm/doc-collections/nuregs/staff/sr0800/`.

The PMT concept was discussed at the 24 July 2006 NOAA/NRC workshop. In spite of the name, the process by which a Probable Maximum Tsunami is specified does not refer to a rigorous probabilistic methodology, such as the Probabilistic Tsunami Hazard Assessment (PTHA) method recently applied to Seaside, Oregon (Tsunami Pilot Study Working Group, 2006). In fact, U.S. NRC (1996) states that a probabilistic approach based only on the limited historic record may underestimate the severity of events, and that a deterministic approach that takes into account the practical physical limitations of the natural phenomenon can avoid this problem.

In the context of the SRP, the phrase "physical limitations of the natural phenomena" refers to the inherent physics of a process that imposes an upper (or lower) limit on the allowable value of a particular parameter. When modified by the word "practical" this phrase is weakened somewhat, presumably through consideration of the likelihood that such limits would actually be

attained. The PMT in this sense is similar to the approach adopted for the Probable Maximum Precipitation (PMP) described by NOAA Hydrometeorological Reports of the National Weather Service (NWS) (U.S. Department of Commerce, National Oceanic and Atmospheric Administration, and U.S. Department of Army Corps of Engineers, 1978).

### *8.3.1 Definition*

A Technical Rationale for the PMT concept is presented in Section 2.4.6 of the U.S. NRC (1996) SRP. Based in large part on this Technical Rationale, NRC adopted the following definition for Probable Maximum Tsunami at the 24 July 2006 workshop:

> A Probable Maximum Tsunami is that tsunami for which the impact at the site is derived from the use of best available scientific information to arrive at a set of scenarios reasonably expected to affect the nuclear power plant site, taking into account (1) appropriate consideration of the most severe of the natural phenomena that have been historically reported for the site and surrounding area, with sufficient margin for the limited accuracy, quantity, and period of time in which the historical data have been accumulated, (2) appropriate combinations of the effects of normal and accident conditions with the effects of the natural phenomena, and (3) the importance of the safety functions to be performed.

Workshop participants discussed certain important phrases in this definition, in order to clarify their meaning:

> "... the impact at the site ..." refers to different categories of phenomena that might threaten the integrity of a nuclear plant, such as deep inundation, high current speed, extensive and sustained drawdown, severe scouring, etc. This implies that multiple PMTs may be needed to fully specify the most severe conditions in each impact category since, in general, the most severe conditions for each impact category may not be produced by a single PMT.
>
> "... best available scientific information ..." refers, in the final analysis, to expert consensus on proper and defensible PMT specification. One of the most effective mechanisms for developing such consensus is an intense, highly focused workshop that brings together recognized experts committed to the development of PMT scenarios and the publication of a report that documents the process, including limitations and the degree of confidence in the results. An example of this process was the workshop held to identify and describe potential tsunami sources in the Puget Sound region (González *et al.*, 2003).
>
> "... historically reported ... " refers indirectly to pre-historic information as well, since reports on paleotsunami deposits, for example, are considered to be historical data.

The latest version of Section 2.4.6 of the U.S. NRC SRP (currently available at `http://www.nrc.gov/reactors/new-licensing/new-licensing-files/srp-table-of-contents.pdf`), modifies the definition of PMT to acknowledge the role of pre-historic information, through addition of the phrase "... or determined from geological and physical data ..." so that the current definition of PMT adopted by the NRC is

> The PMT is defined as that tsunami for which the impact at the site is derived from the use of best available scientific information to arrive at a set of scenarios reasonably expected to affect the nuclear power plant site taking into account (a) appropriate consideration of the most severe of the natural phenomena that have been historically reported or determined from geological and physical data for the site and surrounding area, with sufficient margin for the limited accuracy, quantity, and period of time in which the historical data have been accumulated, (b) appropriate combinations of the effects of normal and accident conditions with the effects of the natural phenomena, and (c) the importance of the safety functions to be performed.

If items (b) and (c) of this PMT definition are excluded, it is then similar to the "credible worst case" concept frequently cited by the U.S. National Tsunami Hazard Mitigation Program, i.e., the most destructive scenario that is defensible on the basis of best available science. Credible worst case scenarios for earthquakes and landslides in Puget Sound, for example, are described in González *et al.* (2003). Addressing items (b) and (c) in the PMT definition requires expert knowledge of NPP operations.

### *8.3.2 PMT development*

As a practical matter, development of a site-specific PMT must be a collaborative, interdisciplinary effort. In general terms, the process of determining PMTs is as follows.

***A. Source Specification Database Development***

> In which geoscientists provide expert consensus on potential tsunami sources, based on "Best Available Science" and including a reasonable range of the source parameters that takes into account the limited accuracy, quantity, and period of time in which data have been accumulated.

Standards for the source specification process have been established by the Senior Seismic Hazard Analysis Committee (1997). An example of the source specification process is the Puget Sound study (González *et al.*, 2003). This study was jointly sponsored by NOAA's Center for Tsunami Inundation Mapping Efforts (now the NOAA Center for Tsunami Research), the USGS, the Washington State Emergency Management Division, and the Washington State Department of Natural Resources.

Careful preparation and preliminary scientific discussions by e-mail and telephone before the 1-day workshop were essential. Starting in April 2002, an organizing committee developed a workshop website and an informational e-mail to 35 individuals, inviting their participation and, importantly, soliciting pre-workshop material to be posted to the website. This website content was generously contributed by individuals, even if they did not plan to attend the workshop. The website content was an invaluable catalyst that stimulated and facilitated the pre-workshop discussions and provided resource material for the workshop itself.

On 10 June 2002, 23 experts on tsunami sources, modeling, and emergency management were brought together at NOAA's Pacific Marine Environmental Laboratory in Seattle, Washington. At the workshop, three expert sub-groups were formed—Earthquake Sources, Delta Failure and Landslide Sources, and Paleotsunami Field Evidence—each to concentrate on specific mechanisms and source issues. The specific goal for each sub-group was to identify all potential tsunami sources in Puget Sound and the development of tables of source parameters, including the reasonably expected range of values for each. The development of these tables continued well after the 1-day workshop, up to publication of the workshop report. These tables serve as a starting point for modeling sources for tsunami inundations studies in Puget Sound.

This process is recommended as an effective means of establishing the consensus of experts on the best available science regarding potential tsunami sources that might threaten a specific candidate NPP site. If sources other than earthquakes and landslides threaten a site, then appropriate experts should be included in the process.

### *B. Inundation Modeling Database Development*

> In which tsunami modelers conduct parametric modeling studies to generate the "Parametric Scenario Database" for tsunami sources identified in A. The database will include tsunami model results such as height and velocity, boundary conditions and initial conditions, as well as field data, a bibliography, and other information specific to the site of interest.

Standards for tsunami modeling are under active development (see Synolakis *et al.*, 2006, provided as Appendix C of this report). These standards include the completion of benchmark tests, hindcasts of actual historical events, and documentation in peer-reviewed journals. Synolakis *et al.* (2006) provide benchmark test cases and other standards and procedures that are in the process of being reviewed and adopted by NOAA and the international tsunami modeling community.

An example of step B, i.e., the development of a tsunami model output database, is given by the Seaside, Oregon, pilot study to improve FEMA Federal Insurance Rate Maps (Tsunami Pilot Study Working Group, 2006). For brevity, this study is referred to here as TPS06 and, for convenience, is reproduced as Appendix D.

What follows is a brief summary of TPS06; important components of the study methodology are described, and references to specific sections of TPS06 are provided in *italicized text*.

(1) Source Specification, consisting of a review of literature, consultation with expert colleagues, and the development of a database of quantitative probabilistic models of local and far-field earthquake tsunami sources in the Cascadia Subduction Zone, the Alaska-Aleutian Subduction Zone, and the Peru-Chile Subduction Zone. *A detailed description of the process is provided in Section 5.2, "Source Specification," of TPS06. In particular, Section 5.2.2 describes the specification of far-field earthquake sources, and Section 5.2.3 describes the development of the near-field earthquakes on the Cascadia Subduction Zone. Also see Section 6.2, "Model Sources," for a discussion of propagation and inundation modeling based on these sources, and model results for selected cases, presented in Figs. 25–28.*

(2) Data Acquisition, including the performance of a paleotsunami deposit mapping and interpretation study and the acquisition of historical records and eyewitness reports. *A thorough discussion of the paleotsunami fieldwork and analyses is provided in Section 4, "Tsunami Deposits," including Figs. 6–11, illustrative of the methodology and the geographical distribution of data acquired for several paleo-events, and Appendix D of TPS06, a listing of geographical coordinates and core results for each individual site. Historical data acquisition, including eyewitness reports, is described in Section 3, "Development of GIS Database," and Appendix C of the TPS06 report, "Summary of eyewitness observations for 1964 Alaska Tsunami in Seaside, Oregon."*

(3) Model Development, Testing, and Application, including the development of a higher resolution Digital Elevation Model (DEM) based on the latest available topography, bathymetry, and tidal information; the development of a state-of-the-art, site-specific tsunami inundation model; testing of the model with all available tsunami field observations, including paleotsunami data, historical records, and eyewitness reports; and, finally, application of the model, using the source database, to generate the corresponding tsunami inundation database. *Appendix B of TPS06, "A digital elevation model for Seaside, Oregon," provides a detailed description of the Seaside DEM development. Section 6.1, "Numerical Model," presents the MOST model mathematical formulation, the numerical scheme for inundation computations, and the use of*

*historical information for model verification. Section 6.3, "Numerical Model Setup and Testing," describes the nested grid system, additional testing against historical data, and discusses the correspondence of model results with eyewitness and paleotsunami data. Section 6.4, "Database of Model Runs," discusses the results of simulations based on the source database, and presents examples of maximum wave heights, inundation, and current speeds for a few selected source scenarios.* (See also Section 5 of the current report, above.)

(4) Probabilistic Computations, including the development of a systematic procedure to process the study data and compute the distributions of 0.01 and 0.002 annual rates of occurrence (100- and 500-yr) quantities, including the effect of ocean tides, and the application of the procedure to create the site-specific tsunami hazard maps. *Section 5.1, "PTHA Overview," provides a summary of the Probabilistic Tsunami Hazard Assessment methodology, and a schematic (Fig. 12) illustrating the application of PTHA to the model results database. Appendices E and F of TPS06 describe methods required for the correct application of PTHA—i.e., accounting for the effect of tides, and determining earthquake recurrence rates, respectively. Section 8, "Results," describes and interprets the resulting 100-yr and 500-yr tsunami maps for the Seaside area.*

(5) Study-Specific Database Development, including documentation of a comprehensive, study-specific, GIS-compatible database with sources, DEM, model output, field observations, and other information relevant to the study, and the creation of a web-based interface for database access. *Section 3, "Development of GIS Database," describes the design and contents of the GIS database developed for all the data relevant to the study. (A more detailed description of the database is given by Wong et al., 2007.)*

(6) Analyses and Interpretation, through use of the GIS database for quality control and error-checking, and to analyze and interpret the primary study results; exploratory analyses and interpretation of various tsunami impact indices to generalize the concepts of tsunami hazard levels in general, and tsunami high-velocity flood zones ($V$-zones) in particular. *Section 7, "Evaluating Tsunami Impact Metrics," describes the development and exploration of several metrics that characterize tsunami impact.* (See also Section 6 of the current report, above.)

### *C. Hazard Assessment Metrics Development*

A number of metrics are important to the tsunami hazard assessment process for NPP sites. The developers of these and other metric products could either be the scientists that conducted the studies and created the databases in Steps B and C, or NPP Operations experts that are also qualified to conduct analyses and interpretations of hydro-

dynamic and geophysical information; optimally, however, this work should be conducted as a collaborative effort of both.

What follows is a brief description of the more obvious metrics that should be considered, and how they can be developed from the basic modeling output and other information available in the site-specific study database.

a. *Impact Metrics*

The fundamental model products available in the database are the multi-dimensional tsunami field variables—i.e., the wave height, $\eta(x,y,t)$, and the $x$ and $y$ components of the current, $u(x,y,t)$ and $v(x,y,t)$, respectively—along with ancillary data, such as the DEM, $d(x,y,t)$, which provides the undisturbed water depth. Given these fundamental quantities, most metrics of interest can be formed, including:

$$\text{Maximum water depth, } h_{\max}(x,y) = [\eta(x,y,t) + d(x,y,t)]_{\max},\ t = 0 \text{ to } t_{\max}\ , \quad (8.1a)$$

$$\text{Minimum water depth, } h_{\min}(x,y) = [\eta(x,y,t) + d(x,y,t)]_{\min},\ t = 0 \text{ to } t_{\max}\ , \quad (8.1b)$$

$$\text{Maximum current speed, } V_{\max}(x,y) = \{[u^2(x,y,t) + v^2(x,y,t)]^{1/2}\}_{\max},\ t = 0 \text{ to } t_{\max}\ . \quad (8.1c)$$

It is worth emphasizing here that the resulting fields do not, as a whole, represent a solution to the equations at a particular moment in time; rather, they are products of the solution, but each point in the domain is considered independently. Examples of such fields are presented in Figs. 26–28 of the TPS06 (Appendix D). Clearly, the maximum extent of inundation and the maximum extent of drawdown can be derived from these basic fields, either graphically or numerically.

Other metrics of interest that address the impact of a tsunami on structures such as cylindrical objects and walls are discussed in Section 6, including acceleration, $d\vec{V}/dt$, and the inertial component, $hd\vec{V}/dt$; but the metric that appears to be most useful as an indicator of potential damage is

$$\text{Momentum flux, } M(x,y,t) = h(x,y,t)V^2(x,y,t)\ , \quad (8.1d)$$

and the associated field of

$$\text{Maximum momentum flux, } M_{\max}(x,y) = [h(x,y,t)V^2(x,y,t)]_{\max},\ t = 0 \text{ to } t_{\max}\ . \quad (8.1e)$$

These metric fields can be derived numerically from the basic field variables ($\eta$, $u$, $v$) or, perhaps more efficiently, generated and stored in the site-specific study database during the actual model runs.

b. *Duration Metrics*

Clearly, the duration of an event must also be considered. A tsunami event involves a series of waves separated in time by individual wave periods (likely in a narrow band around the dominant wave period—see Section 1.3). As a general rule, larger tsunamis are characterized by longer wave period, a consequence of the longer length scales that result from higher energy sources, e.g., larger areas of seafloor deformation associated with larger earthquakes. Typical destructive wave periods range from 20 to 60 min. Furthermore, the largest wave may not be the first, and multiple destructive waves may ultimately strike the coast. Thus, the period of time during which destructive tsunami waves continue to attack a coastline can easily exceed several hours. The 15 November 2006 Kuril Islands tsunami caused $700,000 damage in Crescent City, California, with the 7th wave being the largest inside Crescent City harbor, about 2.5 hr after the first arrival. For now, this is attributed to trapping on the continental shelf. Long duration events need to be considered in the context of background sea level temporal variations, including the tidal cycle, which may serve to increase the destructive power of a tsunami.

Duration is important to at least two aspects of the tsunami hazard:

- *Response*, in which the hazard level must be considered by decision-makers responsible for triggering emergency plans, including the deployment of human and technological assets to contain and mitigate the hazard to NPP personnel, the local and regional population, and the NPP physical plant, itself. The risk that must be managed is the premature deployment of assets that would place them in harm's way as the event continues to unfold.
- *Destructiveness*, in which the cumulative effect of multiple destructive waves would increase the effectiveness of the tsunami to destroy human life and the built environment. Typically, for example, a large tsunami event is characterized by the generation of debris, including massive objects which, when transported by successive waves, become battering rams that dramatically intensify the destructive power of the tsunami. Furthermore, the generation of such debris is enhanced as the built and natural environment succumbs to successive, multiple, attacks. Tsunami currents need to be analyzed as debris currents.

Time series archived in site-specific THA databases are clearly essential to the development of duration metrics. Thus, a general

duration metric could be developed by application of the following computational algorithm to a particular site-specific study database:

**Table 8-1:** General algorithm for a duration metric.

| | |
|---|---|
| a. | Set the location $(x_m, y_n)$ in the model domain |
| b. | Form or retrieve the metric time series $M(x_m, y_n, t)$ |
| c. | Set a "hazard threshold," $M_H$ |
| d. | Identify that time period, $t_M$, beyond which the series is less than the hazard threshold, $M_H$ |
| e. | Increment $m$ and $n$ and return to step a. |

As a specific example, consider a duration metric based on the momentum flux of equation 8.1d. Then, for every model grid point considered, this computation yields the metric:

$$\text{Momentum flux duration, } t_M(x_m, y_n; M_H), \text{ for all } (m, n) \text{ pairs.} \tag{8.2}$$

c. *Hazard Thresholds*

The application of the computational algorithm in Table 8-1 is conceptually straightforward. The accuracy and value of the algorithm, however, is clearly dependent on proper specification of a hazard threshold parameter, $\mathrm{M_H}$. This is true for both impact and duration metrics.

A hierarchy of increasingly complex hazard thresholds can be envisioned. Examples of threshold values based on simple, site-specific physical considerations are

$$h_{H1} = \text{the depth of an NPP water inlet,} \tag{8.3a}$$

or (as in 8.3c and 8.3d)

$$h_{H2} = \text{the height of an NPP flood barrier.} \tag{8.3b}$$

Examples of more complex hazard thresholds based on the ability of NPP structures to withstand a tsunami, are

$$M_H = \text{the maximum momentum flux sustainable by a structure,} \tag{8.3c}$$

or

$$V_H = \text{the minimum current speed required to initiate scouring.} \tag{8.3d}$$

In general, the value of $M_H$ for a specific site is determined by analysis of the engineering design specifications and strength of

the materials to be used in the proposed NPP structure. Similarly, the value of $V_H$ is dependent on the composition of the material adjacent to and underlying the proposed NPP structure.

We note that, in principle, all hazard thresholds can be expected to vary with both space and time; for example, $h_{H2} = h_{H2}(x, y, t)$, since flood barrier height can certainly vary with location and a flood barrier can be partially or totally destroyed during the course of an actual event. In practice, however, such parameters are assumed constant in time, although frequently variable in space—a good example is the specification of tsunami model friction parameters.

***D. Impact-Specific PMT Development***

In which NPP Operations experts and scientists that developed the source and inundation databases identify a PMT scenario that corresponds to each impact mechanism of interest, such as maximum runup, maximum inundation, maximum current, maximum momentum flux, intake exposure, scouring, etc., considering appropriate combinations of the effects of normal and accident conditions with the tsunami and the importance of the safety functions to be performed.

The end users of both studies described in Steps A and B, above, were State Emergency Management officials that then combined the information with their expert knowledge of local community characteristics—population distribution, transportation and communication infrastructure, etc.—to develop appropriate mitigation products such as inundation and evacuation maps, brochures, and educational and training programs. NPP Operations experts that lead the effort in this step can thus be viewed as the direct counterparts of State and local Emergency Management experts. As in the example studies described above (González *et al.*, 2003; Tsunami Pilot Study Working Group, 2006), the active involvement of NPP Operations experts in source and inundation database development is essential; similarly, it is essential that PMT development include scientists that participated in database development.

### *8.3.3 PMT analyses*

The level of tsunami hazard at a site is assessed by an analysis of values of PMT hazard metrics in the context of relevant features of the engineering design for the proposed NPP. In particular, if maximum hazard thresholds are exceeded, this would indicate that the site is not suitable for construction and safe operation of a nuclear power plant (see Hazards Thresholds section, above).

Beyond this analysis of the tsunami hazard associated with the site, per se, it may be necessary in some cases to conduct a formal, comprehensive,

in-depth analysis to determine the ability of a proposed NPP design to withstand the probable impact of tsunamis, as estimated by PMT hazard metric values. Such analyses require expertise that includes structural engineering and other related fields, and guidance on such an effort is beyond the scope of this study.

## 8.4 Real-time THA

Ultimately, a site-specific tsunami hazard assessment must address non-physical issues that bear on the capability of the NPP as an integrated entity, composed of personnel and an NPP infrastructure that includes the physical structure, emergency back-up systems, preparedness programs, etc. Some of these issues, such as personnel education and training, are clearly best addressed after the actual establishment of an NPP. Here we focus on those scientific and technical issues that must be considered before establishment of an NPP, because these issues bear directly on the quality and effectiveness of the infrastructure required to support critical decision-making during an actual tsunami event—i.e., real-time THA (RTHA).

### *8.4.1 Importance of RTHA*

Even if a nuclear power plant is located outside an inundation zone, a destructive tsunami may still threaten the safety of the NPP. Potential tsunami impacts include disruptions of cooling water intake, power transmission systems, and ground transportation to and from the plants; these impacts can occur whether the tsunami generation source is local or distant. It is therefore essential to the safety of the NPP facility and personnel that forecasts and warnings of an incoming tsunami be provided as soon as possible after generation, including reliable estimates of wave heights, currents, and the duration of danger. These real-time tsunami forecast and warning products should guide RTHA that must be conducted during the entire duration of a tsunami event. Consider the value of RTHA to decision-making before and after the arrival of the first tsunami wave:

- ***Before First Wave Arrival.*** RTHA assists decision-makers responsible for initiation (or cancellation) of an NPP response to the hazard, such as evacuation and/or other emergency actions. (In a local event, the tsunami may arrive in minutes, too short a time for any action except those triggered immediately by natural warning phenomena, such as earthquake shaking or anomalous sea level withdrawal or rise. Nonetheless, RTHA must be initiated as soon as possible and continued throughout the entire event.)

- ***After First Wave Arrival.*** The first wave is not necessarily the largest wave, and dangerous waves can continue to arrive for hours. Continual updates of forecast products and THA are therefore required for making decisions that initiate (or cancel) emergency action plans, including evacuation, safely deployment of first responders and other assets, and declaration of an all-clear, i.e., that the tsunami event is terminated.

### *8.4.2 National infrastructure for RTHA*

***8.4.2.1 The NOAA Tsunami Warning System.*** NOAA provides official tsunami warnings for the United States, Puerto Rico, the U.S. Virgin Islands, and the Associated Pacific States. There are presently two NOAA tsunami warning centers. The West Coast/Alaska Tsunami Warning Center (WC/ATWC) in Palmer, Alaska has responsibility for issuing tsunami warnings to the West Coast states and Alaska. After the December 2004 tsunami in the Indian Ocean, the area of responsibility of the WC/ATWC was expanded to include states bordering the Gulf of Mexico and along the East Coast. The Pacific Tsunami Warning Center (PTWC) in Hawaii has responsibility for Hawaii, Puerto Rico, and the Associated Pacific States. PTWC also functions as the international tsunami warning center for nations in the Pacific, Atlantic, and Indian Oceans and the Caribbean Sea. WC/ATWC and PTWC coordinate their efforts, issue consistent warnings, and act as back-up centers for each other. Tsunami warning messages are transmitted via a number of civilian and military means to facilities, agencies, and the Public.

The primary focus of the Tsunami Warning Centers (TWCs) is warning against earthquake-generated tsunamis. After an earthquake occurs near the coast or offshore, the TWCs evaluate real-time seismic data from the global seismic network to determine the likelihood that a dangerous tsunami has been generated. If the earthquake is of sufficient magnitude and occurred near a population center in the TWC's area of responsibility, then a tsunami warning is issued immediately. This warning includes a statement that a dangerous tsunami may have been generated and estimates of arrival times at specific locations along the adjacent coast. As soon as the tsunami has reached the nearest offshore Deep-ocean Assessment and Reporting of Tsunami (DART) system (Fig. 8-2) and/or coastal tide gages, real-time data from these are used to directly observe the tsunami. If the tsunami is found to be too small to be dangerous, then the tsunami warning is promptly cancelled to avoid, if possible, a false alarm. Having one or more DART systems and coastal tide gages near a community or facility has proven very useful for locally generated tsunamis.

When the tsunami source location is such that the tsunami waves will take hours to reach U.S. and other coastal areas within TWC areas of responsibility, there is more time to get additional seismic information and verification from DART systems and coastal tide gages before issuing a tsunami watch and then warning, if these prove to be warranted. The tsunami watch is issued first; a warning is issued to a coastal region when a dangerous tsunami is within 2 hr of reaching that region. DART systems and tide gages near impact areas are also useful for forecast verification and real-time monitoring of tsunami waves incident on the coast during the entire event.

***8.4.2.2 The NOAA Tsunami Forecast System.*** A new forecast system is being developed and installed at the TWCs (Titov *et al.*, 1999; Titov *et al.*, 2001; Titov *et al.*, 2005). This system integrates real-time water level data with tsunami numerical modeling technology to provide site-specific forecasts of tsunami inundation; during the entire event, the

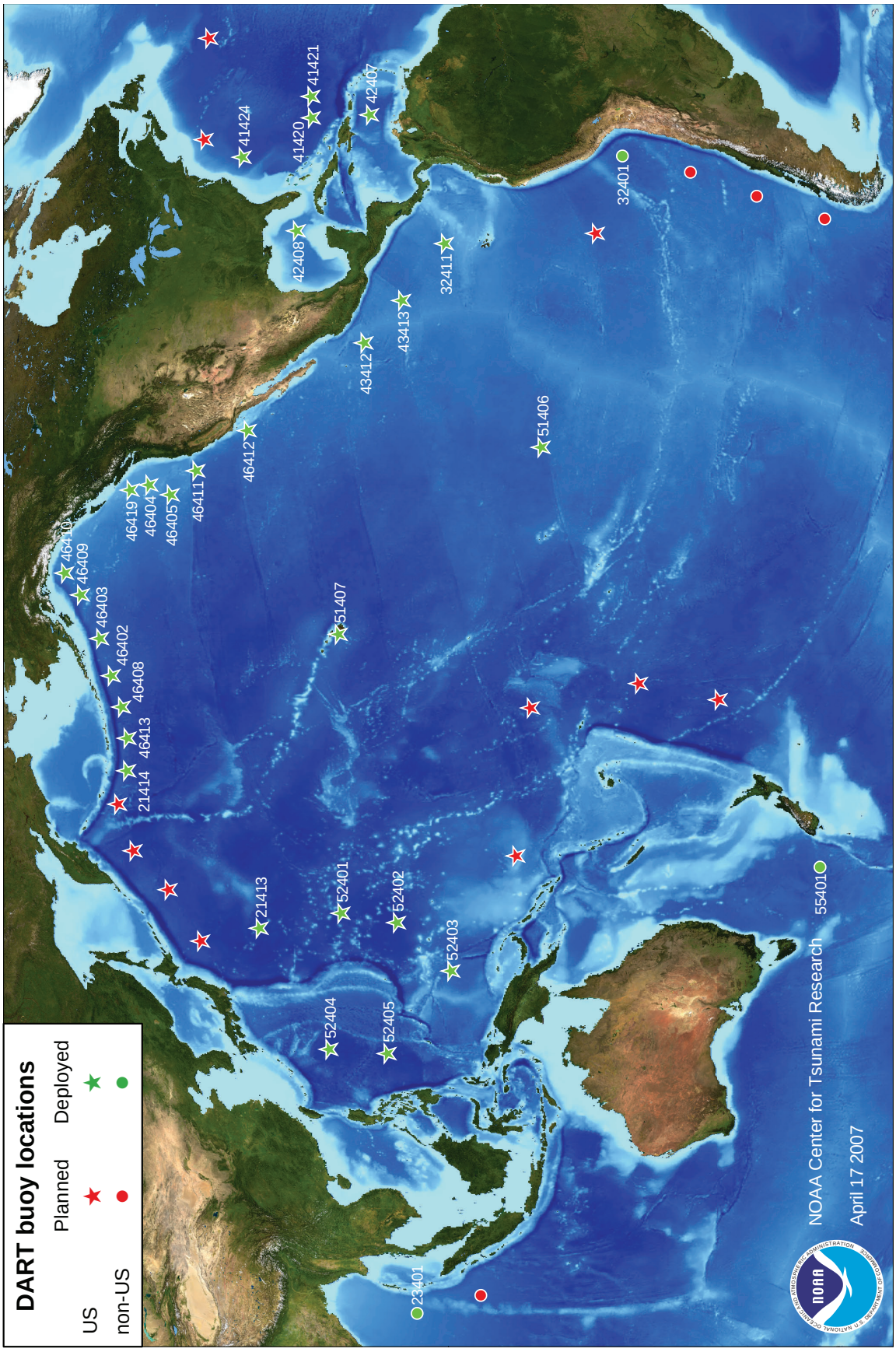


**Figure 8-2:** Existing and planned DART stations.

forecast system will provide continuous updates to monitor and predict the duration of the danger. Site-specific inundation forecast models are planned for approximately 75 locations along the U.S. coast (Fig. 8-3).

The current methodology was designed for earthquake-generated tsunamis only, and utilizes a database of pre-computed, ocean-wide tsunami propagation solutions for individual "unit sources" in regions with known potential of generating tsunamis that threaten U.S. coastlines (see Sections 5.1 and 5.2 and Figs. 5-3 and 5-4). Linear combinations of these solutions can be combined into individual generation/propagation scenarios that formally invert sea level data by optimally matching observed and modeled sea level time series. The resulting generation/propagation scenario then provides the initial and boundary conditions needed for the fine-resolution, site-specific inundation models (see Sections 5.3 and 5.4, and Fig. 5-16). Testing of this methodology indicates that it is sufficiently accurate and robust for forecast and warning purposes (see, e.g., Figs. 5-8 and 5-16).

### *8.4.3 Tsunami preparedness and response*

Clearly, the ultimate effectiveness of RTHA in protecting the safety of an NPP requires that emergency coordinators, the staff, and the facilities be well prepared to respond swiftly and appropriately to RTHA information. This requires, for example, that personnel be educated and trained to recognize natural warnings of a potential tsunami threat—earthquake shaking, anomalous withdrawal or rise in water level, sounds associated with an approaching tsunami, etc.—and respond accordingly; this ability is, in fact, RTHA on an immediate and personal level—a capability that is directly dependent on the NPP preparedness and response program. Beyond this fundamental capability, an infrastructure to provide NPP personnel with reliable RTHA during the course of an entire event is required, as discussed above. This infrastructure includes tsunami forecasts and warnings, robust communication links to TWCs, proper response protocol, training that includes real-time response to updated information, and physical preparation of the facility site and nearby area. All these efforts should be coordinated with local and state emergency management agencies for maximum effectiveness.

### *8.4.4 RTHA enhancement*

Improved RTHA can be achieved for individual NPP sites through the application of the technologies discussed above. To increase the speed and accuracy of the tsunami forecast and warning system, additional DART systems and coastal tide gages are being installed near potential tsunami sources in the Pacific, Atlantic, Caribbean, and Gulf of Mexico Regions (Fig. 8-3). The proximity of such data to an NPP site has a direct impact on the accuracy and reliability of forecasts, and this is especially critical during that period of an event after first wave arrival, when the tsunami hazard must continue to be monitored and assessed and accurate forecasting is essential to RTHA and well-informed decisions to initiate or cancel emergency actions. The

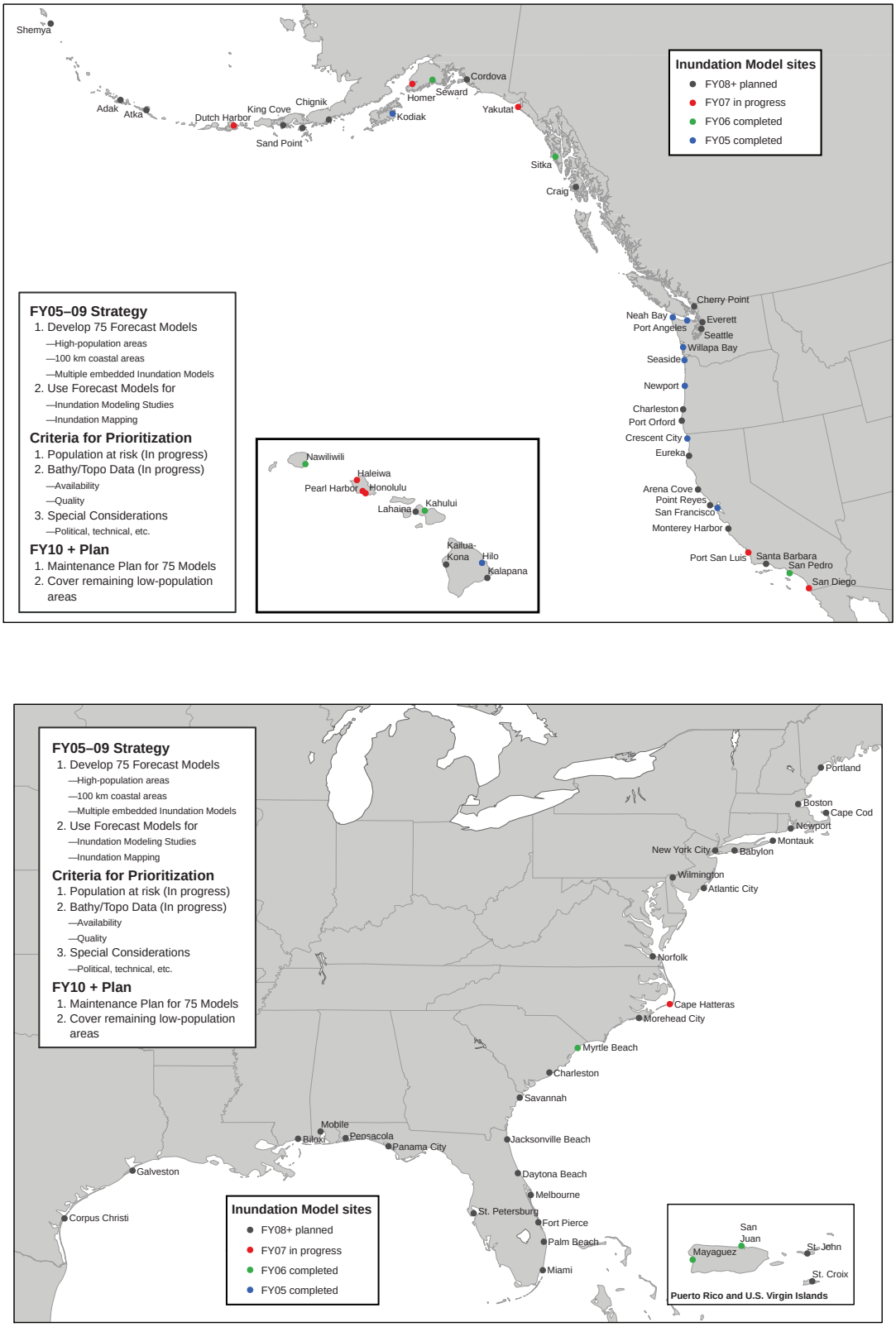


**Figure 8-3:** Real-time inundation forecast models for existing and planned sites on Pacific and Atlantic coasts.

existence of a forecast inundation model that includes the area in which the NPP is located greatly improves the accuracy and reliability of information available for real-time assessment of the hazard. The same model can also be used to prepare inundation maps essential to emergency planning, and to enhance the educational and training component of a preparedness and response plan. Finally, the tsunami hazard can be mitigated if response protocols are developed, for execution on receipt of NOAA forecasts and warnings, and preparedness training programs are established that are coordinated with NOAA TWCs and local and state emergency management agencies.

## 8.5 Probabilistic THA

This report would not be complete without brief mention of Probabilistic THA (PTHA), a topic that is currently the subject of intensive research. In principle, an effective PTHA methodology would provide a more realistic and scientifically rigorous framework for decision-making during NRC reviews of NPP applications, since such reviews would be based on quantitative hazard level estimates—i.e., the probability of occurrence for tsunami events with an estimated level of destructive potential. The PTHA methodology has matured to the point of prototype application at Seaside, Oregon, and is being considered for adoption by Federal agencies and U.S. States charged with THA-related missions (Tsunami Pilot Study Working Group, 2006, included as Appendix D; Dunbar *et al.*, 2006). Indeed, the NRC actively sponsors research directly related to PTHA.

## 8.6 Recommendations

Preceding sections presented a Template THA that provides a scientific/technical framework for the development of more detailed procedures to guide NRC review of tsunami hazard assessments submitted in an application to build and operate an NPP. The Template THA is consistent with current NRC practice that features a hierarchical approach and includes the concept of a Probable Maximum Tsunami. A graphical summary of the Template THA, in the form of a flow chart for major efforts and decision points, is presented in Fig. 8-4.

Regarding the development of improved, more detailed NRC review procedures, we make the following recommendations.

- Form an interdisciplinary team with the required areas of expertise to review the scientific and technical content of the procedures, including an NPP specialist, a geoscientist tsunami expert, a tsunami modeler, a structural engineer, an emergency management professional, and other appropriate experts.

- Require that tsunami hazard assessments include an evaluation of the feasibility and potential effectiveness of RTHA during an event; this evaluation is essential to an assessment of the level of the hazard posed by tsunamis to an operational NPP.

- Conduct frequent evaluations of PTHA development and the status of adoption by other Federal agencies, with the goal of adopting PTHA when the evaluation concludes that an adequately mature PTHA methodology has been achieved.

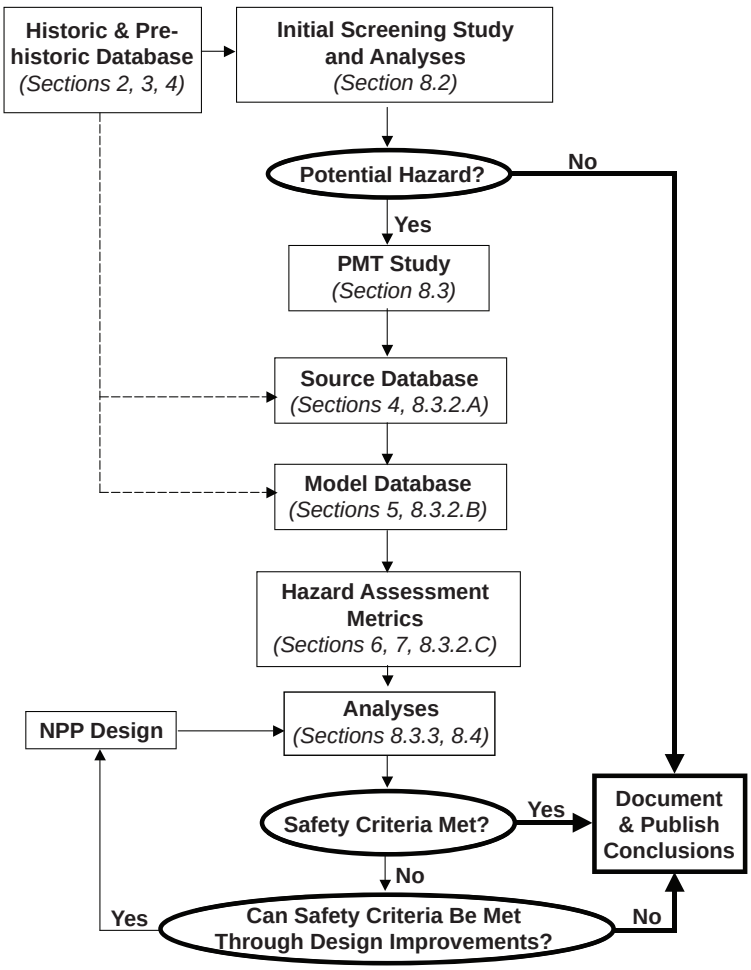


**Figure 8-4:** Flow chart for major efforts (rectangles) and decision points (ovals) of the Template THA. Italicized, parenthetical entries are relevant sections in this report that, in turn, cite the Appendices and additional references.

## 9. Summary and Recommendations

This report reviews scientific issues and technical capabilities that bear on tsunami hazard assessment of U.S. NPP sites. In particular, Section 8 provides a summary of this information in the form of a Template THA, a framework that provides scientific/technical guidance for the development of more detailed, step-by-step procedures for NRC review of tsunami hazard assessments of NPP sites.

Recommendations are also provided in each of Sections 2-8 that address specific technical issues of THA methodology and application. Here we provide more general recommendations to facilitate improvements in nuclear power plant THA, and associated NRC reviews, through collaboration and coordination with other Federal agencies and programs.

A. Establish a formal, interagency partnership of NRC, NOAA, USGS, and FEMA to leverage existing expertise and resources, avoid duplication, and address national needs for tsunami hazard assessment of nuclear power plant sites in a federally consistent and cost-effective manner.

B. Require that tsunami hazard assessments be conducted with source specification and tsunami numerical modeling that meet USGS and NOAA standards, respectively, to ensure Federal consistency of all tsunami hazard assessment methods and the resulting products.

C. Request that NOAA investigate and determine the means and needed resources by which (a) TWCs can provide site-specific warnings for threatened nuclear power plants, and (b) real-time tsunami measurement systems can be established near each NPP to enhance site-specific tsunami forecasts, warnings, and real-time tsunami hazard assessment during an actual event.

## 10. Acknowledgments

Preparation of this report was sponsored by the NRC Division of Engineering. Rajiv Prasad provided valuable comments and suggestions for improvement of the first draft. Harold Mofjeld provided an initial draft of Section 8.4. Ryan Layne Whitney formatted and prepared the final manuscript for publication.

## 11. References


Aalto, K.R., R. Aalto, C.E. Garrison-Laney, H.F. and Abramson (1999): Tsunami sculpturing of the Pebble Beach Wave-cut Platform, Crescent City area, California. *J. Geol., 107*, 607–622.

Abe, K. (1995): Estimate of tsunami run-up heights from earthquake magnitudes. In *Tsunami: Progress in Prediction, Disaster Prevention and Warning*, Y. Tsuchiya and N. Shuto (eds.), Kluwer Academic Publishers, Dordrecht, 21–35.

Abercrombie, R.E., M. Antolik, and G. Ekström (2003): The June 2000 $M_w$ 7.9 earthquakes south of Sumatra: Deformation in the India-Australia plate. *J. Geophys. Res., 108*(B1), 2018, doi: 10.1029/2001JB000674.

Aki, K. (1967): Scaling law of seismic spectrum. *J. Geophys. Res., 72*, 1212–1231.

Allen, J. (1985): *Principles of Physical Sedimentology.* George Allen & Unwin, London, 272 pp.

Andrews, D.J. (1980): A stochastic fault model. 1. Static case. *J. Geophys. Res., 85*, 3867–3877.

Atwater, B.F., and A.L. Moore (1992): A tsunami about 1000 years ago in Puget Sound, Washington. *Science, 258*(5088), 1614–1617.

Begét, J.E. (2000): Volcanic Tsunamis. In *Encyclopedia of Volcanoes*, H. Sigurdsson (ed.), Academic Press, San Diego, 1005–1013.

Belousov, A., B. Voight, M. Belousov, and Y. Muravyev (2000): Tsunamis generated by subaquatic volcanic explosions: Unique data from the 1996 eruption in Karymskoye Lake, Kamchatka, Russia. *Pure Appl. Geophys., 157*, 1135–1143.

Benson, B.E., K.A. Grimm, and J.J. Clague (1997): Tsunami deposits beneath tidal marshes on northwestern Vancouver Island, British Columbia. *Quat. Res., 48*, 192–204.

Berge, C., J.C. Gariel, and P. Bernard (1998): A very broad-band stochastic source model used for near source strong motion prediction. *Geophys. Res. Lett., 25*, 1063–1066.

Bilek, S.L., and T. Lay (1999): Rigidity variations with depth along interplate megathrust faults in subduction zones. *Nature, 400*, 443–446.

Bilek, S.L., and T. Lay (2000): Depth dependent rupture properties in circum-Pacific subduction zones. In *GeoComplexity and the Physics of Earthquakes*, J.B. Rundle, D.L. Turcotte and W. Klein (eds.), Geophysical Monograph, American Geophysical Union, Washington, D.C., 165–186.

Bird, P., and Y.Y. Kagan (2004): Plate-tectonic analysis of shallow seismicity: Apparent boundary width, beta-value, corner magnitude, coupled lithosphere thickness, and coupling in 7 tectonic settings. *Bull. Seismol. Soc. Am., 94*, 2380–2399.

Bird, P. (2003): An updated digital model of plate boundaries. *Geochem. Geophys. Geosyst., 4*(3), 1027, doi: 10.1029/2001GC000252.

Biscontin, G. and J.M. Pestana (2006): Factors affecting seismic response of submarine slopes. *Nat. Haz. Earth Syst. Sci., 6*, 97–107.

Biscontin, G., J.M. Pestana, and F. Nadim (2004): Seismic triggering of submarine slides in soft cohesive soil deposits. *Mar. Geol., 203*, 341–354.

Bondavik, S., F. Løvholt, C. Harbitz, J. Mangerud, A. Dawson, and J.I. Svendsen (2005): The Storegga slide tsunami—comparing field observations with numerical simulations. *Mar. Petrol. Geol., 22*, 195–208.

Borrero, J., M. Ortiz, V. Titov, and C. Synolakis (1997): Field survey of Mexican tsunami produces new data, unusual photos. *Eos Trans. AGU, 78*(8), 85, 87–88.

Bourgeois, J., and M.A. Reinhart (1993): Tsunami deposits from 1992 Nicaragua event: Implications for interpretation of paleotsunami deposits, Cascadia subduction zone. *Eos Trans. AGU, 74*, 350.

Briggs, M.J., C.E. Synolakis, G.S. Harkins, and D.R. Green (1995): Laboratory experiments of tsunami runup on circular island. *Pure Appl. Geophys., 144*(3/4), 569–593.

Bryant, E.A., and R.W. Young (1996): Bedrock-sculpturing by tsunami, South Coast New South Wales, Australia. *J. Geol., 104*, 565–582.

Bryant, E.A., R.W. Young, and D.M. Price (1992): Evidence of tsunami sedimentation on the southeastern coast of Australia. *J. Geol., 100*, 753–765.

Burroughs, S.M., and S.F. Tebbens (2005): Power law scaling and probabilistic forecasting of tsunami runup heights. *Pure Appl. Geophys., 162*, 331–342.

Byrne, D.E., D.M. Davis, and L.R. Sykes (1988): Loci and maximum size of thrust earthquakes and the mechanics of the shallow region of subduction zones. *Tectonics, 7*, 833–857.

Cannon, E.C., R. Bürgmann, S.E. and Owen (2001): Shallow normal faulting and block rotation associated with the 1975 Kalapana earthquake, Kilauea Volcano, Hawaii. *Bull. Seismol. Soc. Am., 91*, 1553–1562.

Chagué-Goff, C., and J.R. Goff (1999): Geochemical and sedimentological signature of catastrophic saltwater inundations (tsunami), New Zealand. *Quat. Australasia, 17*, 38–48.

Chlieh, M., J.-P. Avouac, V. Hjorleifsdottir, T.-R.A. Song, C. Ji, K. Sieh, A. Sladen, H. Hebert, L. Prawirodirdjo, Y. Bock, and J. Galetzka (2007): Coseismic slip and afterslip of the great (Mw 9.15) Sumatra-Andaman earthquake of 2004. *Bull. Seismol. Soc. Am., 97*(1a), S152–S173.

Choy, G.L., and S.H. Kirby (2004): Apparent stress, fault maturity and seismic hazard for normal-fault earthquakes at subduction zones. *Geophys. J. Int., 159*, 991–1012.

Christensen, D.H., and L.J. Ruff (1988): Seismic coupling and outer-rise earthquakes. *J. Geophys. Res., 93*, 13,421–13,444.

Dames and Moore (1980): Design and Construction Standards for Residential Construction in Tsunami-Prone Areas of Hawaii. Prepared for the Federal Emergency Management Agency.

Darienzo, M.E., and C.D. Peterson (1995): Magnitude and frequency of subduction-zone earthquake along the northern Oregon coast in the past 3,000 years. *Oregon Geol., 57*, 3–11.

Dawson, A.G., D. Long, and D.E. Smith (1988): The Storegga Slides: Evidence from eastern Scotland for a possible tsunami. *Mar. Geol., 82*, 271–276.

Dawson, A.G., S. Shi, S. Dawson, T. Takahashi, and N. Shuto (1996): Coastal sedimentation associated with the June 2nd and 3rd, 1994 tsunami in Rajegwesi, Java. *Quat. Sci. Rev., 15*, 901–912.

Dmowska, R., and B.V. Kostrov (1973): A shearing crack in a semi-space under plane strain conditions. *Arch. Mech., 25*, 421–440.

Dmowska, R., J.R. Rice, L.C. Lovison, and D. Josell (1988): Stress transfer and seismic phenomena in coupled subduction zones during the earthquake cycle. *J. Geophys. Res., 93*, 7869–7884.

Dunbar, P., C. Weaver, E. Bernard, D. Dominey-Howes (eds.) (2006): U.S. States and Territories National Tsunami Hazard Assessment—Historical Record and Sources for Waves. NOAA Technical Report (in preparation).

Dziewonski, A.M., and D.L. Anderson (1981): Preliminary reference Earth model. *Phys. Earth Planet. Int., 25*, 297–356.

Edgers, L., and K. Karlsrud (1982): Soil flows generated by submarine slides: Case studies and consequences. In *Proceedings of the 3rd International Conference on the Behavior of Offshore Structures*, C. Chryssostomomidis and J.J. Connor (eds.), Hemisphere Publishing Corporation, 425–437.

Engdahl, E.R., and A. Villaseñor, A. (2002): Global seismicity: 1900–1999. In International Handbook of Earthquake and Engineering Seismology, W.H.K.

Lee, H. Kanamori, P.C. Jennings, and C. Kisslinger (eds.), Part A. Academic Press, San Diego, 665–690.

Federal Emergency Management Agency (2003): Coastal Construction Manual: Principles and Practices of Planning, Siting, Designing, Constructing, and Maintaining Residential Buildings in Coastal Areas, Third Edition.

Fine, I.V., A.B. Rabinovich, E.A. Kulikov, E. Thompson, and B.D. Bonhold (1999): Numerical modeling of landslide-generated tsunamis with application to the Skagway harbor tsunami of 3 November 1994. In *Proceedings of the International Conference on Tsunamis*, Paris, France, 1998, 211–214.

Fine, I.V., Rabinovich, A.B., Bornhold, B.D., Thomson, R. and Kulikov, E.A. (2005): The Grand Banks landslide-generated tsunami of 18 November 1929: Preliminary analysis and numerical modeling. *Mar. Geol., 215*, 45–57.

Fitch, T.J. (1972): Plate convergence, transcurrent faults, and internal deformation adjacent to southeast Asia and the western Pacific. *J. Geophys. Res., 77*, 4432–4460.

Flinn, E.A., E.R., Engdahl, and A.R. Hill (1974): Seismic and geographical regionalization. *Bull. Seismol. Soc. Am., 64*, 771–992.

Frankel, A.D. (1991): High-frequency spectral falloff of earthquakes, fractal dimension of complex rupture, b value, and the scaling of strength on faults. *J. Geophys. Res., 96*, 6291–6302.

Fredsøe, J. (1984): Turbulent boundary layer in wave and current motion. *J. Hydraul. Eng., ASCE, 110*(8), 1103–1120.

Fritz, H.M., W.H. Hager, and H.E. Minor (2003a): Landslide generated impulse waves, Part 1: Instantaneous flow fields. *Exp. Fluids, 35*, 505–519.

Fritz, H.M., W.H. Hager, and H.E. Minor (2003b): Landslide generated impulse waves, Part 2: Hydrodynamic impact craters. *Exp. Fluids, 35*, 520–532.

Fritz, H.M., W.H. Hager, and H.E. Minor (2004): Near field characteristics of landslide generated impulse waves. *J. Waterw. Port Coast. Ocean Eng., 130*, 287–302.

Frohlich, C., M.F. Coffin, C. Massell, P. Mann, C.L. Schuur, S.D. Davis, T. Jones, and G. Karner (1997): Constraints of Macquarie Ridge tectonics provided by Harvard focal mechanisms and teleseismic earthquake locations. *J. Geophys. Res., 102*(B3), 5029–5041, doi: 10.1029/96JB03408.

Fujima, K., and N. Shuto (1989): Friction laws for long waves on dry bed. In *Proceedings of the IUGG/IOC International Tsunami Symposium*, Novosibirsk, USSR, 115–119.

Geist, E.L., and R. Dmowska (1999): Local tsunamis and distributed slip at the source. *Pure Appl. Geophys., 154*, 485–512.

Geist, E.L. (1999): Local tsunamis and earthquake source parameters. *Adv. Geophys., 39*, 117–209.

Gelfenbaum, G., and B. Jaffe (2003): Erosion and sedimentation from the 17 July, 1998 Papua New Guinea tsunami. *Pure Appl. Geophys., 160*, 1969–1999.

Geller, R.J. (1976): Scaling relations for earthquake source parameters and magnitudes. *Bull. Seismol. Soc. Am., 66*, 1501–1523.

Gica, E., M. Spillane, V. Titov, and C. Chamberlin (2006a): Development of the forecasting propagation database for NOAA's Short-term Inundation Forecast for Tsunamis (SIFT). NOAA Tech. Memo ERL PMEL, PMEL, Seattle, WA (in review).

Gica, E., M.H. Teng, P.L.-F. Liu, V. Titov, and H. Zhou (2006b): Sensitivity analysis of source parameters for earthquake generated distant tsunamis. *J. Waterw. Port Coast. Ocean Eng.*, (in review)

Gisler, G., R. Weaver, and M.L. Gittings (2006): SAGE calculations of the tsunami threat from La Palma. *Sci. Tsunami Haz., 24*, 288–301.

Goff, J., P.L. Liu, B. Higman, R. Morton, B.E. Jaffe, H. Frenando, P. Lynett, H. Fritz, and C. Synolakis (2006): The December 26th 2004 Indian Ocean Tsunami in Sri Lanka. *Earthq. Spectra, 22*(S3), S155–S172.

Goff, J.R., and C. Chagué-Goff (1999): A late Holocene record of environmental changes from coastal wetlands: Abel Tasman National Park, New Zealand. *Quat. Int., 56*, 39–51.

González, F.I. (1984): A case study of wave-current-bathymetry interactions at the Columbia River entrance. *J. Phys. Oceanogr., 14*(6), 1065–1078.

González, F.I., B.L. Sherrod, B.F. Atwater, A.P. Frankel, S.P. Palmer, M.L. Holmes, R.E. Karlin, B.E. Jaffe, V.V. Titov, H.O. Mofjeld, and A.J. Venturato (2003): Puget Sound Tsunami Sources—2002 Workshop Report. A contribution to the Inundation Mapping Project of the U.S. National Tsunami Hazard Mitigation Program, NOAA OAR Special Report, NOAA/OAR/PMEL, 34 pp.

Gray, J.P., and J.J. Monaghan (2003): Caldera collapse and the generation of waves. *Geochem. Geophys. Geosyst., 4*, doi: 10.1029/2002GC000411.

Gregory, A.R. (1976): Fluid saturation effects on dynamic elastic properties of sedimentary rocks. *Geophysics, 41*, 895–921.

Gusiakov, V.K. (1972): Generation of tsunami waves and oceanic Reyleigh waves by a submarine earthquake. In *Mathematical Problems of Geophysics, VC SOAN, Novosibirsk, USSR, 3*, 250–272 (in Russian).

Gusiakov, V.K. (1976): Calculation of the tsunami wave energy. *In Ill-posed problems of mathematical physics and interpretation of geophysical data, VC SOAN, Novosibirsk, USSR*, 46–64 (in Russian).

Gusiakov, V.K. (1978): Static displacement on the surface of an elastic space. In *Ill-posed problems of mathematical physics and interpretation of geophysical data, Novosibirsk, VC SOAN, Novosibirsk, USSR*, 23–51, (in Russian).

Hampton, M.A., H. Lee, and J. Locat (1996): Submarine landslides. *Rev. Geophys., 34*, 33–59.

Hanks, T.C., and H. Kanamori (1979): A moment magnitude scale. *J. Geophys. Res., 84*, 2348–2350.

Hanks, T.C. (1979): b values and w-g seismic source models: Implications for tectonic stress variations along active crustal fault zones and the estimation of high-frequency strong ground motion. *J. Geophys. Res., 84*, 2235–2242.

Hartzell, S.H., and T.H. Heaton (1985): Teleseismic time functions for large, shallow, subduction zone earthquakes. *Bull. Seismol. Soc. Am., 75*, 965–1004.

Hearty, P.J. (1997): Boulder deposits from large waves during the last interglaciation on North Eleuthera, Bahamas. *Quatern. Res., 48*, 326–338.

Heinrich, P., A. Mangeney, S. Guibourg, R. Roche, G. Boudon, and J.-L. Cheminée (1998): Simulation of water waves generated by a potential debris avalanche in Monteserrat, Lesser Antilles. *Geophys. Res. Lett., 25*(19), 3697–3700.

Heinrich, P. (1992): Nonlinear water waves generated by submarine and aerial landslides. *J. Waterw. Port Coast. Ocean Eng., 118*, 249–266.

Heinrich, P., A. Piatanesi, and H. Hébert (2001): Numerical modelling of tsunami generation and propagation from submarine slumps: The 1998 Papua New Guinea event. *Geophys. J. Int., 145*, 97–111.

Hemphill-Haley, E. (1995): Diatom evidence for earthquake-induced subsidence and tsunami 300 yr ago in southern coastal Washington. *GSA Bull., 107*, 367–378.

Herrero, A., and P. Bernard (1994): A kinematic self-similar rupture process for earthquakes. *Bull. Seismol. Soc. Am., 84*, 1216–1228.

Higman, B., and B.E. Jaffe (2005): A comparison of grading in deposits from five tsunamis: Does tsunami wave duration affect grading patterns? *Eos Trans. AGU, 86*(52), Fall Meet. Suppl., Abstract T11A-0362.

Hisada, Y. (2000): A theoretical omega-square model considering the spatial variation in slip and rupture velocity. *Bull. Seismol. Soc. Am., 90*, 387–400.

Hisada, Y. (2001): A theoretical omega-square model considering the spatial variation in slip and rupture velocity. Part 2: Case for a two-dimensional source model. *Bull. Seismol. Soc. Am., 91*, 651–666.

Huggel, C., W. Haeberli, A. Kääb, D. Bieri, and S.D. Richardson (2004): An assessment procedure for glacial hazards in the Swiss Alps. *Can. Geotech. J., 41*, 1068–1083.

Hughes, S. (2004): Wave momentum flux parameter: a descriptor for nearshore waves. *Coast. Eng., 51*, 1067–1084.

Iida K. (1956): Earthquakes accompanied by tsunamis occurring under the sea off the islands of Japan. *J. Earth Sciences, 4*(2), 1–43.

Imamura, F., C.E. Synolakis, E. Gica, V. Titov, E. Listanco, and H.G. Lee (1995): Field survey of the 1994 Mindoro Island, Philippines tsunami, *Pure Appl. Geophys., 144*, 875–890.

Imran, J., G. Parker, J. Locat, and H. Lee (2001): A 1-D numerical model of muddy subaqueous and subaerial debris flows. *J. Hydraul. Eng., 127*, 959–958.

Issler, D., F.V. De Blasio, A. Elverhøi, P. Bryn, and R. Lien (2005): Scaling behaviour of clay-rich submarine debris flows. *Mar. Petrol. Geol., 22*, 187–194.

Jaffe, B.E., and G. Gelfenbaum (2002): Using tsunami deposits to improve assessment of tsunami risk. In *Solutions to Coastal Disasters '02*, Conference Proceedings, ASCE, 836–847.

Jaffe, B., G. Gelfenbaum, D. Rubin, R. Peters, R. Anima, M. Swensson, D. Olcese, L. Bernales, J. Gomez, and P. Riega (2003): Tsunami deposits: Identification and interpretation of tsunami deposits from the June 23, 2001 Peru tsunami. In *Proceedings of the International Conference on Coastal Sediments 2003*, CD-ROM Published by World Scientific Publishing Corp and East Meets West Productions, Corpus Christi, TX, USA, ISBN 981-238-422-7, 13 pp.

Jaffe, B.E., and G. Gelfenbaum (2007): A simple model for calculating tsunami flow speed from tsunami deposits. Sediment. Geol., doi: 10.1016/j.sedgeo.2007.01.013, (in press).

Jaffe, B.E., J.C. Borrero, G.S. Prasetya, R. Peters, B. McAdoo, G. Gelfenbaum, R. Morton, P. Ruggiero, B. Higman, L. Dengler, R. Hidayat, E. Kingsley, W. Kongko, Lukijanto, A. Moore, V.V. Titov, and E. Yulianto (2006): Northwest Sumatra and offshore islands field survey after the December 2004 Indian Ocean Tsunami. Earthq. Spectra, 22(S3), S105–S136.

Japan Society of Civil Engineers (2002): Tsunami Assessment Method for Nuclear Power Plants in Japan, 72 pp. (English translation available at `http://www.jsce.or.jp/committee/ceofnp/Tsunami/eng/JSCE_Tsunami_060519.pdf`)

Jeyakumaran, M., and L.M. Keer (1994): Curved slip zones in an elastic half-plane. *Bull. Seismol. Soc. Am., 84*, 1903–1915.

Jeyakumaran, M., J.W. Rudnicki, and L.M. Keer (1992): Modeling slip zones with triangular dislocation elements. *Bull. Seismol. Soc. Am., 82*, 2153–2169.

Jiang, L., and P.H. Leblond (1992): The coupling of a submarine slide and the surface waves which it generates. *J. Geophys. Res., 97*, 12,731–12,744.

Jiang, L., and P.H. Leblond (1993): Numerical modeling of an underwater Bingham plastic mudslide and the waves which it generates. *J. Geophys. Res., 98*, 10,303–10,317.

Jiang, L., and P.H. Leblond (1994): Three-dimensional modeling of tsunami generation due to a submarine mudslide. *J. Phys. Oceanogr., 24*, 559–572.

Johnson, J.M., and K. Satake (1997): Estimation of seismic moment and slip distribution of the April 1, 1946, Aleutian tsunami earthquake. *J. Geophys. Res., 102*, 11,765–11,774.

Kagan, Y.Y., and D.D. Jackson (1991): Seismic gap hypothesis: Ten years after. *J. Geophys. Res., 96*, 21,419–21,431.

Kagan, Y.Y., and D.D. Jackson (1995): New seismic gap hypothesis: Five years after. *J. Geophys. Res., 100*, 3943–3959.

Kagan, Y.Y. (1997): Seismic moment-frequency relation for shallow earthquakes: Regional comparison. *J. Geophys. Res., 102*, 2835–2852.

Kagan, Y.Y. (2002): Seismic moment distribution revisited: I. Statistical Results. *Geophys. J. Int., 148*, 520–541.

Kajiura, K. (1963): The leading wave of a tsunami. *Bull. Earthq. Res. Inst., 41*, 535–571.

Kanamori, H., and D.L. Anderson (1975): Theoretical basis of some empirical relations in seismology. *Bull. Seismol. Soc. Am., 65*, 1073–1095.

Kanamori, H., and M. Kikuchi (1993): The 1992 Nicaragua earthquake: A slow earthquake associated with subducted sediments. *Nature, 361*, 714–716.

Kanamori, H. (1972): Mechanism of tsunami earthquakes. *Phys. Earth Planet. Int., 6*, 346–359.

Kanamori, H., G. Ekström, A.M. Dziewonski, J.S. Barker, and S.A. Sipkin (1993): Seismic radiation by magma injection: An anomalous seismic event near Tori Shima, Japan. *J. Geophys. Res., 98*, 6511–6522.

Kânoğlu, U. (1998): *The Runup of Long Waves Around Piecewise Linear Bathymetries*. Ph.D. Thesis, University of Southern California, Los Angeles, California, 90089-2531, 273 pp.

Kânoğlu, U., and C.E. Synolakis (1998): Long wave runup on piecewise linear topographies. *J. Fluid Mech., 374*, 1–28.

Kânoğlu, U., and C.E. Synolakis (2006): Initial value problem solution of nonlinear shallow water-wave equations. *Phys. Rev. Lett., 97*, 148–501.

Kayen, R.E., and H.J. Lee (1991): Pleistocene slope instability of gas hydrate-laden sediment on the Beaufort Sea magin. *Mar. Geotechnol., 10*, 125–141.

Kelsey, H.M., E. Hemphill-Haley, A.R. Nelson, and R.C. Witter (2005): Tsunami history of an Oregon coastal lake reveals a 4,600 year record of great earthquakes on the Cascadia subduction zone. *Geol. Soc. Am. Bull., 117*, 1009–1032.

Kench, P.S., R.F. McLean, R.W. Brander, S.L. Nichol, S.G. Smithers, M.R. Ford, K.E. Parnell, and M. Asiam ( 2006): Geological effects of tsunami on mid-ocean atoll islands: The Maldives before and after the Sumatran tsunami. *Geology, 34*(3), 177–180, doi: 10.1130/G21907.1.

Kijko, A., and G. Graham (1998): Parametric-historic procedure for probabilistic seismic hazard analysis, Part I: Estimation of maximum regional magnitude $m_{max}$. *Pure Appl. Geophys., 152*, 413–442.

Kijko, A. (2004): Estimation of the maximum earthquake magnitude, $m_{max}$. *Pure Appl. Geophys., 161*, 1655–1681.

Kirby, S., E. Geist, W.H.K. Lee, D. Scholl, and R. Blakely (2005): Tsunami source characterization for Western Pacific subduction zone. A preliminary report, USGS Tsunami subduction zone working group, USGS white paper.

Klein, F.W., A.D. Frankel, C.S. Mueller, R.L. Wesson, and P.G. Okubo (2001): Seismic hazard in Hawaii: High rate of large earthquake and probabilistic ground-motion maps. *Bull. Seismol. Soc. Am., 91*, 479–498.

Kobayashi, N., A.K. Otta, and I. Roy (1987): Wave reflection and runup on rough slopes. *ASCE, J. Waterw. Port Coast. Ocean Eng., 113*(3), 282–298.

Kowalik, Z., and I. Bang (1987): Numerical computation of tsunami runup by the upstream derivative method, Science of tsunami hazards. *Int. J. Tsunami Soc., 5*(2), 77–84.

Lavallée, D., R.J. and Archuleta (2003): Stochastic modeling of slip spatial complexities for the 1979 Imperial Valley, California, earthquake. *Geophys. Res. Lett., 30*(5), 1245, doi: 10.1029/2002GL015839.

Lavallée, D., P. Liu, and R.J. Archuleta (2006): Stochastic model of heterogeneity in earthquake slip spatial distributions. *Geophys. J. Int., 165*, 622–640.

Lay, T., and T.C. Wallace (1995): *Modern Global Seismology*. International Geophysics Series, 58, Academic Press, San Diego, 517 pp.

Lee, H., J.P.M. Syvitski, G. Parker, D. Orange, J. Locat, E.W.H. Hutton, and J. Imran (2002): Distinguishing sediment waves from slope failure deposits: field examples including the "Humboldt slide," and modelling results. *Mar. Geol., 192*(1–3), 79–104.

Lee, H.J., W.R. Normark, M.A. Fisher, H.G. Greene, B.D. Edwards, and J. Locat *et al.* (2004): Timing and extent of submarine landslides in Southern California. Offshore Technology Conference, Houston, Texas, U.S.A., Paper Number 16744.

Lee, H., R.E. Kayen, J.V. Gardner, and J. Locat (2003): Characteristics of several tsunamigenic landslides. In *Submarine Mass Movements and their Consequences*, J. Locat and J. Meinert (eds.), Kluwer, Dordrecht, 357–366.

Lee, H., J. Locat, P. Dartnell, K. Israel, and F. Wong (1999): Regional variability of slope stability: application to the Eel margin, California. *Mar. Geol., 154*, 305–321.

Lee, H.J. (2005): Undersea landslides: Extent and significance in the Pacific Ocean, an update. *Nat. Haz. Earth Syst. Sci., 5*, 877–892.

Legros, F., and T.H. Druitt (2000): On the implacement of ignimbrite in shallow water environments. *J. Volcanol. Geotherm. Res., 95*, 9–22.

Lipman, P.W., B.W. Eakins, and H. Yokose (2003): Ups and downs on spreading flanks of ocean-island volcanoes: Evidence from Mauna Loa and Kilauea. *Geology, 31*, 841–844.

Lipman, P.W., T.W. Sisson, T. Ui, J. Naka, and J.R. Smith (2002): Ancestral submarine growth of Kilauea volcano and instability of its south flank. In *Hawaiian Volcanoes: Deep Underwater Perspectives*, E. Takahashi, P.W. Lipman, M.O. Garcia, J. Naka, and S. Aramaki (eds.), *Geophys. Mono., 128*, American Geophysical Union, 161–191.

Liu, P.L.-F, Y.-S. Cho, M.J. Briggs, U. Kânoğlu, and C.E. Synolakis (1995): Runup of solitary waves on a circular island. *J. Fluid Mech., 302*, 259–285.

Liu, P.L.-F., C.E. Synolakis, and H.H. Yeh (1991): Report on international Workshop on long-wave run-up. *J. Fluid Mech., 229*, 675–688.

Liu, P.L.F., T.-R. Wu, F. Raichlen, C.E. Synolakis, and J.C. Borrero (2005): Runup and rundown generated by three-dimensional sliding masses. *J. Fluid Mech., 536*, 107–144.

Locat, J., and H. Lee (2005): Subaqueous Debris Flows, Chapter 9. In *Debris-Flow Hazards and Related Phenomena*, M. Jakob, and O. Hungr (eds.), Springer, 204–245.

Locat, J., and H.J. Lee (2002): Submarine landslides: Advances and challenges. *Can. Geotech. J., 39*, 193–212.

Locat, J., and J. Mienert (2003): Submarine Mass movements and Their Consequences. *Advances in Natural and Technological Hazards, 19*, Kluwer, Dordrecht, 542 pp.

Locat, J. (1997): Normalized rheological behavior of fine mud and their flow properties in a pseudoplastic regime, Debris—Flow Hazards, mitigation, Mechanics, prediction, and Assessment. Water Resources Engineering Division, American Society of Civil Engineers, New York, 260–269.

Locat, J., H.J. Lee, P. Locat, and J. Imran (2004): Numerical analysis of the mobility of the Palos Verdes debris avalanche, California, and its implication for the generation of tsunamis. *Mar. Geol., 203*, 269–280.

López, A.M., and E.A. Okal (2006): A seismological reassessment of the source of the 1946 Aleutian "tsunami" earthquake. *Geophys. J. Int., 165*, 835–849.

Lynett, P., and P.L.F. Liu (2002): A numerical study of submarine-landslide-generated waves and run-up. *Proc. R. Soc. Lond. A, 458*, 2885–2910.

Lynett, P., and P.L.F. Liu (2006): Three-dimensional runup due to submerged and subaerial landslides. In *Caribbean Tsunami Hazard*, A. Mercado and P.L.F. Liu (eds.), World Scientific Publishing Co., Singapore, 289–307.

Ma, K.-F., H. Kanamori, and K. Satake (1999): Mechanism of the 1975 Kalapana, Hawaii, earthquake inferred from tsunami data. *J. Geophys. Res., 104*, 13,153–13,167.

Mader, C.L., and M.L. Gittings (2002): Modeling the 1958 Lituya Bay mega-tsunami, II. *Sci. Tsunami Haz., 20*, 241–250.

Mai, P.M., and G.C. Beroza (2000): Source scaling properties from finite-fault-rupture models. *Bull. Seismol. Soc. Am., 90*, 604–615.

Mai, P.M., and G.C. Beroza (2002): A spatial random field model to characterize complexity in earthquake slip. *J. Geophys. Res., 107*(B11), 2308, doi: 10.1029/2001JB000588.

Mansinha, L., and D.E. Smylie (1971): The displacement fields of inclined faults. *Bull. Seismol. Soc. Am., 61*, 1433–1440.

Mariotti, C., and P. Heinrich (1999): Modelling of submarine landslides of rock and soil. *Int. J. Numer. Anal. Meth. Geomech., 23*, 335–354.

Masson, D.G., M. Canals, B. Alonso, R. Urgeles, and V. Huhnerbach (1998): The Canary debris flow: Source area morphology and failure mechanisms. *Sedimentology, 45*, 411–432.

Mazzotti, S., X. Le Pichon, P. Henry, and S. Miyazaki (2000): Full interseismic locking of the Nankai and Japan-west Kurile subduction zones: An analysis of uniform elastic strain accumulation in Japan constrained by permanent GPS. *J. Geophys. Res., 105*, 13,159–13,177.

McAdoo, B., L. Pratson, and D. Orange (2000): Submarine landslide geomorphology, U.S. continental slope. *Mar. Geol., 169*, 103–136.

McCaffrey, R. (1992): Oblique plate convergence, slip vectors, and forearc deformation. *J. Geophys. Res., 97*, 8905–8915.

McCann, W.R., S.P. Nishenko, L.R. Sykes, and J. Krause (1979): Seismic gaps and plate tectonics: Seismic potential for major boundaries. *Pure Appl. Geophys., 117*, 1082–1147.

Meckel, T., P. Mann, S. Mosher, and M.F. Coffin (2005): Influence of cumulative convergence on lithospheric thrust fault development and topography along the Australian-Pacific plate boundary south of New Zealand. *Geochem. Geophys. Geosyst., 6*, doi: 10.1029/2005GC000914.

Momoi, T. (1964): Tsunami in the vicinity of a wave origin [I]. *Bull. Earthq. Res. Inst., 42*, 133–146.

Moore, A. (1994): *Evidence for a Tsunami in Puget Sound ∼1000 Years Ago.* M.S. thesis, Seattle, University of Washington.

Moore, A., and D. Mohrig (1994): Size estimate of a 1000-year-old Puget Sound tsunami (abstract). *GSA Abstracts with Programs, 26*, 522.

Moore, A., B.G. McAdoo, and A. Ruffman (2007): Landward fining from multiple sources in a sand sheet deposited by the 1929 Grand Banks tsunami, Newfoundland. *Sediment. Geol.*, Special Issue on Tsunami Deposits (in press).

Moore, A., Y. Nishimura, G. Gelfenbaum, T. Kamataki, and R. Triyono (2006): Sedimentary deposits of the 26 December 2004 tsunami on the northwest coast of Aceh, Indonesia. *Earth Planets Space, 58*, 253–258.

Moore, A.L. (2000): Landward fining in onshore gravel as evidence for a late Pleistocene tsunami on Molokai, Hawaii. *Geology, 28*, 247–250.

Moore, A.L., F. Imamura, I. Yoshida, T., and Hayakawa (2001): Reappraisal of the maximum runup of the 1771 Meiwa tsunami on Ishigakijima. *Tsunami Eng., 18*, 53–60.

Moore, J.G., and G.W. Moore (1984): Deposit from a giant wave on the island of Lanai, Hawaii. *Science, 226*, 1312–1315.

Moore, J.G., W.B. Bryan, and K.R. Ludwig (1994):, Chaotic deposition by a giant wave, Molokai, Hawaii. *Geol. Soc. Am. Bull., 106*, 962–967.

Morgan, J.K., G.F. Moore, and D.A. Clague (2003): Slope failure and volcanic spreading along the submarine south flank of Kilauea volcano, Hawaii. *J. Geophys. Res., 108*(B9), 2415, doi: 10.1029/2003JB002411.

Morton, R.A., G. Gelfenbaum, and B.E. Jaffe (2007): Physical criteria for distinguishing sandy tsunami and storm deposits using modern examples. *Sediment. Geol.*, doi: 10.1016/j.sedgeo.2007.01.003 (in press).

Morton, R.A., B.M. Richmond, B.E. Jaffe, and G. Gelfenbaum (2006): Reconnaissance investigation of Caribbean extreme wave deposits—Preliminary observations, interpretations, and research directions. U.S. Geological Survey Open-File Report OFR-2006-1293, 42 pp., URL: `http://pubs.usgs.gov/of/2006/1293/`.

Murty, T.S. (1977): Seismic Sea Waves Tsunamis. Bulletin 198, Department of Fisheries and the Environment, Fisheries and Marine Service, Ottawa, Canada, 337 pp.

Murty, T.S. (1979): Submarine slide-generated waves in Kitimat Inlet, British Columbia. *J. Geophys. Res., 84*, 7777–7779.

Myers, E.P., and A.M. Baptista (1995): Finite element modeling of the July 12, 1993 Hokkaido-Nansei-Oki tsunami. *Pure Appl. Geophys., 144*(3/4), 769–802.

Nakata, T., and T. Kawana (1993): Historical and prehistorical large tsunamis in the southern Ryukyus, Japan. Tsunamis '93, Proceedings of IUGG/IOC Tsunami Symposium, Wakayama, Japan, 297–307.

Nanayama, F., and K. Shigeno (2005): Inflow and outflow facies from the 1993 tsunami in southwest Hokkaido. *Sediment. Geol., 187*, 139–158.

Nanayama, F., K. Satake, R. Furukawa, K. Shimokawa, B.F. Atwater, K. Shigeno, and S. Yamaki (2003): Unusually large earthquakes inferred from tsunami deposits along the Kuril trench. *Nature, 424*, 660–663.

Nanayama, F., K. Shigeno, K. Satake, K. Shimokawa, S. Koitabashi, S. Miyasaka, and M. Ishii, M. (2000): Sedimentary differences between the 1993 Hokkaido-nansei-oki tsunami and the 1959 Miyakojima typhoon at Taisei, southwestern Hokkaido, northern Japan. *Sediment. Geol., 135*, 255–264.

Newhall, C. (2007) Volcanogenic Tsunami and DART. In *DART Workshop Report*, F.I. González, and E.L. Geist (eds.), NOAA Technical Memorandum OAR PMEL, in preparation.

Nishenko, S.P., and R. Buland (1987): A generic recurrence interval distribution for earthquake forecasting. *Bull. Seismol. Soc. Am., 77*, 1382–1399.

Nishenko, S.P. (1991): Circum-Pacific seismic potential: 1989–1999. *Pure Appl. Geophys., 135*, 169–259.

Nomanbhoy, N., and K. Satake (1995): Generation mechanism of tsunamis from the 1883 Krakatau eruption. *Geophys. Res. Lett., 22*, 509–512.

Nott, J. (1997): Extremely high-energy wave deposits inside the Great Barrier Reef, Australia: Determining the cause—tsunami or tropical cyclone. *Mar. Geol., 141*, 193–207.

O'Brien, J.S., P.-Y. and Julien (1988): Laboratory analysis of mud-flow properties. *J. Hydraul. Eng., 114*, 877–887.

Okada, Y. (1985): Surface deformation due to shear and tensile faults in a half-space. *Bull. Seismol. Soc. Am., 75*, 1135–1154.

Okal, E.A., and C.E. Synolakis (2004): Source discriminants for near-field tsunamis. *Geophys. J. Int., 158*, 899–912.

Okal, E.A. (1988): Seismic parameters controlling far-field tsunami amplitudes: A review. *Nat. Haz., 1*, 67–96.

Okal, E.A., J.C. Borrero, and C.E. Synolakis (2006): Evaluation of tsunami risk

from regional earthquakes at Pisco, Peru. *Bull. Seismol. Soc. Am., 96*, 1634–1648.

Pacific Northwest National Laboratory (2006): Tsunami Hazard Assessment at Nuclear Power Plant Sites in the United States of America. NRC JCN J-3301 Task Order 1 Draft Tsunami Report (in preparation).

Packwood, A.R., and D.H. Peregrine (1981): Surf and runup on beaches: Models of viscous effects. Rep. AM-81-07, School Math., University of Bristol, Bristol, 34 pp.

Parker, L., and M. Holt (2006): Nuclear Power: Outlook for new U.S. Reactors. CRS Report for Congress, Congressional Research Service RL33442, The Library of Congress, 21 pp. (Available at `http://ncseonline.org/NLE/`.)

Pelayo, A.M., and D.A. Wiens (1992): Tsunami earthquakes: Slow thrust-faulting events in the accretionary wedge. J. Geophys. Res., 97, 15,321–15,337.

Peregrine, D.H. (1966): Calculation of the development of an undular bore. *J. Fluid Mech., 22*(2), 321–330.

Peregrine, D.H. (1976): Interaction of water waves and currents. *Adv. Appl. Math., 16*, Academic Press, 9–117.

Peters, B., B. Jaffe, G. Gelfenbaum, and C. Peterson (2003): Cascadia tsunami deposit database. U.S. Geological Survey Open-File Report 03-13, 24 pp. plus electronic database and GIS coverage [`http://geopubs.wr.usgs.gov/open-file/of03-13/`].

Peters, R., B.E. Jaffe, and G. Gelfenbaum, G. (2007): Distribution and sedimentary characteristics of tsunami deposits along the Cascadia margin of western North America. *Sediment. Geol.*, Special Issue on Tsunami Deposits, in press.

Pinegina, T.K., and J. Bourgeois (2001): Historical and paleo-tsunami deposits on Kamchatka, Russia: Long-term chronologies and long-distance correlations. *Nat. Haz. Earth Syst. Sci., 1*, 177–185.

Pinegina, T.K., J. Bourgeois, L.I. Bazanova, I.V. Melekestsev, and O.A. Braitseva (2003): A millennial-scale record of Holocene tsunamis on the Kronotskiy Bay coast, Kamchatka, Russia. *Quat. Res., 59*, 36–47.

Poddyapolsky, G.S. (1968): Generation of a long gravity wave in ocean by a seismic source in the earth crust. *Izvestia AN SSSR, Physics of the Earth, 1*, 7–24 (in Russian).

Polet, J., and H. Kanamori (2000): Shallow subduction zone earthquakes and their tsunamigenic potential. *Geophys. J. Int., 142*, 684–702.

Ramming, H.-G., and Z. Kowalik (1980): *Numerical modelling of marine hydrodynamics.* Elsevier, Amsterdam, 368 pp.

Reinhart, M.A. (1991): Sedimentological analysis of postulated tsunami-generated deposits from Cascadia great-subduction earthquakes along southern coastal Washington. Seattle, WA, University of Washington.

Reinhart, M.A., and J. Bourgeois, J. (1989): Tsunami favored over storm or seiche for sand deposit overlying buried Holocene peat, Willapa Bay, WA. *Eos Trans. AGU, 70*, 1331.

Richardson, S.D., and J.M. Reynolds (2000): An overview of glacial hazards in the Himalayas. *Quat. Int., 65/66*, 31–47.

Rong, Y., D.D. Jackson, and Y.Y. Kagan (2003): Seismic gaps and earthquakes. *J. Geophys. Res., 108*(B10), 2471, doi: 10.1029/2002JB002334.

Rubino, A., S. Pierini, and J.O. Backhaus (1998): Dispersive mudslide-induced tsunamis. *Nonlin. Proc. Geophys., 5*, 127–136.

Rudnicki, J.W., and M. Wu (1995): Mechanics of dip-slip faulting in an elastic half-space. *J. Geophys. Res., 100*, 22,173–22,186.

Rybicki, R. (1986): Dislocations and their geophysical application. *In Continuum Theories in Solid Earth Physics*, R. Teisseyre (ed.), Elsevier, Amsterdam, 18–186.

Saffer, D.M., K.M. Frye, C. Marone, and K. Mair (2001): Laboratory results indicating complex and potentially unstable frictional behavior of smectite clay. *Geophys. Res. Lett., 28*, 2297–2300.

Salzmann, N., A. Kääb, C. Huggel, B. Allgöwer, and W. Haeberli (2004): Assessment of the hazard potential of ice avalanches using remote sensing and GIS-modelling. *Norweg. J. Geog., 58*, 74–84.

Satake, K., J. Bourgeois, K. Abe, Y. Tsuji, F. Imamura, Y. Io, H. Katao, E. Noguera, and F. Estrada (1993): Tsunami field survey of the 1992 Nicaragua earthquake. *Eos Trans. AGU, 74*(13), 145–156.

Satake, K., and H. Kanamori (1991): Abnormal tsunamis caused by the June 13, 1984, Torishima, Japan, earthquake. *J. Geophys. Res., 96*, 19,933–19,939.

Satake, K., and Y. Kato (2001): The 1741 Oshima-Oshima eruption: Extent and volume of submarine debris avalanche. *Geophys. Res. Lett., 28*, 427–430.

Satake, K., and Y. Tanioka (1995): Tsunami generation of the 1993 Hokkaido-Nansei-Oki earthquake. *Pure Appl. Geophys., 144*(3/4), 803–822.

Satake, K., and Y. Tanioka (1999): Sources of tsunami and tsunamigenic earthquakes in subduction zones. *Pure Appl. Geophys., 154*, 467–483.

Satake, K., and Y. Tanioka (2003): The July 1998 Papua New Guinea earthquake: Mechanism and quantification of unusual tsunami generation. *Pure Appl. Geophys., 160*, 2087–2118.

Satake, K. (2002): Tsunamis. In *International Handbook of Earthquake and Engineering Seismology, Part A*, W.H.K. Lee, H. Kanamori, P.C. Jennings, and C. Kisslinger (eds.), Academic Press, San Diego, 437–451.

Satake, K., J.R. Smith, and K. Shinozaki (2002): Volume estimate and tsunami modeling for the Nuuanu and Wailau landslides. In *Hawaiian Volcanoes: Deep Underwater Perspectives*, E. Takahashi, P.W. Lipman, M.O. Garcia, J. Naka, and S. Aramaki (eds.), Geophysical Monograph 128, American Geophysical Union, 333–348.

Scheffers, A.M. (2002): Paleotsunami evidence from boulder deposits on Aruba, Curaao and Bonaire. *Sci. Tsunami Haz., 20*, 26–37.

Schindelé, F., D. Reymond, E. Gaucher and E.A. Okal (1995): Analysis and automatic processing in near field of eight 1992–1994 tsunamigenic earthquakes: Improvements towards real-time tsunami warning. *Pure Appl. Geophys., 144*(3/4), 381–408.

Scholz, C.H. (1982): Scaling laws for large earthquakes: Consequences for physical models. *Bull. Seismol. Soc. Am., 72*, 1–14.

Scholz, C.H. (1990): *The mechanics of earthquakes and faulting.* Cambridge University Press, Cambridge, 439 pp.

Scholz, C.H. (1994): A reappraisal of large earthquake scaling. *Bull. Seismol. Soc. Am., 84*, 215–218.

Schwab, W.C., H.J. Lee, and D. Twichell (1993): Submarine Landslides: Selected Studies in the U.S. Exclusive Economic Zone. U.S. Geological Survey Bulletin 2002, 204 pp.

Seed, H.B., K.L. Lee, and F.I. Makdisi (1975): The slides in the San Fernando Dams during the earthquake of February 9, 1971. *J. Geotech. Eng., ASCE, 101*(GT7), 651–689.

Senior Seismic Hazard Analysis Committee (1997): Recommendations for Probabilistic Seismic Hazard Analysis: Guidance on Uncertainty and Use of Experts. U.S. Nuclear Regulatory Commission, Main Report NUREG/CR-6372 UCRL-ID-122160, Vol. 1, 256.

Shields, A. (1936): Application of similarity principles and turbulence research to bed-load movement. Hydrodynamics Laboratory Publ. No. 167, W.P. Ott and J.C. van Uchelen (trans.), U.S. Department of Agriculture, Soil Conservation

Service Cooperative Laboratory, California Institute of Technology, Pasadena, Calif.

Shokin, Y.I., L.B. Chubarov, V.A. Novikov, and A.N. Sudakov (1987): Calculations of tsunami travel time charts in the Pacific Ocean—Models, algorithms, techniques, results. *Sci. Tsunami Haz., 5*, 85–113.

Shuto, N. (1991): Numerical simulation of tsunamis. In *Tsunami Hazards*, E. Bernard (ed.), Kluwer Academic Publishers, Dordrecht, The Netherlands, 171–191.

Shuto N., and H. Matsutomi (1995): Field survey of the 1993 Hokkaido Nansei-Oki tsunami. *Pure Appl. Geophys., 144*(3/4), 649–664.

Siebert, L. (1996): Hazards of large volcanic debris avalanches and associated eruptive phenomena. In *Monitoring and Mitigation of Volcano Hazards*, R. Scarpa and R.I. Tilling (eds.), Springer-Verlag, Berlin/New York, 541–572.

Siebert, L., and T. Simkin (2002): *Volcanoes of the World: An Illustrated Catalog of Holocene Volcanoes and their Eruptions*. Smithsonian Institution, Global Volcanism Program Digital Information Series, GVP-3, (`http://www.volcano.si.edu/world/`), Washington, D.C.

Smith, W.H.F., and D.T. Sandwell (1997): Global seafloor topography from satellite altimetry and ship depth soundings. *Science, 277*, 1957–1962.

Smolik, G., and K. Newell (2006): 2006–2007 Information Digest. U.S. Nuclear Regulatory Commission NUREG-1350, Vol. 18, 133 pp. (Available at `http://www.nrc.gov/reading-rm.html`)

Somerville, P., K. Irikura, R. Graves, S. Sawada, D. Wald, N. Abrahamson, Y. Iwasaki, T. Kagawa, N. Smith, and A. Kowada (1999): Characterizing crustal earthquake slip models for the prediction of strong ground motion. *Seismol. Res. Lett., 70*, 59–80.

Synolakis, C.E. (1986): *The Runup of Long Waves*. Ph.D. Thesis, California Institute of Technology, Pasadena, California, 91125, 228 pp.

Synolakis, C.E. (1987): The runup of solitary waves. *J. Fluid Mech., 185*, 523–545.

Synolakis, C.E., E. Bernard, V. Titov, U. Kânoğlu, and F. González (2007): Standards, criteria and procedures for NOAA evaluation of tsunami numerical models. NOAA Technical Memorandum OAR PMEL-135, Seattle, WA, in preparation.

Takagi, T. (1996): Finite element analysis in benchmark problems 2 and 3. In *Long Wave Runup Models*, World Scientific Publishing Co., Singapore, 258–264.

Takahashi, To., Ta. Takahashi, N. Shuto, F. Imamura, and M. Ortiz (1995): Source models for the 1993 Hokkaido-Nansei-Oki earthquake tsunami. *Pure Appl. Geophys., 144*(3/4), 747–768.

Tanioka, Y., and K. Satake (1996): Tsunami generation by horizontal displacement of ocean bottom. *Geophys. Res. Lett., 23*, 861–865.

Tanioka, Y., and K. Satake (2001): Detailed coseismic slip distribution of the 1944 Tonankai earthquake estimated from tsunami waveforms. *Geophys. Res. Lett., 28*, 1075–1078.

ten Brink, U.S., and J. Lin (2004): Stress interaction between subduction earthquakes and forearc strike-slip faults: Modeling and application to the northern Caribbean plate boundary. *J. Geophys. Res., 109*, B12310, doi: 10.1029/2004JB003031.

ten Brink, U.S. (2005): Vertical motions of the Puerto Rico Trench and Puerto Rico and their cause. *J. Geophys. Res., 110*, doi: 10.1029/2004JB003459.

ten Brink, U.S., E.L. Geist, and B.D. Andrews (2006a): Size distribution of submarine landslides and its implication to tsunami hazard in Puerto Rico. *Geophys. Res. Lett., 33*, L11307, doi: 10.1029/2006GL026125.

ten Brink, U.S., E.L. Geist, P.J. Lynett, and B.D. Andrews (2006b): Submarine

slides north of Puerto Rico and their tsunami potential. In *Caribbean Tsunami Hazard*, A. Mercado and P. Liu (eds.), World Scientific, Singapore, 67–90.

Thomson, L. (1985): Biot-consistent elastic moduli of porous rocks: Low-frequency limit. *Geophysics, 50*, 2797–2807.

Tinti, S., E. Bortolucci, and C. Romagnoli (2000): Computer simulations of tsunamis due to sector collapse at Stromboli, Italy. *J. Volcanol. Geotherm. Res., 96*, 103–128.

Tinti, S., A. Maramai, and A.V. Cerutti (1999): The Miage Glacier in the Valley of Aosta (Western Alps, Italy) and the extraordinary detachment which occurred on August 9, 1996. *Phys. Chem. Earth, Part A: Solid Earth and Geodesy, 24*, 157–161.

Titov, V.V., and C.E. Synolakis (1995): Modeling of breaking and nonbreaking long-wave evolution and runup using VTCS-2. *J. Waterw. Port Coast. Eng., 121*, 308–316.

Titov, V.V., and F.I. González (2001): Numerical study of the source of the July 17, 1998 PNG tsunami. In *Tsunami Research at the End of a Critical Decade*, G.T. Hebenstreit (ed.), Kluwer Academic Publishers, 197–207.

Titov, V.V., F.I. González, E.N. Bernard, M.C. Eble, H.O. Mofjeld, J.C. Newman, and A.J. Venturato (2005): Real-time tsunami forecasting: Challenges and solutions. In Developing Tsunami-Resilient Communities, The National Tsunami Hazard Mitigation Program, E. Bernard (ed.), *Nat. Haz. 35/1*, 40–58.

Titov, V.V., H.O. Mofjeld, F.I. González, and J.C. Newman (1999): Offshore forecasting of Hawaiian tsunamis generated in Alaskan-Aleutian subduction zone. NOAA Tech. Memo. ERL PMEL-114, NTIS: PB2002-101567, NOAA/Pacific Marine Environmental Laboratory, Seattle, WA, 22 pp.

Titov, V.V., H.O. Mofjeld, F.I. González, and J.C. Newman (2001): Offshore forecasting of Alaskan tsunami in Hawaii. In *Tsunami Research at the End of a Critical Decade*, G.T. Hebenstreit (ed.), Kluwer Academic Publishers, Dordrecht, The Netherlands, 75–90.

Trifunac, M.D., A. Hayir, and M.I. Todorovska (2002): A note on the effects of nonuniform spreading velocity of submarine slumps and slides on the near-field tsunami amplitudes. *Soil Dyn. Earthq. Eng., 22*, 167–180.

Trifunac, M.D., A. Hayir, and M.I. Todorovska (2003): A note on tsunami caused by submarine slides and slumps spreading in one dimension with nonuniform displacement amplitudes. *Soil Dyn. Earthq. Eng., 23*, 223–234.

Tsai, C.P. (1997): Slip, stress drop and ground motion of earthquakes: A view from the perspective of fractional Brownian motion. *Pure Appl. Geophys., 149*, 689–706.

Tsunami Pilot Study Working Group (2006): Seaside, Oregon Tsunami Pilot Study-Modernization of FEMA flood hazard maps. NOAA OAR Special Report, NOAA/OAR/PMEL, Seattle, WA, 94 pp. + 7 appendices.

Tuttle, M.P., A. Ruffman, T. Anderson, and H. Jeter (2004): Distinguishing tsunami from storm deposits in eastern North America: The 1929 Grand Banks tsunami versus the 1991 Halloween storm. *Seismol. Res. Lett., 75*, 117–131.

U.S. Nuclear Regulatory Commission, Office of Nuclear Reactor Regulation, Division of Inspection and Support Programs (1996): Standard Review Plan for the Review of Safety Analysis Reports for Nuclear Power Plants, LWR Edition, Draft for Public Comment, June, 1996.

U.S. Department of Commerce National Oceanic and Atmospheric Administration and U.S. Department of Army Corps of Engineers, (1978): Probable Maximum Precipitation Estimates, United States East of the 105th Meridian, Hydrometeorological Report No. 51.

Ui, T., S. Takarada, and M. Yoshimoto (2000): Debris Avalanches. In *Encyclopedia of Volcanoes*, H. Sigurdsson (ed.), Academic Press, San Diego, 617–626.

Urgeles, R., D.G. Masson, M. Canals, A.B. Watts, and T. Le Bas (1999): Recurrent large-scale landsliding on the west flank of La Palma, Canary Islands. *J. Geophys. Res., 104*, 25,331–25,348.

Utsu, T. (2002): A list of deadly earthquakes in the world: 1500–2000. In *International Handbook of Earthquake and Engineering Seismology, Part A*, W.H.K. Lee, H. Kanamori, P.C. Jennings, and C. Kisslinger (eds.), Academic Press, San Diego, 691–717.

Varnes, D.J. (1978): Slope movement types and processes. In *Landslides: Analysis and Control*, R.L. Schuster and R.J. Krizek (eds.), National Academy of Sciences, Washington, D.C., 11–33.

Walder, J.S., P. Watts, O.E. Sorensen, and K. Janssen (2003): Tsunamis generated by subaerial mass flows. *J. Geophys. Res., 108*(B5), 2236, doi: 10.1029/2001JB000707.

Walsh, T.J., C.G. Caruthers, A.C. Heinitz, E.P. Meyers III, A.M. Baptista, G.B. Erdakos, and R.A. Kamphaus (2000): Tsunami hazard map of the southern Washington coast: Modeled tsunami inundation from a Cascadia Subduction Zone earthquake. Washington Division of Geology and Earth Resources, Geologic Map GM-49.

Ward, S.N., and S. Day (2003): Ritter Island Volcano—lateral collapse and the tsunami of 1888. *Geophys. J. Int., 154*, 891–902.

Ward, S.N. (1980): Relationships of tsunami generation and an earthquake source. *J. Phys. Earth, 28*, 441–474.

Ward, S.N. (2001): Landslide tsunami. *J. Geophys. Res., 106*, 11,201–11,215.

Watts, P. (1998): Wavemaker curves for tsunamis generated by underwater landslides. *J. Waterw. Port Coast. Ocean Eng., ASCE, 124*(3), 127–137.

Watts, P., and C.F. Waythomas (2003): Theoretical analysis of tsunami generation by pyroclastic flows. *J. Geophys. Res., 108*(B12), 2563, doi: 10.1029/2002JB002265.

Waythomas, C.F., and C.A. Neal (1998): Tsunami generation by pyroclastic flow during the 3500-year B.P. caldera-forming eruption of Aniakchak Volcano, Alaska. *Bull. Volcanol., 60*, 110–124.

Weiss, R. (2007): Sediment grains moved by a passing tsunami wave. *Earth Planet. Sci. Lett.* (in preparation).

Wells, D.L., and K.J. Coppersmith (1994): New empirical relationships among magnitude, rupture length, rupture width, rupture area, and surface displacement. *Bull. Seismol. Soc. Am., 84*, 974–1002.

Wesnousky, S.G. (1994): The Gutenberg-Richter or characteristic earthquake distribution, which is it? *Bull. Seismol. Soc. Am., 84*, 1940–1959.

Wong, F.L., A.J. Venturato, and E.L. Geist (2007): Seaside, Oregon, Tsunami Pilot Study: Modernization of FEMA Flood Hazard Maps. GIS Data: U.S. Geological Survey Digital Series (in review).

Wyss, M. (1979): Estimating maximum expectable magnitude of earthquake from fault dimensions. *Geology, 6*, 336–340.

Xu, J.P., M.A. Noble, and L.K. Rosenfeld (2004): In-situ measurements of velocity structure within turbidity currents. Geophys. Res. Lett., 31, L09311, doi: 10.1029/2004GL019718.

Yalin, M. (1977): *Mechanics of Sediment Transport*. Pergamon Press, 2nd edition, 360 pp.

Yamashita, T., and R. Sato (1974): Generation of tsunami by a fault model. *J. Phys. Earth, 22*(4), 415–440.

Yeh, H., F. Imamura, C.E. Synolakis, Y. Tsuji, P.L.-F. Liu, and S. Shi (1993): The Flores island tsunamis. *Eos Trans. AGU, 7*(33), 369, 371–373.

Yeh, H., P.L.-F. Liu, M. Briggs, and C.E. Synolakis (1994): Propagation and amplification of tsunamis at coastal boundaries. *Nature, 372*, 353–355.

Yeh, H., P. Liu, and C. Synolakis (eds.) (1996): *Long Wave Runup Models.* World Scientific Publishing Co., Singapore, 403 pp.

Yeh, H., V. Titov, V.K. Gusiakov, E. Pelinovsky, V. Khramushin, and V. Kaistrenko (1995): The 1994 Shikotan earthquake tsunami. *Pure Appl. Geophys., 144*(3/4), 569–593.

Yin, Z.M., and G.C. Rogers (1996): Toward a physical understanding of earthquake scaling relations. *Pure Appl. Geophys., 146*, 661–675.

Yomogida, K. (1988): Crack-like rupture process observed in near-fault strong motion data. *Geophys. Res. Lett., 15*, 1223–1226.

Yoshii, T. (1979): A detailed cross-section of the deep seismic zone beneath northeastern Honshu, Japan. *Tectonophysics, 55*, 349–360.

Yoshioka, S., M. Hashimoto, and K. Hirahara (1989): Displacement fields due to the 1946 Nankaido earthquake in a laterally inhomogeneous structure with the subducting Philippine Sea plate—A three-dimensional finite element approach. *Tectonophysics, 159*, 121–136.

Zeng, J.L., T.H. Heaton, and C. DiCaprio (2005): The effect of slip variability on earthquake slip-length scaling. *Geophys. J. Int., 162*, 841–849.

Zhao, S., R.D. Müller, Y. Takahashi, and Y. Kaneda (2004): 3-D finite-element modeling of deformation and stress associated with faulting: Effects of inhomogeneous crustal structures. *Geophys. J. Int., 157*, 629–644.

# APPENDICES

The following appendices are on the CD included in the back cover of this report:

**A:** Sources of Historic and Prehistoric Tsunami Data

- Paula Dunbar, NOAA National Geophysical Data Center, Boulder, CO

**B:** Tsunami Science Overview

- Synolakis, C.E., and E.N. Bernard (2006): Tsunami science before and beyond Boxing Day 2004. *Proc. Roy. Soc. Lon. A, 364*(1845), doi: 10.1098/rsta.2006.1824, 2231–2265.

**C:** Tsunami Modeling Standards and Procedures

- Synolakis, C.E., E.N. Bernard, V.V. Titov, U. Kânoğlu, and F.I. González (2007): Standards, criteria, and procedures for NOAA evaluation of tsunami numerical models. NOAA Tech. Memo. OAR PMEL-135, NOAA/Pacific Marine Environmental Laboratory, Seattle, WA, 55 pp.

**D:** Example of Site-specific Assessment, Including a Mathematical Treatment of Tsunamis

- Tsunami Pilot Study Working Group (2006): Seaside, Oregon Tsunami Pilot Study-Modernization of FEMA flood hazard maps. NOAA OAR Special Report, NOAA/OAR/PMEL, Seattle, WA, 83 pp. + 7 appendices.